

Copyright

by

Trevor Jones Budge

2008

**The Dissertation Committee for Trevor Jones Budge Certifies that this is the
approved version of the following dissertation:**

**DELINEATING CONTRIBUTING AREAS FOR KARST SPRINGS
USING NEXRAD DATA AND CROSS-CORRELATION ANALYSIS**

Committee:

John M. Sharp, Jr., Supervisor

Ronald J. Steel

Zong Liang Yang

Steven C. Young

Hongjie Xie

**DELINEATING CONTRIBUTING AREAS FOR KARST SPRINGS
USING NEXRAD DATA AND CROSS-CORRELATION ANALYSIS**

by

Trevor Jones Budge, BS; MS

Dissertation

Presented to the Faculty of the Graduate School of

The University of Texas at Austin

in Partial Fulfillment

of the Requirements

for the Degree of

Doctor of Philosophy

The University of Texas at Austin

August, 2008

Dedication

This work is dedicated to Camea, Courtney, MacKenzie, and Alexis.

Acknowledgements

I would like to acknowledge the contribution of many people who made this dissertation possible. Specifically I would like to thank Jack Sharp for his help in formulating the initial hypothesis and his encouragement and help throughout this process. Also, I would like to thank the other members of my committee for their review and suggestions for this work. I would like to acknowledge the generous funding provided by the Jackson School of Geosciences and the Geology Foundation. The Barton Springs Edwards Aquifer Conservation District, Edwards Aquifer Authority, and the Texas Water Development Board aided in this research by providing me a forum to discuss this research with the scientific community at large. The meetings they set up for me to present these results aided in the process of refining the scope of this research. Will Asquith (USGS) and Greg Shelton (NWS) were key in obtaining time series data for the analysis. Finally, I would like to acknowledge and thank Steve Young for his mentorship in my early career that made seeking this degree possible.

DELINEATING CONTRIBUTING AREAS FOR KARST SPRINGS USING NEXRAD DATA AND CROSS-CORRELATION ANALYSIS

Publication No. _____

Trevor Jones Budge, PhD

The University of Texas at Austin, 2008

Supervisor: John M. Sharp, Jr.

The use of cross-correlation analysis on spring discharge and precipitation data in karst aquifer basins has been used for many years to develop a conceptual understanding of an aquifer and estimate aquifer properties. However, to this point, the application of these processes has relied on gaged precipitation at discrete locations. The use of spatially varying precipitation data and cross-correlation analysis provides a means of spatially characterizing recharge locations on a karst aquifer. NEXRAD provides a spatial estimate of precipitation based by combining reflectivity measurements from radar stations and traditional precipitation gages. This study combines NEXRAD precipitation data with spring discharge data to develop maps of contributing areas for two karst springs in Central Texas. By calculating the cross-correlation of each NEXRAD measurement to spring flow data for the same period of time a map showing the locations hydraulically connected to the spring can be developed. Both numerical experiments and

field applications were conducted as part of the study. The numerical experiments conducted by Padilla and Pulido-Bosch are revisited using the numerical groundwater model MODFLOW. This allowed the introduction of spatially varying parameters into the model. The results show that spatially varying parameters can be inferred based on the results cross-correlation of spatially varying precipitation with respect to a single spring discharge location. Also, contributing area maps are prepared for both Barton Springs and Jacob's Well. Barton Springs has a precise estimate of the recharge area. The current map of the recharge area and the NEXRAD derived map show good agreement with the cross-correlation results. Conversely, Jacob's Well has not been sufficiently studied to delineate a contributing area map. This study provides an preliminary estimate of the area contributing to flow at Jacob's Well. Finally, the development of these maps can also be applied to the construction of regional groundwater models. An application of this methodology with the groundwater availability model for the Barton Springs portion of the Edward's aquifer is introduced. The application of spatial cross-correlation analysis to constrain recharge in the model showed a reduction in the objective function with respect to discharge at Barton Springs of 15%.

Table of Contents

List of Tables	x
List of Figures	xi
Chapter 1. Introduction	1
Motivation	2
Contributions to the Scientific Community	2
Overview	5
Chapter 2. Background	8
Methods	9
NEXRAD	13
Barton Springs	18
Jacob’s Well	20
Chapter 3. Methodolgy	33
Cross-Correlation Equations	33
Statistical Significance	35
Process NEXRAD Data	37
Spring Discharge Pre-Processing	39
Time Series Formatting	40
Run Cross-Correlation Analysis in R Software	41
R Software	41
Import Results into GIS	41
Chapter 4. Numerical Modeling	51
One-dimensional Experiments	51
Two-Dimensional Experiments	53
Chapter 5. Field Applications	77
Comparison of Barton Springs and Jacob’s Well	77
Cross-Correlation Analysis at Two Springs	79
Limitations of Cross-Correlation with NEXRAD	87

Chapter 6. Application to GAM.....	112
Applying SCC Under Different Aquifer Conditions	112
Constraining BSEA GAM	116
Comparison of Results from SCC and GAM Applications	123
Chapter 7. Summary and Conclusions.....	141
Summary and Conclusions	142
Future Work.....	143
Appendix A.....	145
Header File.....	145
Source File	148
Bibliography	181
Vita	189

List of Tables

Table 4.1 – Modeled aquifer properties for each simulation in.....	56
Table 4.2 -Equivalent Hyrdraulic Conductivity estimates for the BSEA based on Halihan (2000).....	64

List of Figures

Figure 1.1 – Location of the Barton Springs portion of the Edwards Aquifer (BSEA) including the delineation of contributing, recharge, and artesian zones.....	7
Figure 2.1 – Stage III NEXRAD gridded data for the West Gulf River Forecast Center.	23
Figure 2.2 – Location of the cell centers of NEXRAD data near Barton Springs used for the cross-correlation analysis.....	24
Figure 2.3 – Example of how staged process of NEXRAD processing alters the precipitation estimate for a single radar location.....	25
Figure 2.4 – NWS River Forecast Regions responsible for flood forecasting across the US.	26
Figure 2.5 – Segments of the Edwards aquifer.	27
Figure 2.6 – Stratigraphic column showing major formations found in the Barton Springs portion of the Edwards Aquifer. The formations shaded in blue are part of the aquifer and the formations not shaded Represent bounding confining units both above and below (Sharp, 1990).....	28
Figure 2.7 – Map showing locations of dye-tracing experiments carried out at BSEA showing possible pathways for recharge in the aquifer to Barton Springs.....	29
Figure 2.8 – Jacob’s Well spring discharge orifice located in the creek bed of Cypress Creek, Wimberley, Texas.	30
Figure 2.9 – Map of the surficial geology near Jacob’s Well.....	31
Figure 2.10 – Stratigraphic column of formations near Jacob’s Well (Ashworth, 1983)	32
Figure 3.1 – A correlogram illustrating the maximum correlation at a lag of 2.	43
Figure 3.2 – The process for determining the maximum correlation significance threshold for two time series (shown in (a)) includes creating 99 correlograms based on randomizing the timing of precipitation events in the precipitation time series (b). A cumulative distribution function (c) for the 99 values of maximum correlation is created to determine the significant threshold . The significant threshold can then be compared the maximum correlation (d) of the original correlogram to verify it is statistically significant.....	44
Figure 3.3 – Website for downloading Stage III and MPE data from the NWS.	45
Figure 3.4 – Discharge recorded at Barton Springs from 1993 to 2004. The hydrograph is broken into components based on a baseflow hydrograph separation using the USGS software BFI.....	46
Figure 3.5 – Correlograms from a NEXRAD cell in the recharge zone of Barton Springs. The Blue Correlogram is derived using the baseflow separated discharge at Barton Springs and the red correlogram results when the baseflow is not separated. The orange dashed line is the statistically significant line.....	47
Figure 3.6 – Discharge recorded at Barton Springs for 1995. The hydrograph is broken into components based on a baseflow hydrograph separation using the USGS software BFI. The figure illustrates the detail of how the large scale temporal trend in the discharge hydrograph is removed by baseflow separation.	48
Figure 3.7 – R source code for carrying out the cross-correlation for an individual cell of NEXRAD data	49

Figure 3.8 – Plot of maximum correlation values at NEXRAD grid cell locations georeferenced with other data for the area around Barton Springs. The currently delineated recharge zone is shaded in grey.	50
Figure 4.1 – Kernel function, precipitation and flow hydrograph, and corresponding correlogram used to model flow in a karst aquifer for conduit-controlled system.	65
Figure 4.2 – Kernel function, precipitation and flow hydrograph, and corresponding correlogram used to model flow in a karst aquifer for matrix-controlled system.	66
Figure 4.3 – Kernel function, precipitation and flow hydrograph, and corresponding correlogram used to model flow in a karst aquifer for mixed-control system.	67
Figure 4.4 – Plan view map of the MODFLOW model domain with the associated boundary conditions.	68
Figure 4.5 – The time series data used for precipitation events used to create discrete recharge for the MODFLOW model using the well package.	69
Figure 4.6 – The locations of the NEXRAD cells used for the precipitation input series used at location Well A and Well B.	70
Figure 4.7 – A set of correlograms that reproduce the three numerical experiments presented by Padilla and Pulido-Bosch.	71
Figure 4.8 – Correlograms for Well A and Well B using a homogenous K field with two precipitation inputs. While differences in the correlogram can be seen, they are extreme.	72
Figure 4.9 – Correlogram for numerical model with hydraulic properties for a conduit flow field.	73
Figure 4.10 – Correlograms for several simulations using multiple precipitation inputs and the conduit flow MODFLOW simulation.	74
Figure 4.11 – Correlogram for Well A and B using a daily timestep in the model. Maximum correlation is found at a negative lag which is physically impossible.	75
Figure 4.12 – Correlograms for Well A and B using the numerical model with aquifer properties equivalent to those in the BSEA. The lag for this correlogram is hours as opposed to days for other correlograms in this chapter.	76
Figure 5.1 – Map of dye trace studies completed by the BSEACD and the City of Austin near Barton Springs.	90
Figure 5.2 – Locations of NEXRAD Cells in the study domain and rain gages near the study domain. The Fischer Store, Wimberley, Dripping Springs, Austin Bergstrom, and Camp Mabry (underlined) gages all had a period of record that overlapped with the NEXRAD data.	91
Figure 5.3 – Bar chart and cumulative precipitation chart for the Camp Mabry gage. Due to the large time scale the bar chart is not as useful in comparing precipitation depths because the width of the bars is so small.	92
Figure 5.4 – Cumulative precipitation plot of Fischer’s Store gage and NEXRAD data for the corresponding NEXRAD cell.	93
Figure 5.5 – Cumulative precipitation plot of Wimberley gage and NEXRAD data for the corresponding NEXRAD cell.	94
Figure 5.6 – Cumulative precipitation plot of Dripping Springs gage and NEXRAD data for the corresponding NEXRAD cell.	95

Figure 5.7 – Cumulative precipitation plot of Camp Mabry gage and NEXRAD data for the corresponding NEXRAD cell.	96
Figure 5.8 – Cumulative precipitation plot of Austin Bergstrom gage and NEXRAD data for the corresponding NEXRAD cell.	97
Figure 5.9 – Cumulative precipitation plot of Fischer’s Store gage and NEXRAD data for the corresponding NEXRAD cell.	98
Figure 5.10 – Cumulative precipitation plot of Wimberley gage and NEXRAD data for the corresponding NEXRAD cell.	99
Figure 5.11 – Cumulative precipitation plot of Dripping Springs gage and NEXRAD data for the corresponding NEXRAD cell.	100
Figure 5.12 – Cumulative precipitation plot of Camp Mabry gage and NEXRAD data for the corresponding NEXRAD cell.	101
Figure 5.13 – Cumulative precipitation plot of Austin Bergstrom gage and NEXRAD data for the corresponding NEXRAD cell.	102
Figure 5.14 – Correlagrams from a NEXRAD cell in the recharge zone of Barton Springs. The Blue Correlagram is derived using the baseflow separated discharge at Barton Springs and the red correlagram results when the baseflow is not separated. The orange dashed line is the statistically significant line.	103
Figure 5.15 – The spatial variation in maximum correlation superimposed over recharge zone of the BSEA. The recharge zone is color-filled in light green.	104
Figure 5.16 – The spatial variation in difference between the maximum correlation and the statistically significant threshold superimposed over recharge zone of the BSEA. The recharge zone is color-filled in light green.	105
Figure 5.17 – The boundaries of the Barton Springs Aquifer with left to right: the contributing zone, the recharge zone, and the confined or artesian zone (USGS, 2008). The table contains the results from cross-correlation analysis based on averaging precipitation time series over each of these zones.	106
Figure 5.18 – Comparison of cross-correlation analysis using MPE and Stage III data over the BSEA recharge zone using the same color ramp for maximum correlation.	107
Figure 5.19 – Comparison of cross-correlation analysis using MPE and Stage III data over the BSEA recharge zone using the natural breaks (Jenks) method for color coding maximum correlation.	108
Figure 5.20 – Example of a typical correlagram of a NEXRAD cell near Jacob’s Well.	109
Figure 5.21 – Maximum correlation plot near Jacob’s well for data from 2005 and 2006. The red square indicates the location of a previously conducted dye-trace study.	110
Figure 5.22 Plot of amount above the statistically significant value NEXRAD cells near Jacob’s well. The darkened area is the surface water catchment above Jacob’s well derived from the 10 m.	111
Figure 6.1 – Flyer produced by the BSEACD that shows both of these locations and gives the current drought status of the aquifer.	125
Figure 6.2 – Location of the Lovelady Well and Barton Springs with respect to the BSEA.	126
Figure 6.3 – Discharge hydrograph at Barton Springs from 1994 to 2004 including the alarm stage threshold at 38 cfs.	127

Figure 6.4 – Maximum correlation plot for BSEA when aquifer conditions were above alarm stage.	128
Figure 6.5 – Maximum correlation plot for BSEA when aquifer conditions were below alarm stage.	129
Figure 6.6 – Pumping distribution used for calibration of the BSEA GAM. Based on pumping rates received from BSEACD. The majority of the pumping occurs in the southern portion of the aquifer.	130
Figure 6.7 – Karst aquifer under different hydraulic conditions. Red circles show locations where during low conditions water may be stored in areas in perched locations that are not hydraulically connected to other locations of the aquifer. (Altered from ESI, 2007)	131
Figure 6.8 – Hydraulic conductivity used in the calibrated BSEA GAM.	132
Figure 6.9 – Locations of springs (modeled using drain cells) and horizontal flow barrier representing major faults in the BSEA GAM.	133
Figure 6.10 – Cross-plots for hydraulic head measurements for both the steady state calibration of the BSEA GAM.	134
Figure 6.11 – Transient calibration of spring discharge hydrograph on a one-month time interval at Barton Springs	135
Figure 6.12 – Calibrated recharge pattern for the BSEA GAM. The pattern is a constant rate within each zone showed in the Figure.	136
Figure 6.13 – PEST optimization can be used along with any numerical model that is based on command line arguments.	137
Figure 6.14 – Locations of pilot points used for sensitivity analysis of recharge in BSEA GAM. Values ranged in value from 0.0 to 3.0.	138
Figure 6.15 – Warping values used to multiply the model recharge when the spring discharge indicated drought conditions.	139
Figure 6.16 – Warping values used to multiply the model recharge when spring discharge indicated normal conditions.	140
Figure A.1 – Graphical user interface for the NEXRAD data processing software to facilitate the conversion of xmrg file format into an ASCII format.	180

Chapter 1. Introduction

In Summer of 2005 The University of Texas at Austin Hydro Field class spent three days at Jacob's Well (a karst spring near Wimberly, Texas) to perform a dye trace study on the spring under the direction of the United States Geological Survey (USGS) and the Edwards Aquifer Authority (EAA). The study ended without recovering any dye at the spring. While there are various hypotheses as to why no dye was recovered, one hypothesis is the location selected to inject the dye was not hydraulically connected to the spring (UT, 2005). The 2005 dye-trace study is the only known dye-trace conducted at Jacob's Well. At the time of the dye-trace experiment, no map precisely delineating the recharge area of the spring was available. As part of the group performing the dye-tracing experiment, I began to ponder a preliminary method that could have been used for pre-selecting dye injection locations. The method of spatial cross-correlation analysis using NEXRAD data was developed as a way to provide a preliminary delineation of recharge for Jacob's Well.

Cross-correlation analysis on spring discharge and precipitation data in karst aquifers has been used in several instances to develop a conceptual understanding of an flow in the aquifer and estimate aquifer properties (Moore, 1992, Padilla and Pulido-Bosch, 1995, Laroque, 1998, Birk, 2004, Aquilina, 2005, Panagopoulos & Lambrakis, 2006). However, to this point, the application of these processes has relied on gauged precipitation at discrete locations. Birk (2004) noted that while the methods are useful for characterizing springs with small catchment areas, using precipitation gages lacks the ability to characterize springs with large catchment areas. The use of spatially varying

precipitation data and cross-correlation analysis is hypothesized here to provide a means of spatially characterizing recharge locations for karst springs. Next Generation Radar (NEXRAD) provides a spatial estimate of precipitation based by combining reflectivity measurements from radar stations and traditional precipitation gages (Fulton, 1998). To investigate the use of these algorithms cross-correlation of NEXRAD precipitation data with spring discharge data was performed with data from two karst springs (Barton Springs and Jacob's Well shown in Figure 1.1) in Central Texas. By calculating the cross-correlation of each NEXRAD cell with respect to spring discharge, a map of the likely locations contributing to recharge at the spring can be developed.

MOTIVATION

The Karst Waters Institute (2007) estimates that over 25 percent of the world's population derives its water supply from karst aquifers. Also, the quality and quantity of water discharging from karst springs is used to gage the health of the karst aquifer. In order to protect the resources in karst aquifers, scientists must evaluate and estimate flow paths and recharge locations for the aquifer. Unfortunately many of the current techniques used for developing this information require large capital investment. The method presented in this dissertation can be used a means to provide insight into the recharge and contributing areas to spring discharge using data sets that are already available.

CONTRIBUTIONS TO THE SCIENTIFIC COMMUNITY

Several obstacles to completing this research existed at its inception. By introducing methods for overcoming these obstacles this research has contributed to the

ability of stakeholders and scientists evaluate recharge to karst springs. These obstacles included; 1) developing algorithms to work with NEXRAD data; 2) processing and analyzing cross-correlation results for large geospatial data sets; 3) dealing with a large period of record; 4) utilizing baseflow separation as a method to filter the discharge signal analyze cross-correlation results; and 5) looking for a method to test statistical significance. These obstacles are discussed below.

Obtaining and manipulating the NEXRAD dataset was a major obstacle at the inception of this research. NEXRAD data is archived by the National Weather Service (NWS) in a format called “xmrg”. This format is binary in nature and is not user friendly in many respects. Johnson et al. (2001) concluded that the use of NEXRAD was so difficult that it was not economically feasible for scientists and engineers outside of the NWS to use it for project work. They also noted that, with time, tools could be developed to allow for general use of these data. However, at these were not available at the time this research began (Xie et al., 2005). This research produced a quick and efficient method for parsing through the NEXRAD period of record to extract precipitation time series data for analysis.

Typical cross-correlation analyses, mentioned previously, included one spring and one or two precipitation gages. By developing algorithms to utilize the spatial variability of NEXRAD data another level of organization was necessary to analyze and interpret data. Not only was it necessary to increase the number of cross-correlation calculations by an order of magnitude, the results also needed to be presented in the proper geospatial context. Otherwise, the comparison of whether recharge likelihood at a given location could not be compared to adjoining locations. Coupling the output from statistical

software with GIS was used in order to produce maps for comparing existing conceptual models of recharge with the cross-correlation analysis.

Typically, the previous studies involving cross-correlation analysis on karst springs involved one-year record of precipitation and discharge data. This research was unique in that it analyzed a 10-year period of record for Barton Springs. These large of data sets taxed the tools used for this analysis to the point that custom software was required to parse through the data and organize it. Without these tools the computer resources used for this research would not have been sufficient for completing the project.

The discharge data for Barton Springs included temporally large scale patterns that caused enough noise in the correlation analysis to render the results unusable for estimating recharge locations. As part of this study an innovative approach to using baseflow separation techniques typically used for surface water applications to filter out the large scale patterns. This step will be key for application of these algorithms at other spring locations with a period of record for the discharge data as long as Barton Springs.

Finally, none of the previous studies involving karst and cross-correlation analysis evaluated the statistical significance of the correlations. Statistical significance testing is used to provide insight into whether the results from the study could possibly be the result of random chance. To overcome this obstacle a method used extensively in the neuroscience field to test statistical significance (Kwan, 2004) was introduced into the analysis of groundwater cross-correlation.

By overcoming these obstacles and developing the algorithms for the creation of maps of recharge likelihood for these regions, this research has developed a useful tool

that allows scientists and stakeholders increased manage and conserve the karst aquifer. The results of this research have been presented to several of these groups including the Barton Springs Edwards Aquifer Conservation District (BSEACD), EAA, and the Texas Water Development Board (TWDB).

OVERVIEW

This dissertation is broken into several chapters discussing specific aspects of the research. This section gives an overview of each of these chapters.

Chapter 2 discusses background information about methods used for delineating karst recharge. These include numerical modeling, dye-trace experiments, and time series statistical analysis. Also, background information on NEXRAD data and the hydrogeology of Barton Springs and Jacob's Well are discussed. A literature review of work in these areas is included with the discussion.

The algorithms developed for conducting this analysis are the subject of Chapter 3. Both cross-correlation analysis and methods of processing NEXRAD and spring discharge data are discussed in this chapter.

Chapter 4 discusses the theoretical experiments conducted by Padilla and Pulido-Bosch (1995) and how they were revisited using the numerical groundwater model MODFLOW. By using MODFLOW similar results to those produced by Padilla and Pulido-Bosch are produced and spatially varying parameters are introduced (e.g., hydraulic conductivity and precipitation) into the modeling exercise. The results indicate that variations in flow paths can be inferred based on the cross-correlation of spatially varying precipitation data and a single spring discharge location.

Also, chapter 5 discusses the preparation of contributing area maps for both Barton Springs and Jacob's Well. Barton Springs portion of the Edwards Aquifer (BSEA) has a precise estimate of the recharge area. The current map of the recharge area (BSEACD, 2005) and the NEXRAD derived map show good agreement in the spatial location of the recharge areas. Conversely, no precise delineation of the contributing area has been completed for Jacob's Well. While several studies investigate groundwater flow (Grimshaw, 1970, Ashworth, 1983, Bluntzer, 1992, Hanson and Small, 1995, Mace et al., 2000, and Scanlon, 2001), none have attempted to map the contributing areas. This study provides an estimate of the area contributing to flow at Jacob's Well. Also, the results provide insights into why no dye was recovered during the dye tracing experiment at Jacob's Well in 2005 discussed previously.

Chapter 6 discusses how the contributing area maps of BSEA can be used to investigate how recharge changes with respect to hydraulic head conditions of the aquifer. These changes are compared to a numerical model of BSEA to show how these results could be used to constrain calibration of a regional groundwater model. A sensitivity analysis using PEST was used to compare model improvements to the results of the cross-correlation analysis. Model sensitivities and cross-correlation results showed similar trends in recharge patterns over BSEA.

Finally, Chapter 7 summarizes the major findings and future directions of this research.

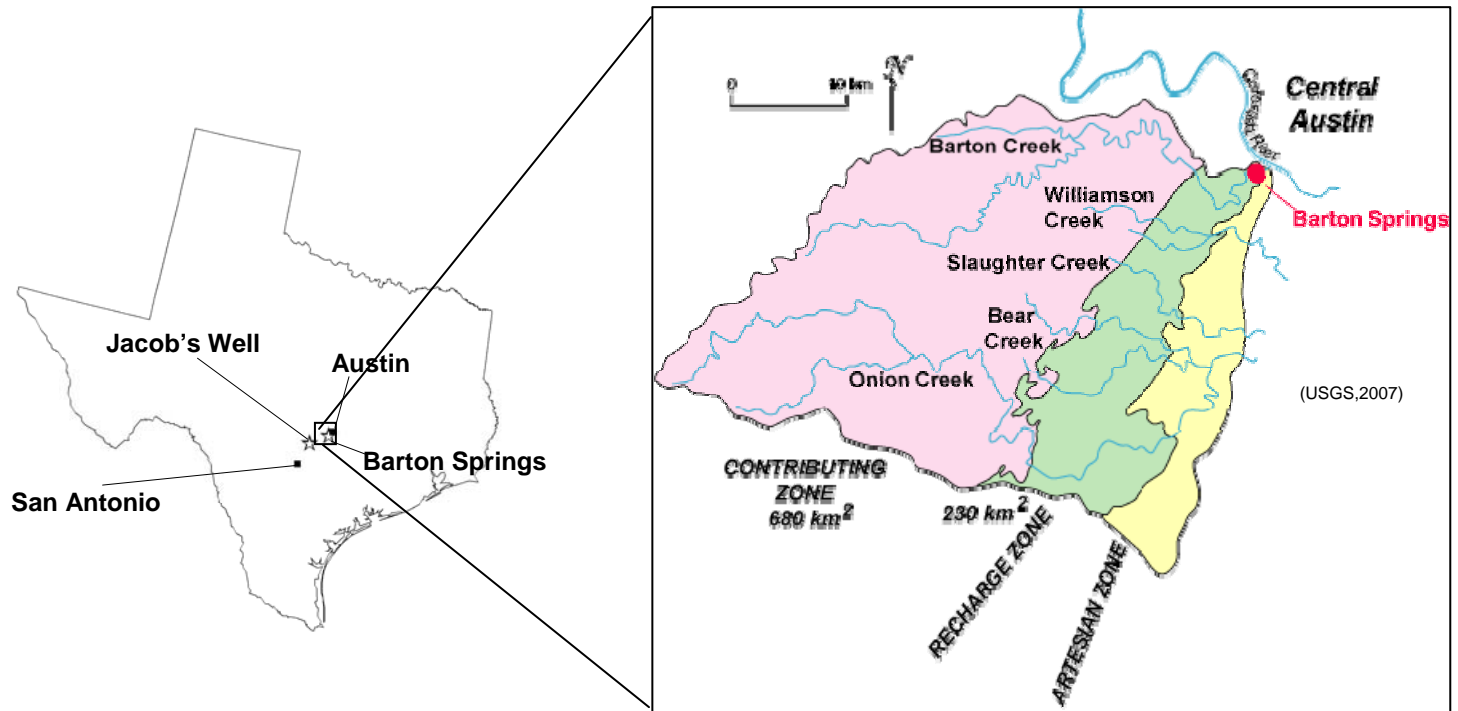


Figure 1.1 – Location of the Barton Springs portion of the Edwards Aquifer (BSEA) including the delineation of contributing, recharge, and artesian zones.

Chapter 2. Background

Karst refers to a geologic terrain or surface landscape with distinctive characteristics of relief and drainage arising primarily from dissolution of rock (or soils) by natural waters. A typical scenario for karst development may include tectonic stresses or overburden that produce fractures in the matrix, enlarging of the fractures through dissolution to form caverns, conduits, and sinkholes that act as preferential flow paths for groundwater and discrete recharge features. Due to the formation of these preferential flow paths, characterizing the flow direction through a karst aquifer can be difficult. Moreover, these preferential flowpaths also transmit pollutants and contaminants that can devastate the usefulness of the water resource (Small, 1996). One example of a karst aquifer that is susceptible to contamination is the Barton Springs portion of the Edwards Aquifer (BSEA) located near Austin, Texas (see Figure 1.1). Groundwater within the aquifer travels through conduits, fractures and the matrix as is normal with many other karst aquifers (Hunt, 2007, Hauwert, 2006, and Scanlon, 2004).

There are many tools available for characterizing karst aquifers. These include dye tracing experiments, models (analytical, numerical and stochastic), and statistical time series analysis. The purpose of this Chapter is to introduce and review literature available describing these methods for characterizing karst and how they have been applied at BSEA. Also, a new method for karst characterization using next generation radar precipitation data (NEXRAD) is introduced. This includes a discussion of past applications of NEXRAD in related fields of study.

METHODS

Several methods including numerical modeling, tracer analysis, and statistical time-series analysis have been developed and applied to characterization of karst aquifers. This section discusses several of these techniques and describes their application to karst aquifers.

Numerical modeling

Several types of numerical models are used for modeling karst regimes. Green et al. (2006) and Neumann (2005) each summarizes the state of modeling flow through fractures. However, Green et al. specifically address karst terrains. The most common types of numerical models used for karst include equivalent porous media models (e.g., MODFLOW (Harbaugh, 1988) , FEMWATER (Lin et al, 2001)), discrete fracture models (e.g., FEFLOW (Diersh, 2002) and Hydrosphere (Therrien et al, 2004), and dual porosity/conductivity models (e.g., MODFLOW-SURFACT (HGL, 2005), MODFLOW-DCM (Painter, 2004)). Numerical models of groundwater aquifers divide the aquifer into discrete volumes called cells or elements. Each cell and/or element is assigned hydraulic properties reflective of properties determined from field data or assumptions. Water level distributions and velocities are then estimated by the models through analytical methods, finite differencing methods, or finite element methods. The results of these models can be used to delineate a zone of influence by tracking the flow directions estimated by the model. A map delineating the zone of influence for any location in the aquifer can be generated by this method. The use of these methods have been used in several studies including Scanlon (2001), Dufrense (1999), Worthington et al. (2002), and Cunningham et al. (2004).

Tracer analysis

One of the most popular methods for delineating recharge locations in karst regions include dye trace studies (BSEACD, 2003, Connair, 2002, Smart, 1988) and stable isotope analysis (Katz, 1996, Kattan, 1997, Barnes, 1998, Nativ, 1999, Vandenschrick, 2001, Emblanch, 2003). In dye tracing experiments a non-volatile dye that is not native to the region is selected and injected into recharge features. The dye is transported through forced convection while discharge features and monitoring wells are monitored for the dye. Concentration breakthrough at another location implies a hydraulic connection between the recharge and discharge feature used for the experiment. By running many dye trace experiments a map of recharge and corresponding discharge zones along with travel times based on the breakthrough curves can be developed. This method can provide reliable results when the experiment is carried out properly. In stable isotope analysis the tracers are naturally occurring and require chemical analysis of water samples from the aquifer to determine where the recharge originated. Both of these methods include significant capital expense in the form of chemical analysis and analytical hardware. In some cases these costs may be prohibit their use as a delineation tool.

Statistical Time Series Analysis

Time series analysis for hydrologic investigation is common in hydrology. Moore (1992), Padilla and Pulido-Bosch (1995) , Laroque et al. (1998), Birk et al. (2004), Aquilina et al. (2005), Panagopoulos & Lambrakis(2006) , and Massei and Mahler (2007) all demonstrate the usefulness of time series analysis as applied to karst aquifers. Specifically, their work has involved the analysis of spring discharge time series. Each of

these studies specifically involves the use of statistical tools to characterize karst aquifers. Therefore, each of these research projects is briefly discussed below.

Moore (1992) used recession curves to determine lag intervals from rainfall events and the corresponding runoff in streams flowing in a shallow karst aquifer near Oak Ridge National Labs in Tennessee. 17 piezometers were used to determine the change in storage in the shallow system over time after a rain event. The slope of recession in the storage volume was used to estimate aquifer properties including hydraulic conductivity, transmissivity, and specific yield. To estimate these values, the properties of the entire system were assumed to be homogenous and isotropic.

Padilla and Pulido-Bosch (1995) used cross-correlation analysis methods to characterize several karst aquifers. Cross-correlation analysis (see Chapter 3) consists of comparing the correlation of two time-series while shifting data over several lag times to calculate a correlogram. They conducted numerical experiments to illustrate the different responses of the correlogram based on different flow regimes and applied the methods to field data to characterize several karst aquifers. By looking at the characteristics of the correlogram of precipitation and discharge they identified the significance of matrix flow and quickflow or conduit flow to discharge of the aquifers. The cross-correlation analysis was useful in determining the dominant flow type (conduit flow or matrix flow) of the karst aquifer along with estimating the lag time between precipitation events and increased discharge at a spring.

Laroque (1998) built upon the work completed by Padilla and Pulido-Bosch by using more than one precipitation gage to characterize the La Rochefoucauld karst aquifer near Charten, France. He also used both spring discharge and electric

conductivity of the water to calculate correlograms for the different precipitation gages. He illustrated that correlograms from different precipitation gages will result in different behavior of the correlogram. Therefore, he was able to infer different levels of contribution to spring flow from different locations in the aquifer.

Birk et al. (2004) combined the use of spectral analysis with temperature and electric conductivity data to investigate location recharge to springs. The study was able to use to correlate recharge events with temperature change in the spring discharge. However, the karst system was localized (3 km²). Birk et al. concluded that the methods lacked the ability to characterize the recharge for a spring with a larger catchment area.

Aquilina (2005) used stable isotope analysis over time to evaluate contribution to spring discharge. By using calculated mean concentrations deuterium and oxygen-18 from rainfall samples and spring flow samples the typical residence time for the water was also estimated. His results indicated that epikarst was a major factor in recharge to the aquifer by providing increased storage resulting in increased residence time.

Panagopoulos and Lambrakis(2006) applied the methods described by Padilla and Pulido-Bosch (1995) to the Trifilia and Almyros Crete aquifers in Greece. They determined that the Trifilia aquifer was dominated by baseflow and did not have well developed karst. However, discharge from the Almyros Crete aquifer was dominated by conduit flow. This application further legitimized the ability of cross-correlation analysis to investigate the nature of flow in karst aquifers.

Massei and Mahler (2007) studied specific conductance of discharge waters at BSEA to investigate differences in flow regimes and paths in the aquifer. Four years of data were studied to determine the specific conductance frequency distribution (CFD).

For each year, the general shape of the CFD was approximately the same. However, differences in the of the peak and specific conductance at the peak frequency illustrated how flow through the system behaves differently under different aquifer conditions.

Each of the studies discussed above show that statistical analysis of spring discharge time series can be a powerful tool in characterizing karst aquifers. The studies of particular interest to this study include the use of precipitation data and the calculation of correlograms to characterize karst aquifers. These algorithms are used with NEXRAD data to create an algorithm to characterize recharge at karst springs.

NEXRAD

Recent developments have been made using NEXRAD data to characterize the spatial location of recharge areas in karst aquifers (Budge and Sharp, 2008). The purpose of this section is to define NEXRAD data, discuss the application of NEXRAD data in fields related to recharge characterization, and introduce how these data are used for characterizing karst environments.

General NEXRAD

NEXRAD is a weather radar network used to collect nationwide precipitation estimates for the United States starting in 1994. The acronym stands for “NEXt generation RADar”. Weather radars work by transmitting energy pulses through the atmosphere and measuring the amount of energy that is reflected by the atmosphere. Different substances reflect different amounts of energy. However, as the particle’s size and the number of particles increase more energy is reflected. The reflected energy can be converted to an amount of precipitation (e.g., rain, snow, hail) based on empirical

observation (Fulton, 1998). The reflected data can be stored in a gridded format to give estimates of precipitation on a spatial basis (see Figure 2.1)

Two issues arise from the use of weather radar data. The first is the distance from radar where reflectivity values are considered accurate and the second is interference from other reflectors other than precipitation. Radar data typically have an effective radius of approximately 100 to 150 km and can obtain measurements from as far as 300 to 450 km (Fulton, 1998). Also, snow and hail have been known to interfere with the accuracy of the measurements when applying empirical relationships (McIlveen, 1992). To overcome these issues two strategies are employed. First, weather radar are placed in networks. The distance between each radar is designed to overcome possible effects due to distance from the radar source. Second, all weather radar goes through ground-truthing algorithms based on other methods of precipitation estimation, most notably the use of precipitation data collected at rain gages.

Carpenter (2001) and Young (2000) each investigated the suitability of NEXRAD data use for hydrologic investigation. In each case, the NEXRAD data were deemed suitable use in hydrologic studies. The majority of current research involving NEXRAD data investigate its usefulness with surface water resources (Smith et al, 2004). The spatial nature of NEXRAD data allows surface water models which for the most part have been lumped parameter models to shift towards spatially variable surface water models. Recently, NWS has been conducting research on how distributed models improve their ability to predict hydrologic response to weather. Results of this research were reported as part of a special issue of the Journal of Hydrology (October 2004). The issue was dedicated to the Distributed Model Intercomparison Project (DMIP).

was a joint project between 12 domestic and international research agencies. It illustrated the usefulness of distributed parameter modeling with NEXRAD as its base precipitation estimate for hydrologic investigation (Smith, 2004). On the other hand little work involving NEXRAD data and groundwater has been completed. Glenn (2003) used NEXRAD data to assess the amount of rainfall that fell for an aquifer recharge zone to help quantify recharge estimates. They concluded that spatial recharge patterns could be quantified using NEXRAD data and slightly improved model prediction. Another conclusion of the study showed the ability to conduct real-time groundwater modeling using MODFLOW with recharge files generated from NEXRAD data. Also, the USGS (2006) recently altered the methodology for calculating recharge for the Edwards Aquifer San Antonio Segment from traditional rain gages to NEXRAD data.

NEXRAD Products

The National Weather Service (NWS) collects and archives the rainfall data in a 4 km by 4 km grid for the entire continental US (Maddox, 2002). This grid is called the Hydrologic Rainfall Analysis Project (HRAP) grid. Figure 2.2 shows the grid locations that are available near the BSEA. The data are archived on an hourly time step. The NEXRAD data used in this study is stored in a file format called XMRG. For this reason the terms NEXRAD and XMRG are sometimes used interchangeably. However, NEXRAD refers to the weather radar network while data collected by this network is stored in XMRG files.

The NWS provides NEXRAD data in several types of products. Two major sets of products that are available from NWS at the following website:

<http://dipper.nws.noaa.gov/hdsb/data/nexrad/nexrad.html> . The two products are Stage III and Multi-sensor Precipitation Estimator (MPE) data. These products are available in the XMRG format. The details of these data along with a discussion of the XMRG format are discussed below.

Staged NEXRAD Products

Stage III data get their title from the levels of processing that occur to produce the estimate. There are up to four stages of calculations that are a part of developing this product. The differences in each stage are briefly discussed below. A more detailed discussion of these processes is available in NWS (2002) and Fulton (1998).

Stage I

In Stage I data the precipitation depth is estimated from an empirical formula shown in equation 2.1 (Fulton, 1998). R is the magnitude of radar reflectivity, Z is the precipitation depth. An example precipitation depth map at the stage I level is shown in Figure 2.3a. The precipitation depth is based purely on the reflectivity measurement captured by the WSR-88D radar. In tropical locations equation 2.2 is substituted for equation 2.1 as the empirical formula. These estimates are the basis for every other staged product.

$$Z=350*R^{1.4} \quad (2.1)$$

$$Z=225*R^{1.2} \quad (2.2)$$

Stage II

Stage II data enhances on Stage I data by including ground truthing. The empirically derived values are altered based with gaged precipitation estimates and radar operator judgment. In either case the estimates are altered to reflect what is believed to be more accurate precipitation depth. Figure 2.3c shows an example of stage II data for the same time period as in Figure 2.3a. The gage data used to alter this precipitation field is shown in Figure 2.3b.

Stage III and IV

Stage III and IV data are essentially the same product with different spatial domains. To create Stage III and IV data the Stage II maps are placed in a mosaic of many radar locations and the overlapping areas are averaged. Stage III data consist of all radar locations within the domain of each NWS river forecasting region. There are 13 regions across the US shown in Figure 2.4. Stage IV NEXRAD data consist of a mosaic of Stage II data covering the entire contiguous 48 states.

MPE

Like Stage III data, MPE data results from an algorithm that estimates a precipitation depth by combining several measurements including, reflectivity, gaged depths, and expert analysis. However, the MPE data includes corrections from other data sources including satellite precipitation estimates obtained through the Geostationary Operational Environmental Satellite (GOES) system and the PRISM rainfall data set in areas where coverage is affected by terrain. The MPE algorithms also include an extra step to correct local bias on a cell-to-cell basis that is not included in the staged products (NWS-MPE, 2007). The West Gulf River Forecast Center, the NWS office responsible

for flood forecasting in the study domain, began using MPE data on a provisional basis in 1999. In 2001 it adopted the MPE program as the standard precipitation estimator operational purposes (Shelton, 2008). In a study comparing the Stage III and MPE data, Wang et al. (2007) concluded that MPE is better at detecting rainfall than Stage III, MPE tends to correlate better with gage data, and that while Stage III overestimates precipitation by 20%, MPE data tends to underestimate rain gage depths by 7%.

XMRG

The XMRG format used to store the NEXRAD stage III and MPE data are binary and cumbersome to work with. Reed and Maidment (1999) and Xie et al. (2005) have worked on making the data formats more accessible to earth scientists and engineers. Each of these projects is involved with integrating NEXRAD data with GIS data. However, these efforts to this point have focused on the use of this data for surface water applications. Also, although the work makes NEXRAD data available to hydrologists for research work, the algorithms are computationally intensive and not practical for large data sets used as part of this research. For this reason custom software was written for processing this data (see Chapter 3 and Appendix A).

BARTON SPRINGS

Barton Springs is a karst spring that is located in Austin, Texas (see Figure 1.1) and is considered one of the most important landmarks in Austin. It has served as a water supply, swimming hole, and gathering locale for central Texas even before Austin existed. Development of the property into its current condition began in the early part of the 20th century. Within the last twenty years, due to environmental concerns about the

Edwards Aquifer and the rapid development of the area considered to influence flow to the springs, Barton Springs has become the subject of intense debate and scientific scrutiny. The focus has increased the availability of data for the springs and the surrounding aquifer.

Barton Springs discharges groundwater from the Edwards Aquifer. The Edwards Aquifer is a karst aquifer that roughly coincides with the Balcones Fault System in Texas (see Figure 2.5). The Edwards Aquifer is classified into three segments: San Antonio, Barton Springs, and the Northern Segment. The BSEA is the portion of the aquifer that discharges to Barton Springs. The stratigraphy of the BSEA was documented by Small et al. (1996). The BSEA is bounded vertically by the Del Rio Clay above and the uppermost member of the Glen Rose Limestone below. A schematic of the formations that make up the BSEA, including the Georgetown, Person, and Kainer formations, are illustrated in Figure 2.6. The southern boundary of the BSEA is located at a ground water divide south of Onion Creek to its northern boundary at the Colorado River. Senger (1984) determined the Mount Bonnell fault was the up dip boundary of the aquifer and the southern boundary is the bad water line to the south-east. Groundwater flow is north-northeast and discharge from the aquifer occurs along several springs along the Colorado River. Water quality in the aquifer is generally good and is the sole source of potable water for nearly 66,000 residents (BSEACD, 2007).

The zone of influence for Barton Springs is an area of current research for both the City of Austin, Texas and Barton Spring Edwards Aquifer Groundwater Conservation District (BSEACD). Dye-tracing has been a major area of focus for determining zone of influence. BSEACD (2003) outlined an extensive series of dye-tracing experiments

conducted on the BSEA. Figure 2.7 illustrates the locations where dye-tracing has been conducted and the potential pathways that are being followed by the groundwater. Twenty-two dye trace experiments have been conducted to determine flow paths and travel times of groundwater through the aquifer system. The results show a system that can transmit water over long distances in a relatively short amount of time.

JACOB'S WELL

Jacob's Well is a large spring located near Wimberley, Texas, USA. It produces water from a 30 m deep vertical cavern in Cretaceous Glen Rose Limestone. The base of the cavern is connected to conduits large enough for divers to navigate. Figure 2.8 shows the spring orifice. The spring forms the headwaters of Cypress Creek, a tributary of the Blanco River. The unique spring is a center of cultural and historical significance to the surrounding community. Mace et al. (2000), Scanlon (2001), Hanson and Small (1995), Bluntzer (1992), Ashworth (1983), and Grimshaw (1970) each studied the groundwater in Hays County near the area surrounding Jacob's Well. Hanson and Small focused on the groundwater resources in the Edwards Aquifer and Mace et al. and Bluntzer (1992) and Ashworth (1983) worked on the Trinity Aquifers from which Jacob's Well receives its recharge. Grimshaw (1970) mapped the surface geology (see Figure 2.9) and discussed how this impacts flow at Jacob's Well. A description of the geologic history, hydrogeology, groundwater use, and available data for the spring is given below.

Geologic History

The formations that make up the Trinity Aquifers (Upper, Middle, and Lower) are sedimentary beds that overly a Paleozoic igneous basement. Figure 2.10 shows the

stratigraphic column for these deposits. The Hensel Sands were deposited during a Cretaceous transgressive-regressive cycle with the Upper and Lower Glen Rose deposits forming later when a shallow sea covered the North American craton (George and others, 1952, Rose, 1972, and Bebout and Loucks, 1974).

Hydrogeology

The groundwater in the Trinity Aquifers near Jacob's well typically flows towards stream beds with groundwater divides near topographic highs. The majority (approximately 90%) of recharge for the aquifers is generally derived from local sources and infiltrates through fractures and sinkholes with a minority fraction of the recharge coming from the underlying Paleozoic formations (Bluntzer, 1992). Natural discharge from the aquifers generally occurs in springs along creek and river beds (such as Jacob's Well) and cross-formational flow into the Edwards Aquifer (Bluntzer, 1992). Grimshaw noted that flow to Jacob's well is most likely caused by the Jacob's Well Fault that occurs just downstream of Jacob's Well. According to Grimshaw, the fault acts as a flow barrier that causes the groundwater to flow out of the spring.

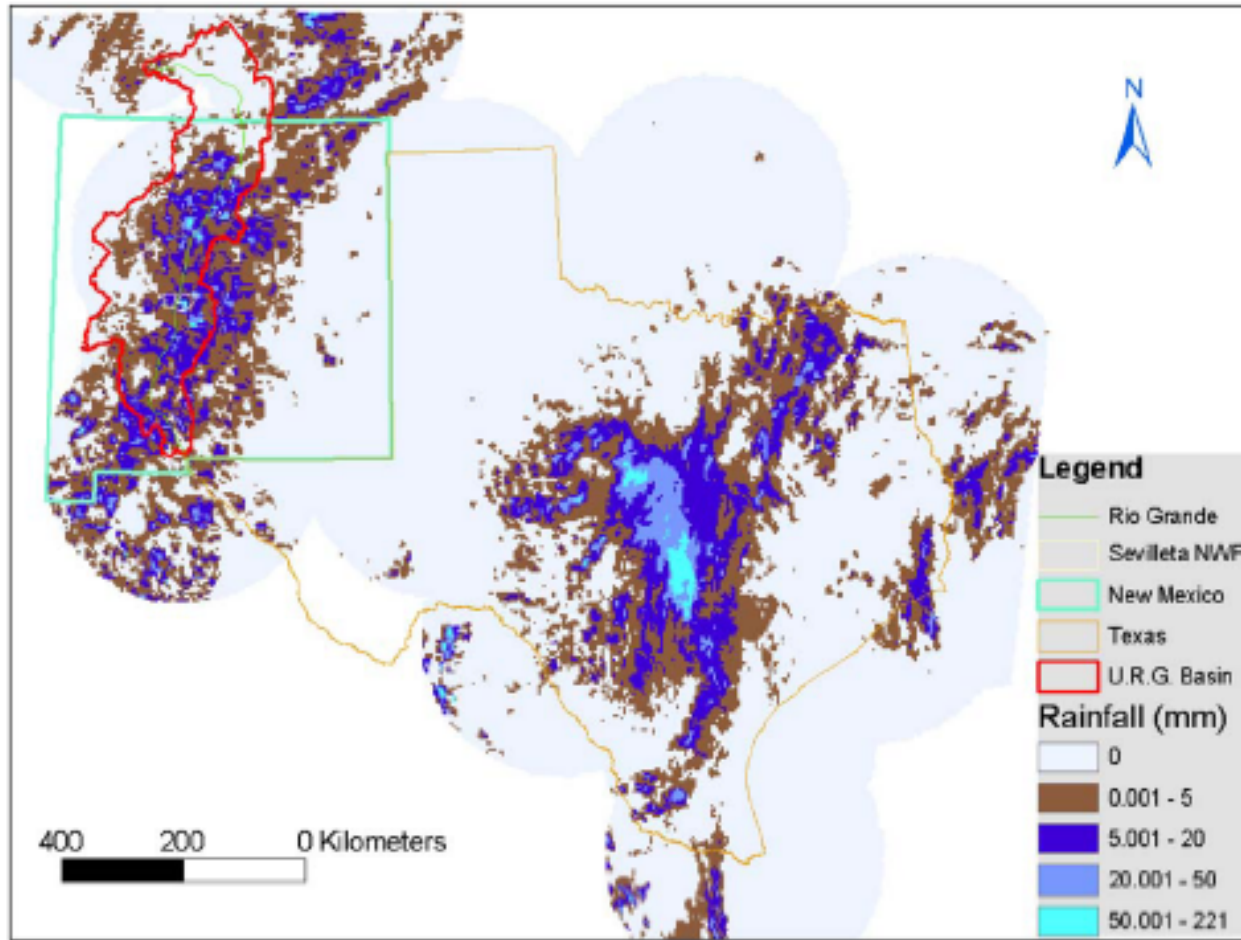
Groundwater Use

Beyond natural groundwater discharge in the Trinity Aquifers discharge also occurs due to wells. Mace (2000), Bluntzer (1992), and Ashworth (1983) report domestic and livestock pumping as the main use of groundwater within Hays County. Specifically, Mace (2000) reports that over 90% of this ground water is used for domestic purposes. Pumping use projections show that domestic use will increase in volume and as a percentage of use as population increases in Hays County into the future. Both Ashworth

(1983) and Blunzter (1992) point out that a decline in overall hydraulic head in the area has been caused by groundwater extraction through wells and that increases in pumping will cause more decline.

Available Data

Little spring discharge data were available at Jacob's Well at the start of this study. Ashworth (1983) recorded an estimate of instantaneous discharge at the spring. However, during a recent drought (pre-2005), the spring stopped flowing for the first time in recorded history (WVWA, 2007). Due to concern of the impacts local pumping and drought were having on the spring, the USGS began monitoring discharge and water quality on a continuous basis since 2005. Also, NEXRAD data are available for the entire period of record that the USGS has monitored the spring. This provided adequate data to perform a cross-correlation analysis on the spring. The results of this study are discussed in Chapter 5.



(Xie, 2005)

Figure 2.1 – Stage III NEXRAD gridded data for the West Gulf River Forecast Center.

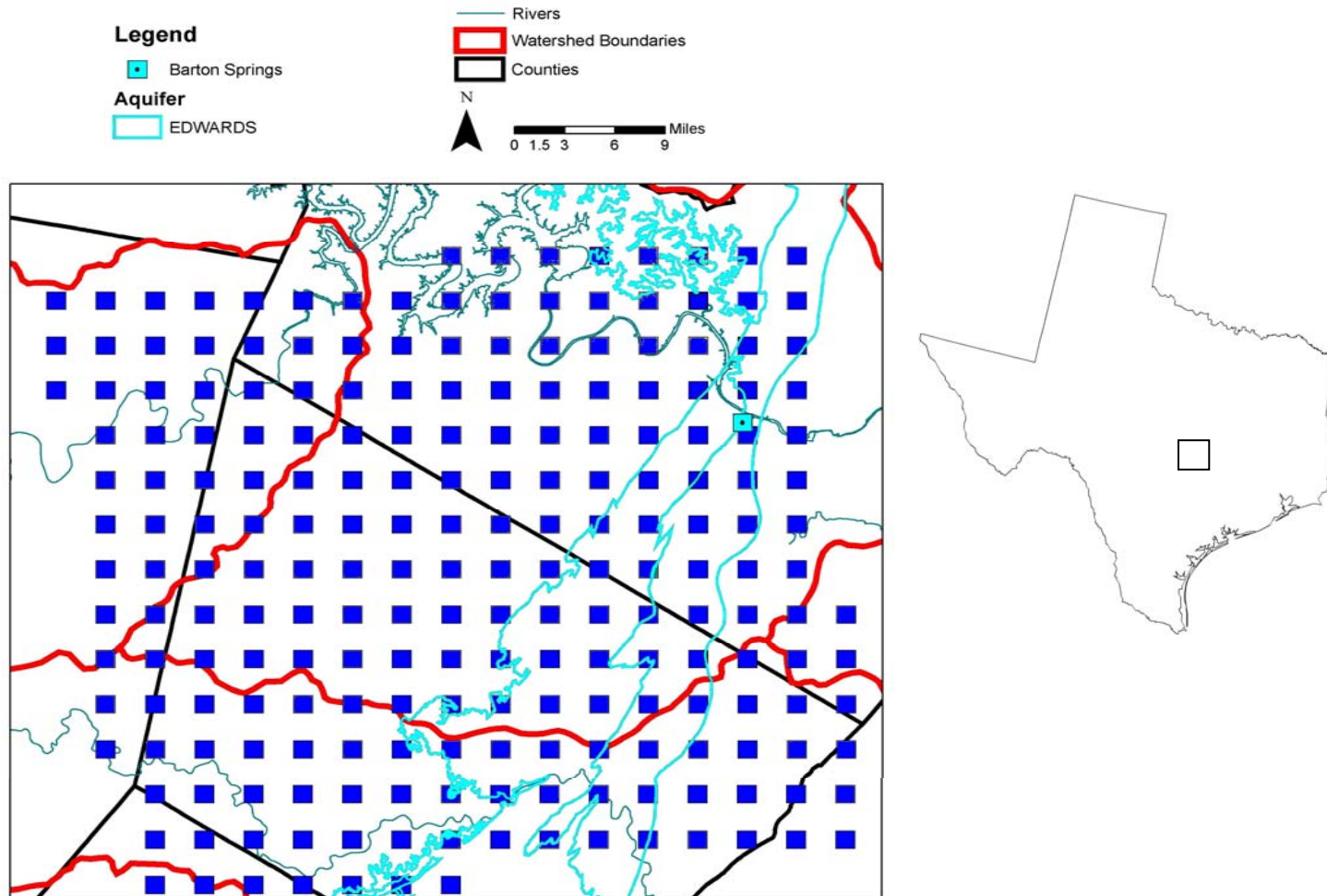
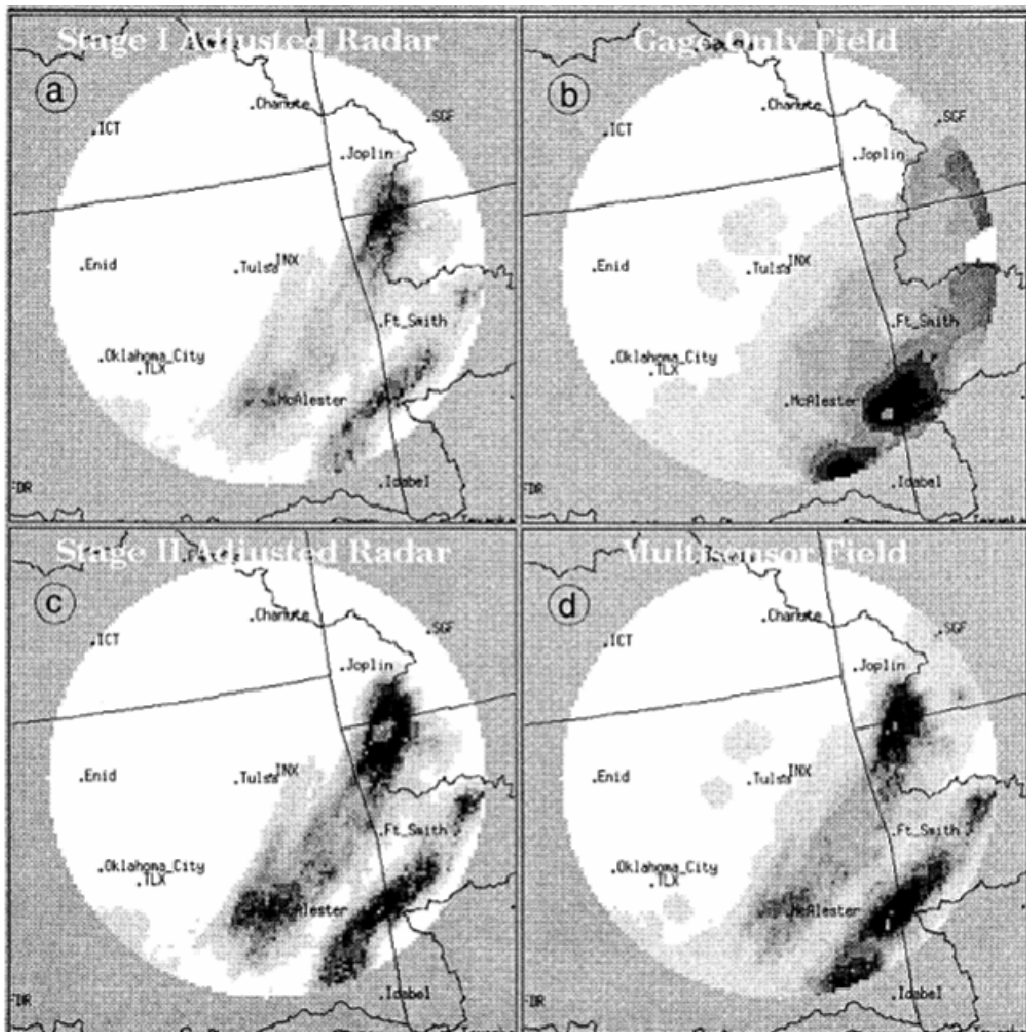
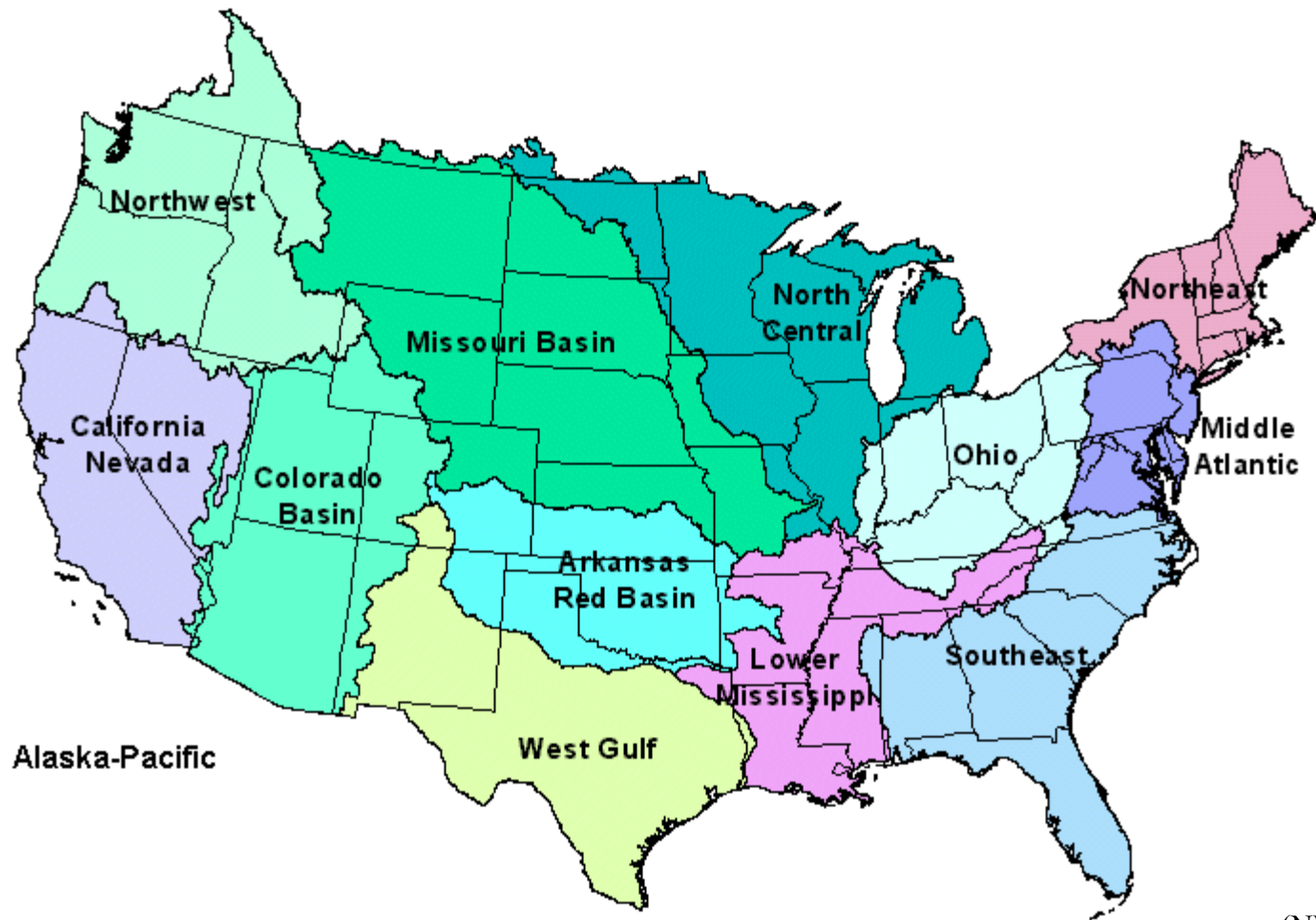


Figure 2.2 – Location of the cell centers of NEXRAD data near Barton Springs used for the cross-correlation analysis.



(Fulton, 1998)

Figure 2.3 – Example of how staged process of NEXRAD processing alters the precipitation estimate for a single radar location.



(NWS, 2007)

Figure 2.4 – NWS River Forecast Regions responsible for flood forecasting across the US.

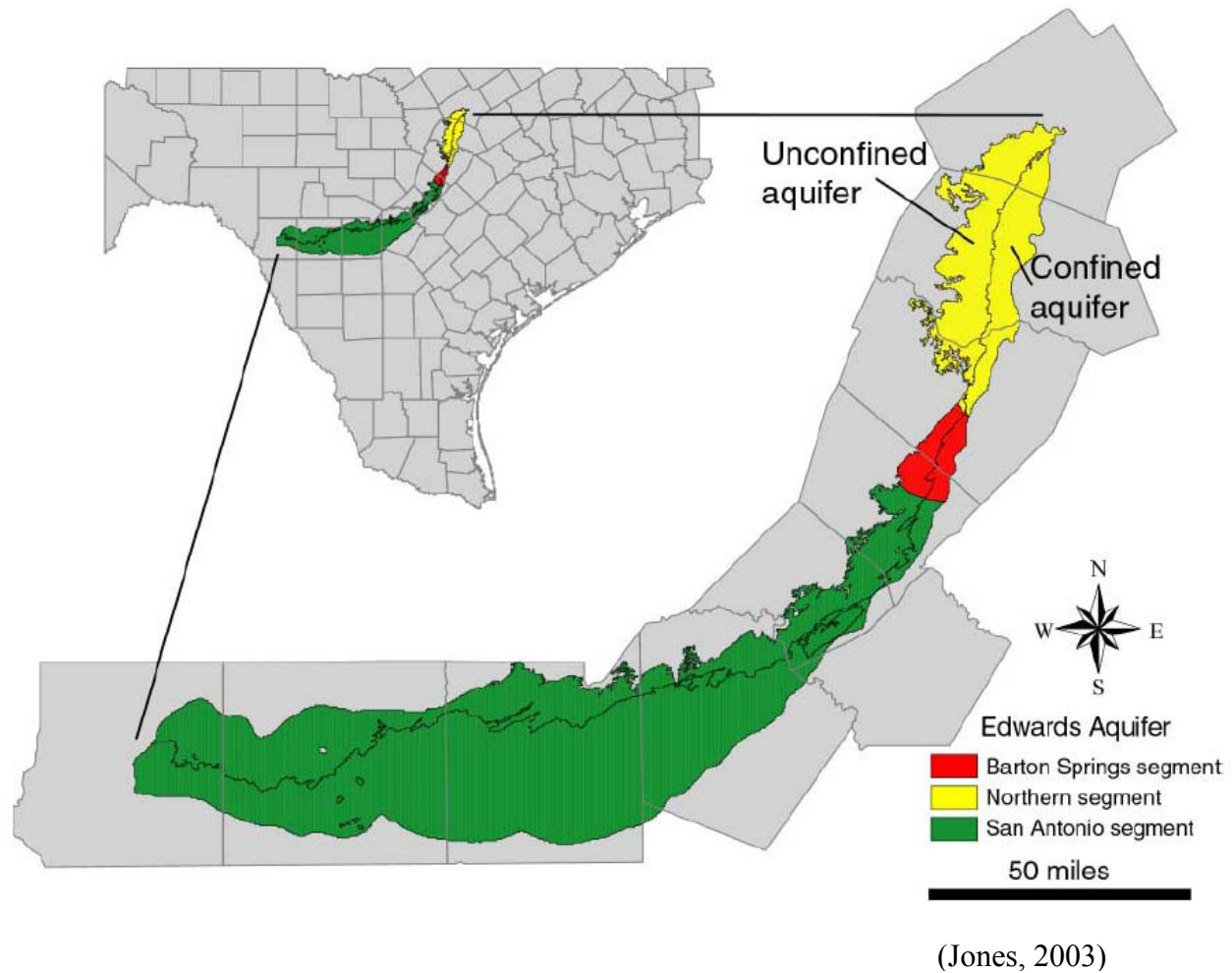


Figure 2.5 – Segments of the Edwards aquifer.

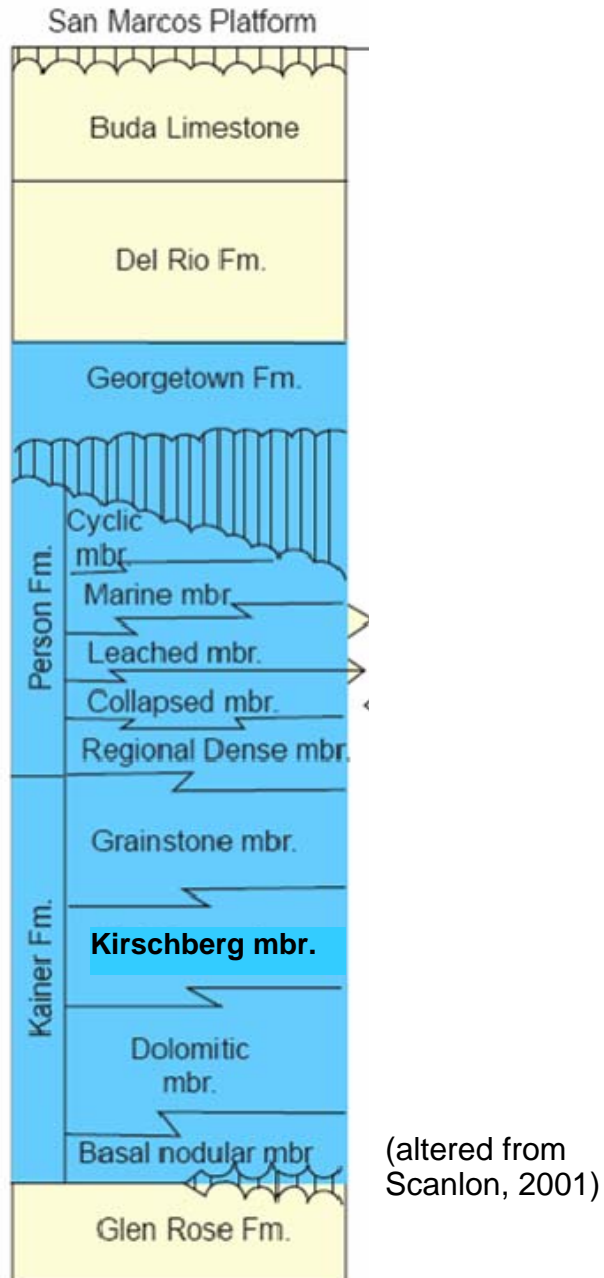
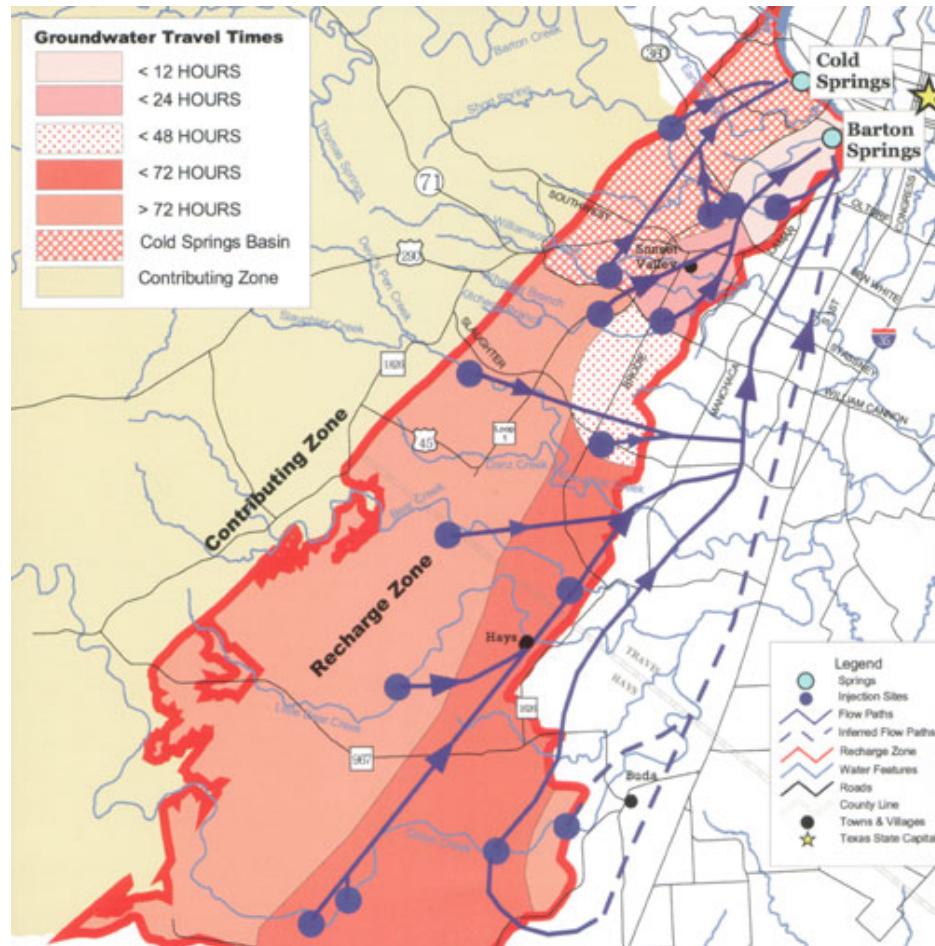


Figure 2.6 – Stratigraphic column showing major formations found in the Barton Springs portion of the Edwards Aquifer. The formations shaded in blue are part of the aquifer and the formations not shaded Represent bounding confining units both above and below (Sharp, 1990)



(BSEACD, 2003)

Figure 2.7 – Map showing locations of dye-tracing experiments carried out at BSEA showing possible pathways for recharge in the aquifer to Barton Springs.



Figure 2.8 – Jacob's Well spring discharge orifice located in the creek bed of Cypress Creek, Wimberley, Texas.

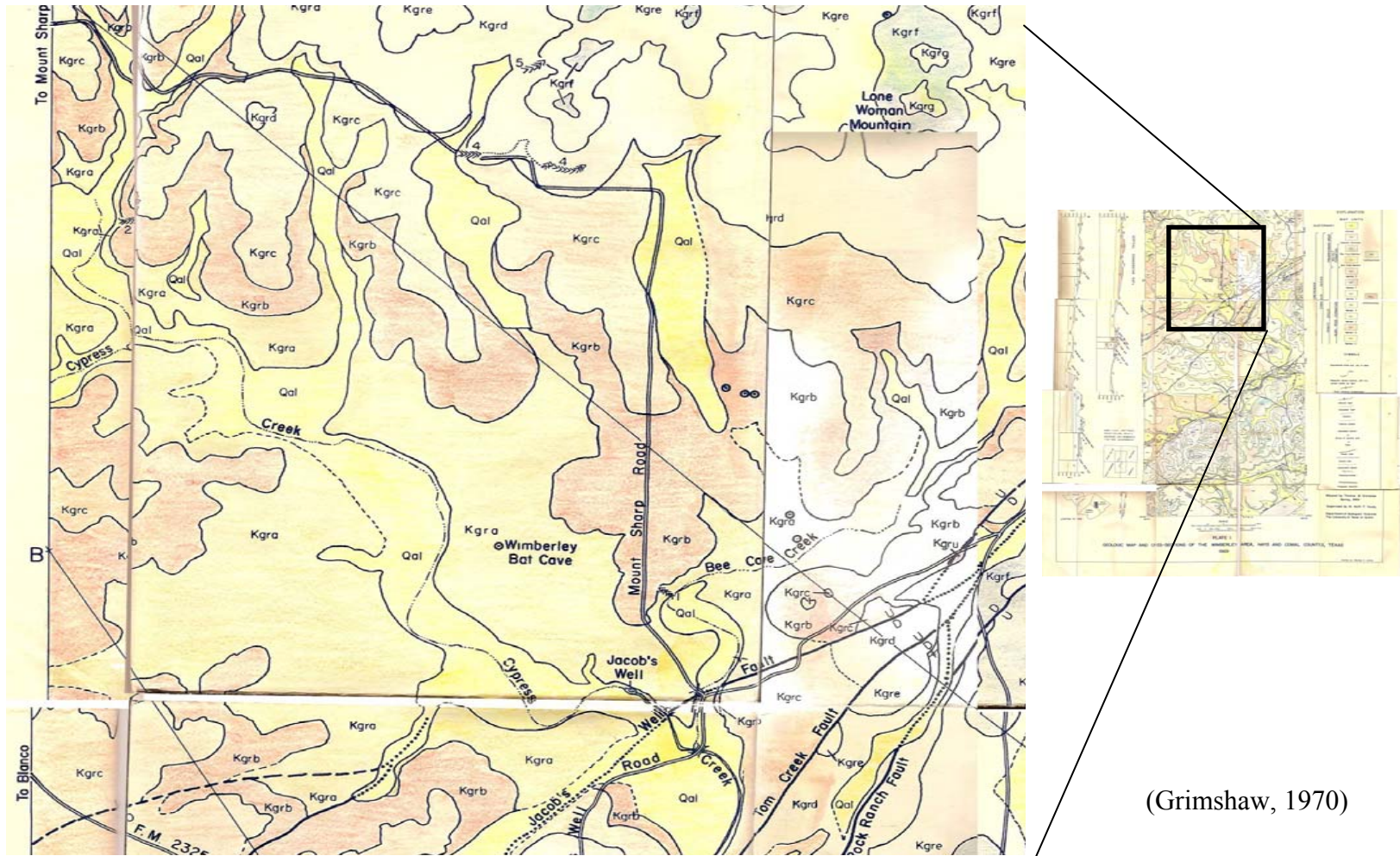
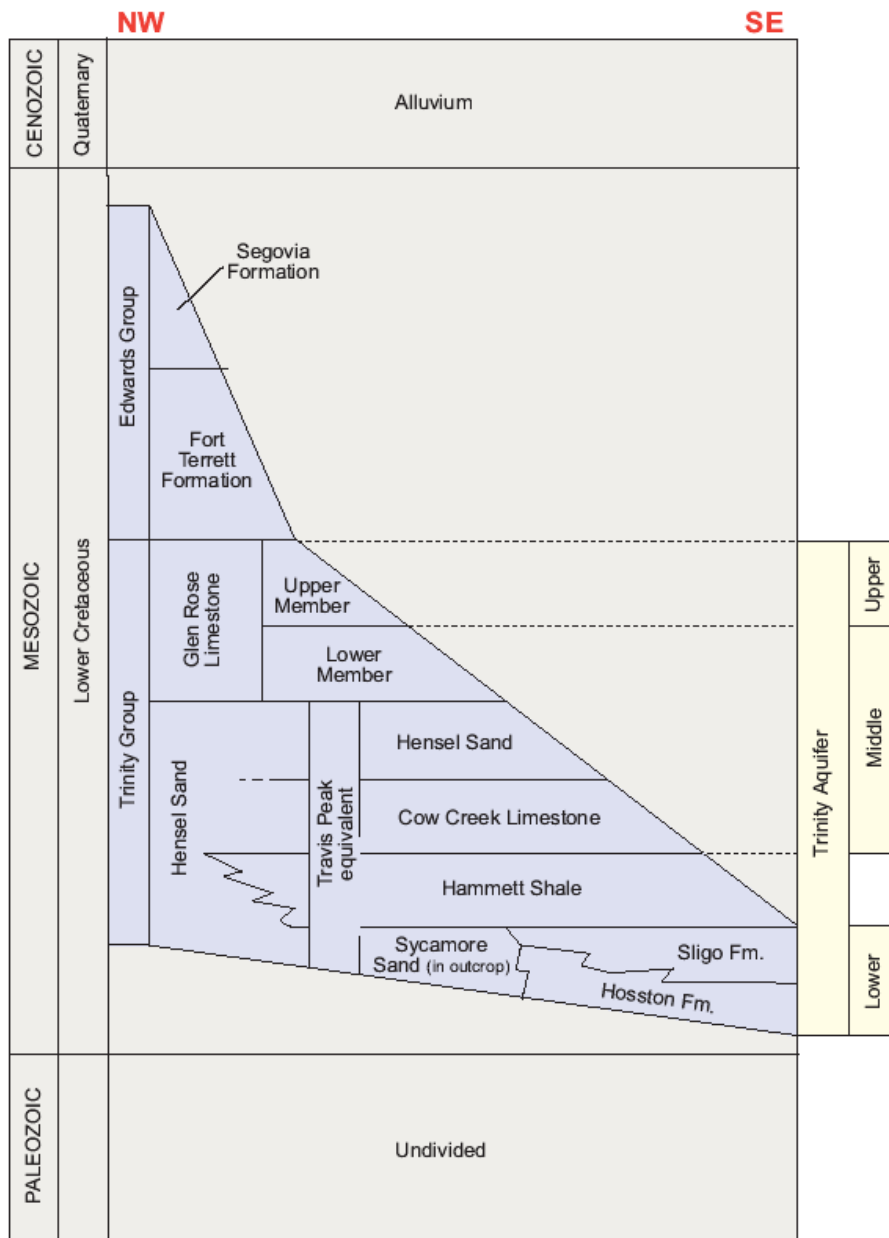


Figure 2.9 – Map of the surficial geology near Jacob's Well



(altered from Mace, 2001)

Figure 2.10 – Stratigraphic column of formations near Jacob's Well (Ashworth, 1983)

Chapter 3. Methodolgy

Padilla and Pulido-Bosch (1995), Laroque (1998), and Pangalous and Lambrakis (2006) demonstrated the usefulness of cross-correlation analysis for the characterization of karst aquifers. Laroque (1998) showed that the spatial heterogeneities typical in karst aquifers may require more than one precipitation measurement to capture these heterogeneities. This study presents the use of cross-correlation analysis coupled with spatially varying rainfall data, NEXRAD, to estimate spatial differences in recharge patterns. This chapter describes the algorithms used in carrying out this analysis including:

- calculation of the correlograms using cross-correlation equations,
- pre-processing rainfall and spring discharge data,
- running calculations with R Software (R),
- and the post-processing the results for GIS

These processes are discussed in the following sections.

CROSS-CORRELATION EQUATIONS

Cross-correlation analysis is based on the correlation coefficient. A correlation coefficient is a statistical measure of how well two variables co-vary. A correlation coefficient of 1 represents perfect match in variation of the data about a mean value. A correlation coefficient of -1 two sets of data perfectly mismatch about the mean of each data set. Cross-correlation is calculated by carrying out the calculation of the correlation

coefficient at several lag intervals (k). Equations 1 through 6 are used for these calculations. Then, these correlation coefficients are plotted versus the lag to create a correlogram (see Figure 3.1). The key aspects of the correlogram that this research utilizes are the maximum correlation coefficient and the lag distance that produces the maximum correlation. Padilla (1995) noted the maximum correlation represents the timing of the impulse response of the aquifer. Furthermore, the value of the maximum correlation is greater when the rainfall and the spring discharge time-series are more correlated and vice versa. Therefore, an increase in the magnitude of maximum correlation results from increased likelihood that the location of the NEXRAD cell is hydraulically connected to the spring.

$$r_{+k} = r_{xy}(k) = \frac{C_{xy}(k)}{\sqrt{C_x^2(0)C_y^2(0)}} \quad (1)$$

$$r_{-k} = r_{yx}(k) = \frac{C_{yx}(k)}{\sqrt{C_x^2(0)C_y^2(0)}} \quad (2)$$

where

$$C_{xy}(k) = \frac{1}{n} \sum_{t=1}^{n-k} (x_t - \bar{x})(y_{t+k} - \bar{y}) \quad (3)$$

$$C_{yx}(k) = \frac{1}{n} \sum_{t=1}^{n-k} (y_t - \bar{y})(x_{t+k} - \bar{x}) \quad (4)$$

$$C_x(0) = \frac{1}{n} \sum_{t=1}^n (x_t - \bar{x})^2 \quad (5)$$

$$C_y(0) = \frac{1}{n} \sum_{t=1}^n (y_t - \bar{y})^2 \quad (6)$$

where,

k = lag interval for each calculation of the correlation coefficient

n = The number of data in the data set

t = an integer representing the order in the location the value is value of the current data point in the data set

y_t = The value of y at the t th location in the dataset

y = The mean value of data set y

x_t = The value of x at the t th location in the dataset

x = The mean value of data set x

r_{+k} or $r_{xy}(k)$ = The correlation coefficient at negative lag k

r_{-k} or $r_{yx}(k)$ = The correlation coefficient at positive lag k

$C_{yx}(k)$ = Covariance of y with respect to x at lag k

$C_{xy}(k)$ = Covariance of x with respect to y at lag k

$C_y(0)$ = Covariance of y

$C_x(0)$ = Covariance of x

STATISTICAL SIGNIFICANCE

Similar work with spatial varying readings and cross-correlation analysis has been conducted by neuroscientists. Neuroscientists use cross-correlation analysis to estimate locations on the brain responsible for control of specific bodily functions (Wiegner et al., 1987; Zygierewicz, 2006). In the case of neuroscience the input signal is a CT scan of the brain and the output signal is some function of the body.

For instance, to verify the portion of the brain that controls smiling, a subject would smile several times while the activity of their brain was being monitored. Then the spatial patterns showing the active portion of the brain are cross-correlated with the time-series representing each smile. The maximum correlations are used to indicate what portion of the brain controls smiling. However, the possibility exists that the maximum correlation is the result of random chance. Therefore, there must be a means found to calculate whether the results are statistically significant.

Kwan (2004) described the methodology for calculating a threshold value for statistical significance of the maximum correlation in cross-correlation analysis. Figure 3.2 illustrates this methodology as it is applied to cross-correlation for precipitation and spring discharge data. Figure 3.2a shows example time series data for precipitation and spring discharge. A correlogram for these data is shown in Figure 3.2d. To determine the statistically significant threshold for these data the following steps are followed. First, the timing of precipitation events in the precipitation time series are randomized and a correlogram is computed. The maximum correlation for that correlogram is extracted and stored for future use. The process of randomizing the timing of precipitation events and extracting the maximum correlation value is repeated 99 times (see Figure 3.2b). The set of 99 maximum correlation values can be used to construct a cumulative distribution function (cdf) of maximum correlation values. The significant threshold value for the two time series data is the 99th percentile value on the cdf (see Figure 3.2c). If the maximum correlation for the non-randomized data is larger than the significance threshold, then the result is considered statistically significant

Calculating the statistically significant threshold provides a quantitative measure as to whether or not the maximum correlation values obtained from the correlograms could be based on random occurrence. The statistical significance threshold can be applied to the cross-correlation of precipitation and spring discharge to verify that our maximum correlations are not occurring by random chance.

PROCESS NEXRAD DATA

The NWS maintains a database of several years of NEXRAD data on their servers. Figure 3.3 shows the web page that allow access to these servers. The internet address of the servers is <http://dipper.nws.noaa.gov/hdsb/data/nexrad/nexrad.html>. NEXRAD data are generally available from 1994 thru 2005. However, there are periods in each year that are unavailable. Processing these data is completed in several steps. These are:

- Unzip and decompress data files
- Process hourly files
- Create a comma delimited ASCII file

Each of these steps was completed using custom computer software developed for this application. The software written for these processes is included in Appendix A of this dissertation. The steps carried out by this computer code are discussed in the following sections.

Unzip and decompress data files

The archived stage III and MPE NEXRAD data described in the previous section

are stored in UNIX compressed archive files. The compressed file format used by NWS is tape archive (tar) format. To read and process these data, the files must be unzipped and decompressed from the tar format to the xmrg format. This task proved problematic due to the large amount of space required to decompress and unzip the tar files. To alleviate the storage problem, a script was written that automatically unzipped and decompressed these files until they were fully processed. Once the precipitation estimates were extracted from the XMRG files, the files were compressed and zipped for compact storage. To complicate the process of decompressing the tar files, the filenames structure used to organize of archived stage III and MPE data have been changed from time to time. Therefore, the script included templates for several naming conventions employed by the NWS. Unzipping and decompressing these files resulted in one binary XMRG file for every hour of recorded data. Each XMRG contained raster data stored on the HRAP coordinate system discussed in Chapter 2.

Process hourly files

The NWS provides source code in the C language called “read_xmrg” (NWS, 2007) to aid in the translation of binary XMRG files to ASCII values. Each file contains the total rainfall depth estimates for a one hour period. In order to create time series, data from these hourly estimates each XMRG file was read into memory and parsed to extract values for the locations used in our analysis. The “read_xmrg” program from the NWS was expanded to aid in the processing the xmrg files. One change included adding references to the scripts discussed in the previous section for unzipping and decompressing data. Second, functionality to read all XMRG files within a range of

dates based on user selected beginning and ending date and time. Finally, an input file was created that allows the user to select a subset of the complete XMRG spatial extent to reduce the amount of data stored on the hard drive.

Create a comma delimited ASCII file

As the expanded “read_xmrg” program extracted values from individual XMRG files, the data extracted was placed in a comma delimited ASCII text file. The file includes a header containing the HRAP grid location for each cell. After the header row the file contains one row for each hour of NEXRAD data processed by these algorithms. The first column in the file contains the date and time of the XMRG file followed by each precipitation measurement for the NEXRAD cells processed.

SPRING DISCHARGE PRE-PROCESSING

Figure 3.4 shows the discharge hydrograph at Barton Springs from 1993 through 2004. The level of the flow at the springs varies on a daily basis. There is a larger pattern on a temporal scale revealing periods of relatively high discharge amounts and low discharge amounts. These time periods roughly coincide with the rainy season (months) and dry seasons (months) in the central portion of Texas (TWDB, 2007).

The effects of the large scale temporal patterns on correlograms are illustrated in Figure 3.5. The correlogram resulting from cross-correlation analysis of the unaltered discharge data indicate a matrix controlled response when compared to the conceptual models developed by Padilla and Pulido-Bosch (1995). No short-term effect is visible. However, it is still generally accepted (Hauwert, 2006) that the main mechanism of

recharge at Barton Springs is through sinkholes into caves and conduits. Also, reducing the temporal scale to a one-year period reveals the short-term response of the spring discharge hydrograph to precipitation events (see Figure 3.6). To capture only the small temporal scale fluctuations in the spring discharge hydrograph rather than the large scale patterns, a baseflow separation technique was run on the hydrograph. The United States Bureau of Reclamation Software BFI was used to remove the large-scale temporal discharge component from the Barton Springs hydrograph. By using a baseflow separation technique, the discharge hydrograph only reflects the incremental change in discharge rather than the long term change in aquifer storage. The correlogram resulting from the altered discharge hydrograph (Figure 3.5) only reflects the portion of the water that enters the aquifer and travels quickly through preferential flow paths. While this is only a percentage of the total water that discharges at the spring, it still reflects the location and mechanism of recharge in the aquifer, namely, discrete recharge locations. The percentage reflected in the larger temporal scale also enters the aquifer at these discrete locations; however, conceptually, this water is retained in storage.

TIME SERIES FORMATTING

One final step was necessary to format the data for use in cross-correlation. The time series for each individual NEXRAD cell was placed in an individual ASCII file with the spring discharge data. A script was written that read the processed NEXRAD data and the spring discharge data and created these files. This required many files and resulted in redundant information being stored on the hard drive. However, this reduced the amount of NEXRAD data that was required to be read into memory while processing.

By reducing the amount of NEXRAD data in active memory, the processing time of the correlograms was significantly decreased.

RUN CROSS-CORRELATION ANALYSIS IN R SOFTWARE

This section discusses the methods for implementing the cross-correlation algorithm using R Software. This includes pre-processing both the spring discharge and NEXRAD time-series data into a format usable by R is discussed and exporting the data into GIS for comparison with other data.

R SOFTWARE

R software (R Software, 2007) is an open-source statistical computing environment used throughout the world by both industry and academicians. Based on command line arguments and scripting routines R can be used to automate complex statistical analysis. All cross-correlation equations used in this study are built into the base R software package. R source files were generated to organize commands that carried out the analysis. Figure 3.7 shows an example R source file generated to carry out each of the R commands necessary for running the cross-correlation analysis for one NEXRAD cell including statistical significance calculations. Included in the commands are output commands for creating GIS files.

IMPORT RESULTS INTO GIS

R software package, using the R source code shown in Figure 3.7, creates comma delimited ASCII text files that can be imported by ArcGIS. These files can be used as XY Event theme layers for plotting correlogram attributes spatially along with other

geologic and hydrogeologic data. The primary purpose of plotting in GIS is to investigate the spatial nature of correlations in the basin. The main plot developed for this purpose is the maximum correlation at each NEXRAD grid center. The highest values for maximum correlation delineate the most likely locations for recharge in the aquifer. Figure 3.8 gives an example of this plot for the BSEA. Another plot similar to Figure 3.8 is created using GIS, however, it involves subtracting the statistically significant threshold correlation value from the maximum correlation. This plot illustrates those locations where the correlations are least likely to be based on the random nature of the precipitation data set. In each case a comparison between the estimates of recharge area and the cross-correlation analysis can be made by visual inspection.

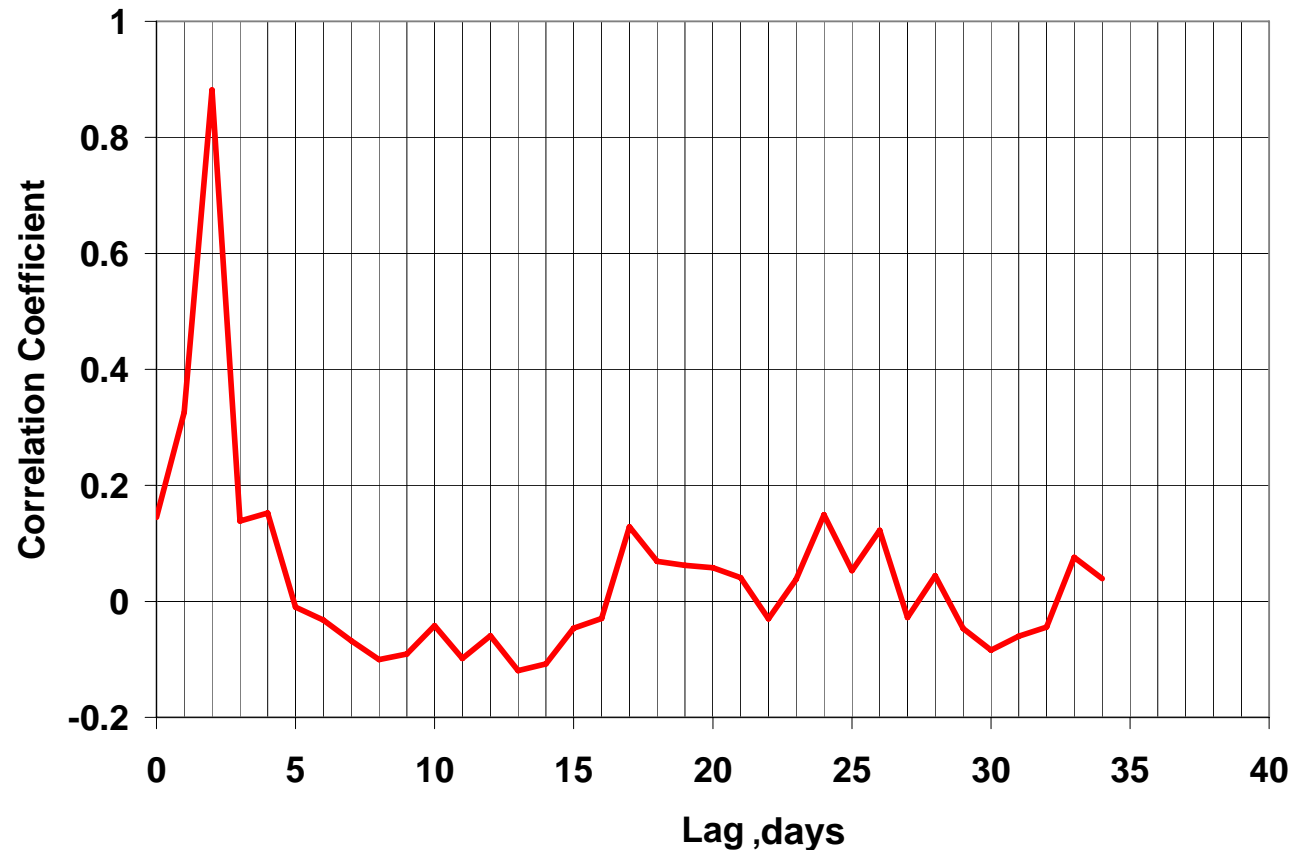


Figure 3.1 – A correlogram illustrating the maximum correlation at a lag of 2.

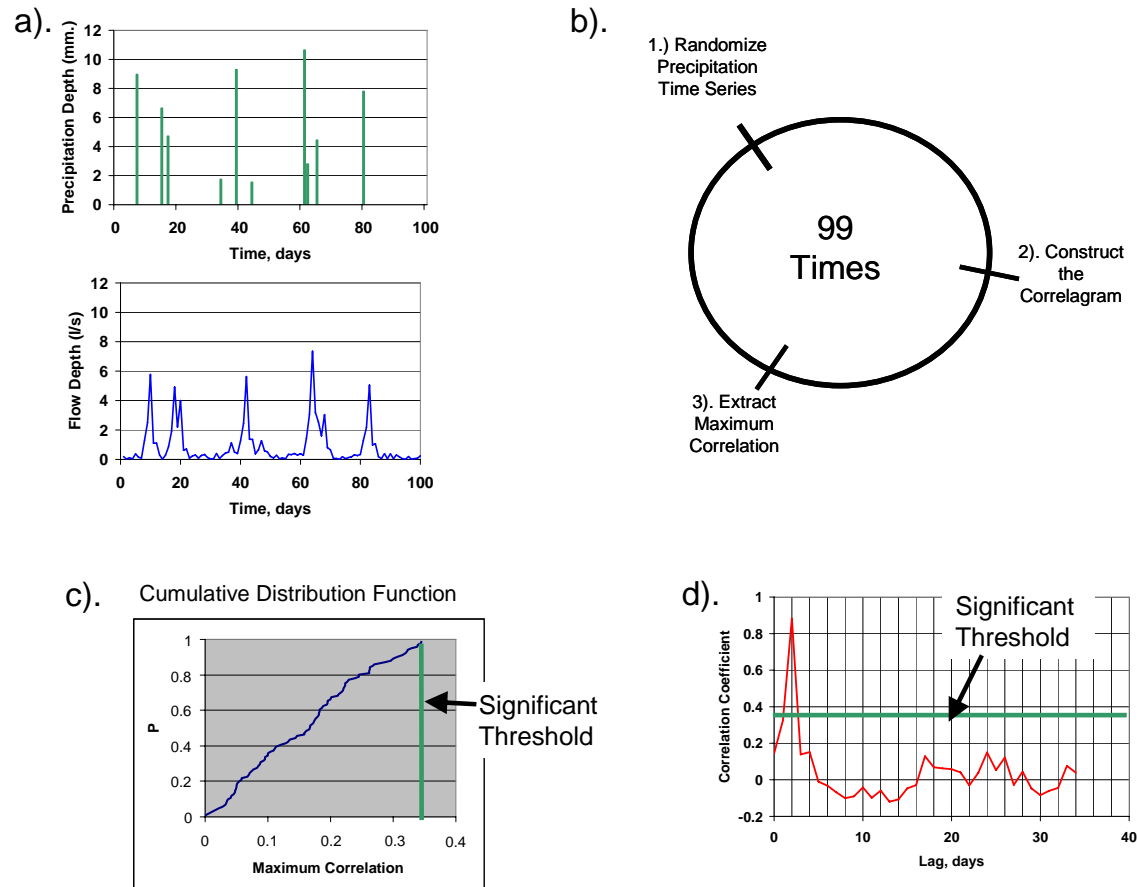


Figure 3.2 – The process for determining the maximum correlation significance threshold for two time series (shown in (a)) includes creating 99 correlagrams based on randomizing the timing of precipitation events in the precipitation time series (b). A cumulative distribution function (c) for the 99 values of maximum correlation is created to determine the significant threshold. The significant threshold can then be compared the maximum correlation (d) of the original correlagram to verify it is statistically significant.

National Weather Service - NHDS - NOAA Hydrologic Data Systems Group - Microsoft Internet Explorer provided by Compaq

File Edit View Favorites Tools Help

Back Search Favorites Media

Address http://dipper.nws.noaa.gov/hdsb/data/nexrad/nexrad.html

NOAA's National Weather Service
NOAA Hydrologic Data Systems Group

Site Map News Organization Search Enter Search Here

Special Announcement
The Office of Hydrologic Development maintains historical hydrologic data up to September 30, 2005.

Archive of River Forecast Center Operational NEXRAD Data
The Stage I, Stage III and MPE data files are collected from the RFCs on a daily basis. The daily files are constructed and archived as monthly files via the UNIX 'tar' utility.

Dates and types of Nexrad archived data are indicated in the table below.

	Stage I	Stage III	MPE
ABRFC	Oct 1995-Sep 2005	May 1993-Dec 2004	Jun 2003-Sep 2005
APRFC	Sep 1997-Sep 2005		Jul 2002-Sep 2005
CBRFC	Sep 1996-Sep 2005	Sep 1996-Mar 2002	Feb 2002-Sep 2005
CNRFC	Jan 1996-Sep 2005	Sep 1996-Jan 2005	May 2003-Sep 2005
LMRFC	Apr 1996-Sep 2005	Apr 1996-Aug 2003	Aug 2003-Sep 2005
MARFC	Oct 1995-Sep 2005	Oct 1995-Dec 2001	Oct 1999-Sep 2005
MBRFC	Nov 1995-Sep 2005	Nov 1994-Jun 2003	Jan 2003-Sep 2005
NCRFC	Sep 1995-Sep 2005	Dec 1994-Apr 2002	Feb 2002-Sep 2005
NERFC	Sep 1996-Sep 2005	Feb 1996-Aug 2002	Aug 2002-Sep 2005
NWRFC	Nov 1995-Sep 2005	Jan 1996-Nov 2002	Nov 2002-Sep 2005

Operational Data Archives
IHFS Database Tables
NEXRAD Data
NPVU Data
Flash Flood Guidance

Historical Data
Data Index

Links
Office of Hydrologic Development
Webmaster

Figure 3.3 – Website for downloading Stage III and MPE data from the NWS.

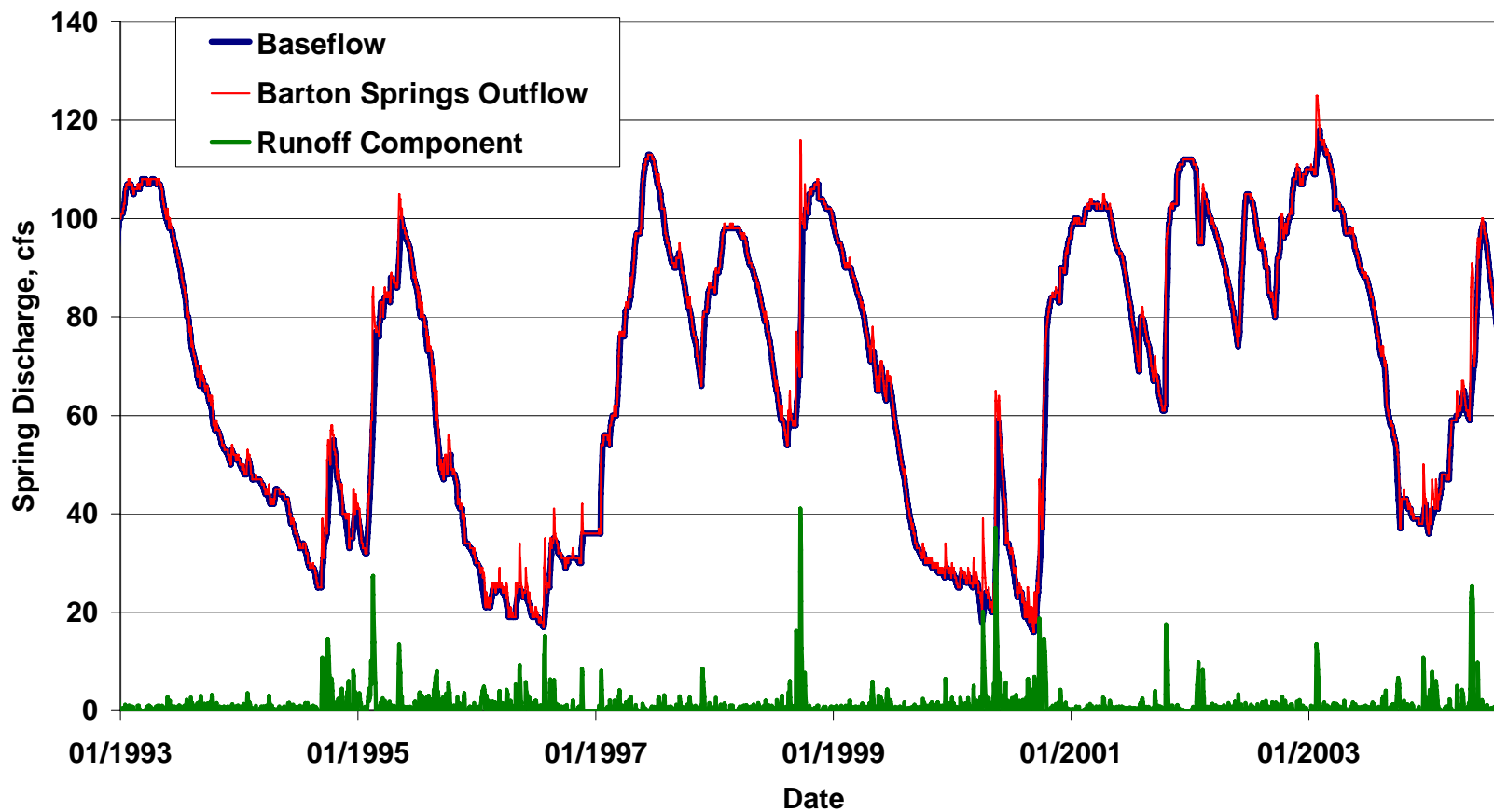


Figure 3.4 – Discharge recorded at Barton Springs from 1993 to 2004. The hydrograph is broken into components based on a baseflow hydrograph separation using the USGS software BFI.

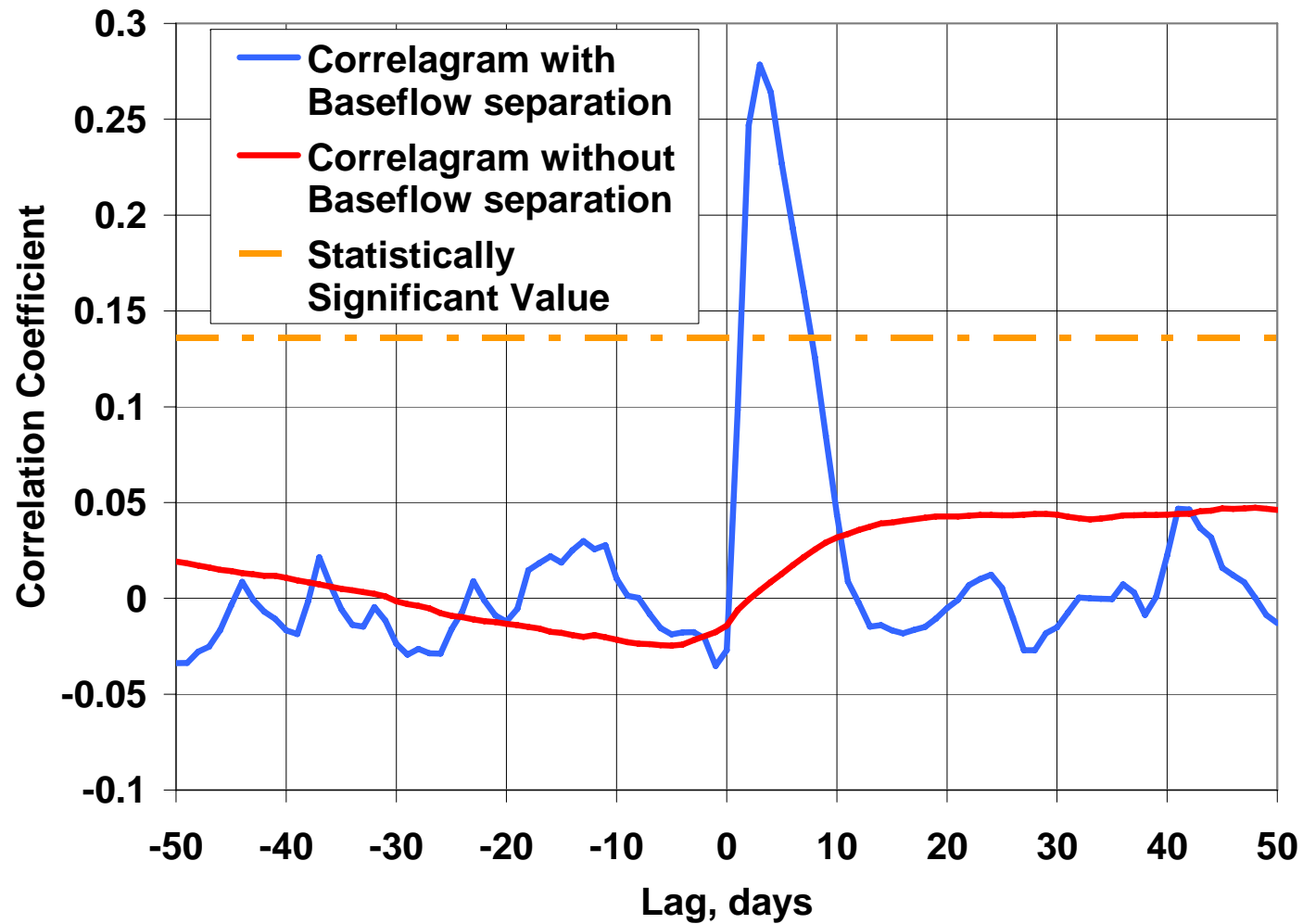


Figure 3.5 – Correlograms from a NEXRAD cell in the recharge zone of Barton Springs. The Blue Correlogram is derived using the baseflow separated discharge at Barton Springs and the red correlogram results when the baseflow is not separated. The orange dashed line is the statistically significant line.

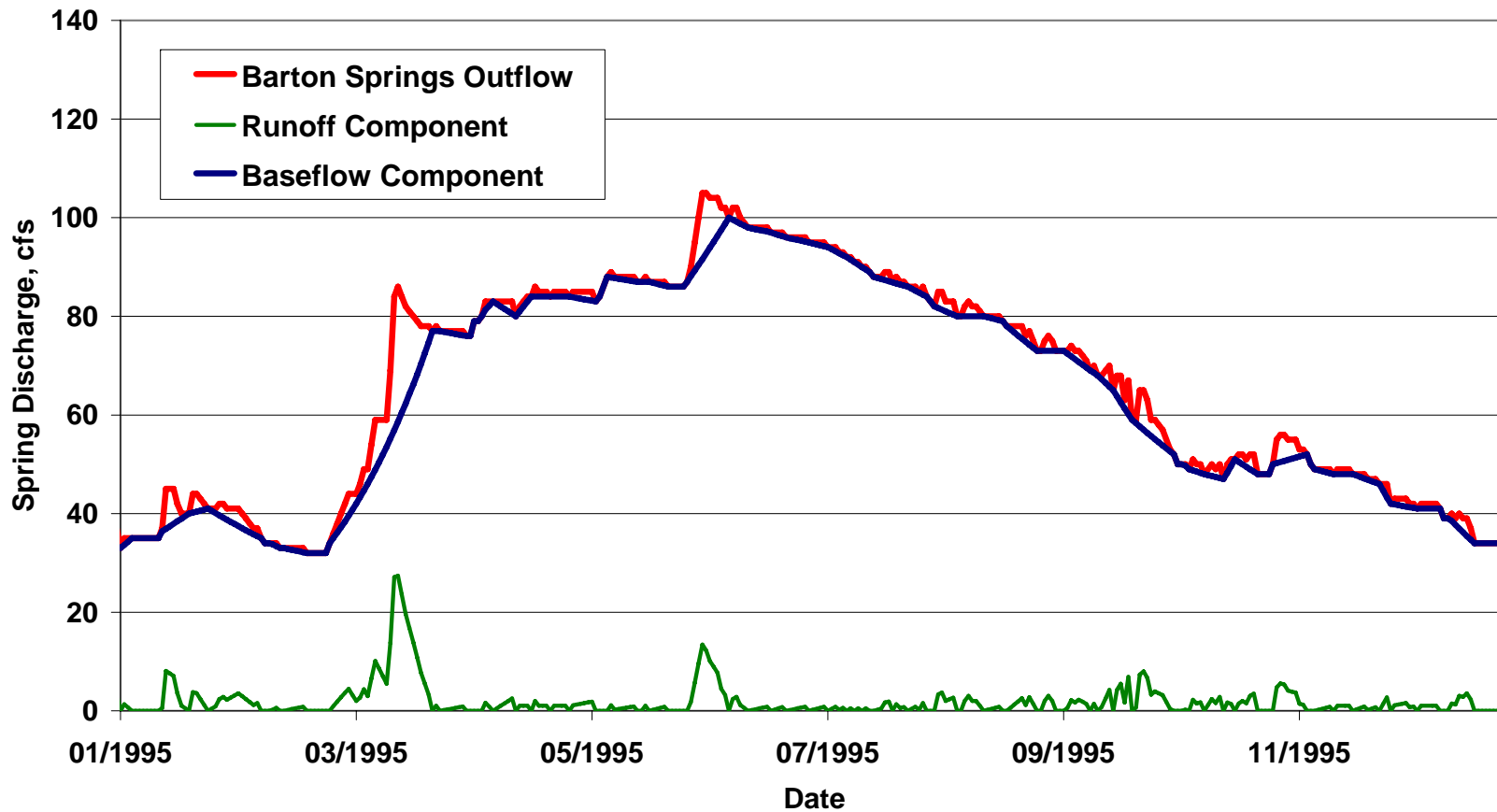


Figure 3.6 – Discharge recorded at Barton Springs for 1995. The hydrograph is broken into components based on a baseflow hydrograph separation using the USGS software BFI. The figure illustrates the detail of how the large scale temporal trend in the discharge hydrograph is removed by baseflow separation.

```
p<-read.table("daily.txt1_prp.txt")
r<-read.table("daily.txt1_flw.txt")
attach(r)
rd<-aggregate(V3,list(Day=V1),mean)
detach(r)
attach(p)
pd<-aggregate(V3,list(Day=V1),sum)
detach(p)
ld<-ccf(rd[2],pd[2],lag.max=50)
dev.print(jpeg, file="/tmp/jpgs/cell1.jpg", width=1024, height=768)
dev.off()
write.table(ld$acf,"GISOUT.txt",row.names=FALSE,col.names=FALSE,sep=" ",eol=" ",append=TRUE)
write.table(which.max(ld$acf),"GISOUT.txt",row.names=FALSE,col.names=FALSE,sep=" ",eol=" ",append=TRUE)
write.table(max(ld$acf),"GISOUT.txt",row.names=FALSE,col.names=FALSE,sep=" ",eol="\n",append=TRUE)
win.graph(width=4,height=4,pointsize=12)
```

Figure 3.7 – R source code for carrying out the cross-correlation for an individual cell of NEXRAD data

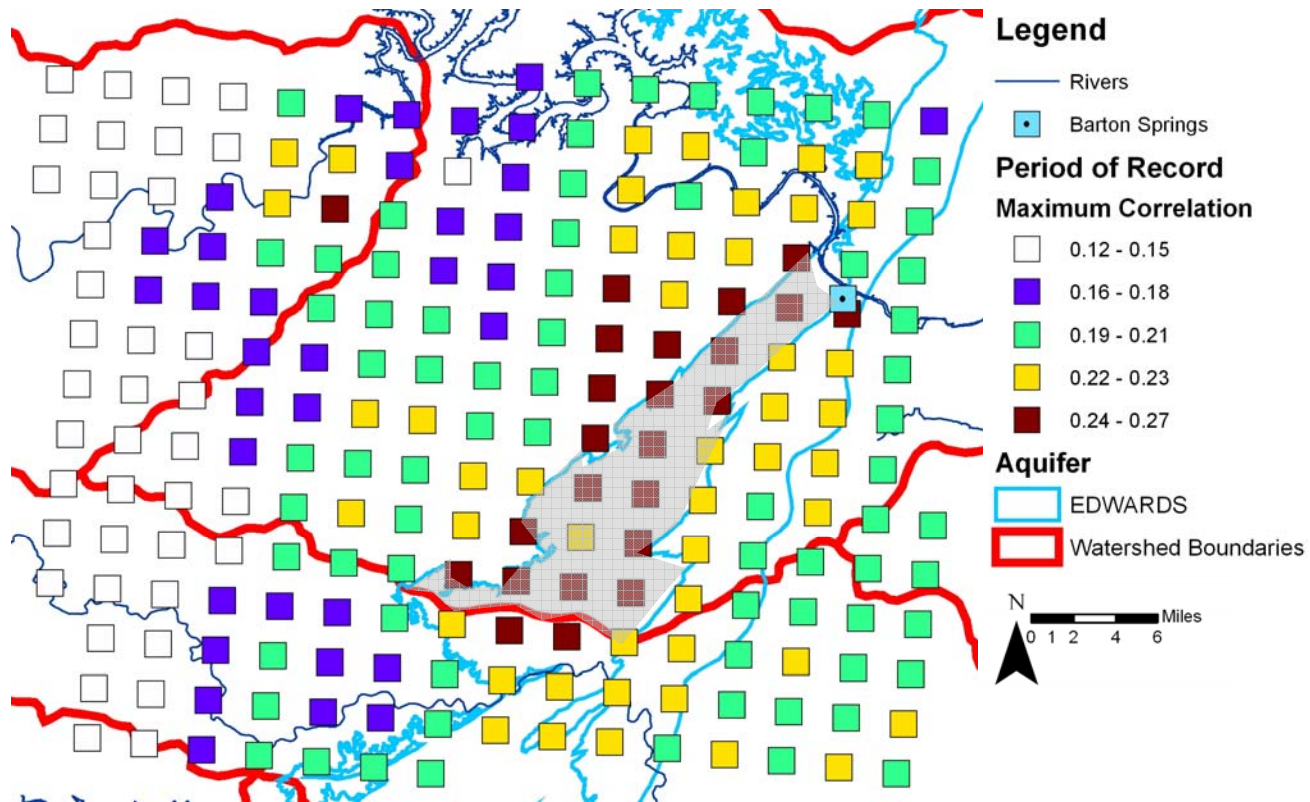


Figure 3.8 – Plot of maximum correlation values at NEXRAD grid cell locations georeferenced with other data for the area around Barton Springs. The currently delineated recharge zone is shaded in grey.

Chapter 4. Numerical Modeling

Padilla and Pulido-Bosch (1995) used three mathematical experiments to illustrate the usefulness of cross-correlation analysis in characterizing a karst aquifer. These experiments aided in illustrating correlogram response based on dominant flow type in a karst aquifer. However, the model Padilla and Pulido-Bosch was one-dimensional, and thus, could not model spatial heterogeneity. To investigate how cross-correlation analysis could aid in characterizing spatial heterogeneity (specifically, heterogeneity in aquifer recharge) a new set of numerical experiments were developed. This chapter discusses the one-dimensional numerical experiments performed by Padilla and Pulido-Bosch; introduces the new two-dimensional numerical experiments designed to introduce spatial heterogeneity into the model; and discusses the results of several numerical experiments.

ONE-DIMENSIONAL EXPERIMENTS

The numerical experiments performed by Padilla and Pulido-Bosch illustrated the correlogram response expected for different dominant flow types in a karst aquifer. This section discusses the model used for the experiment, the resulting conceptual models developed from the numerical experiments, and the limitations related to its use.

Model

Equation 4.1 gives the model used by Padilla and Pulido-Bosch (1995) to simulate conditions in a karst aquifer. Precipitation was modeled using random noise and the response of karst system to the input precipitation was modeled using a kernel function,

shown in Figure 4.1. The kernel function translated the input precipitation signal into the resulting spring discharge through convolution. The kernel functions represented a conduit flow controlled, a matrix flow controlled, and a mixed flow systems. Figure 4.1 shows the kernel function representing the conduit flow transferred the entire precipitation volume to the spring discharge flow within three days. In the case of the matrix flow kernel function shown in figure 4.2, the precipitation volume was spread over a period of 45 days simulating the longer flowpath in a matrix controlled aquifer. The mixed kernel function, shown in figure 4.3, combines the characteristics of both systems, an initial sharp peak with slower discharge over time.

$$Q_t = E_t + \sum_{j=0}^n P_{t-j} \lambda_j \quad (4.1)$$

where, E_t = random variable of the same variance as P
 P_{t-j} = rainfall on the day t-j
 λ_j = are the kernel-function coefficients

Results

The hydrographs for each of the kernel functions and the resulting correlograms are shown in Figures 4.1 thru 4.3 for the conduit, matrix, and mixed systems respectively. These characteristic shapes of correlograms are the basis for classifying karst systems with this method. The correlogram of the simulated karst system dominated by conduit flow has a sharp peak followed by a tailing off of the correlation as the lag interval increases. The correlogram of the simulated karst system dominated by matrix flow results in a correlogram with a smooth rise to a lower peak than in the conduit controlled system, followed by smooth decrease in the correlation coefficient as the lag interval

increases. The mixed system has characteristics of both of the end members, an initial sharp peak followed by a slow decrease of correlation as lag increases.

Limitations of One-Dimensional Experiments

These mathematical experiments are simple in that they are one-dimensional analytical experiments. Therefore, they do not have the ability to investigate the effects of heterogeneity over the domain of a single karst system on the cross-correlation results. Using spatially varying precipitation from NEXRAD data where each precipitation measurement acts as a unique precipitation gage, the resulting correlograms may identify aquifer heterogeneities that cannot be discerned with only one precipitation input time-series. To test whether spatially varying maps of precipitation can be used to classify heterogeneities throughout a karst aquifer is viable, a new mathematical experiment was developed. MODFLOW was used to simulate the aquifer system and actual precipitation measurements from NEXRAD data were used to develop model input time series. The development of these experiments is discussed below.

TWO-DIMENSIONAL EXPERIMENTS

A set of experiments were designed to evaluate the effectiveness of cross-correlation analysis in determining spatial heterogeneities in karst aquifers. Specifically, the experiments evaluated whether or not differences in flowpaths can be inferred from correlograms of multiple precipitation gages versus spring discharge hydrographs. This section discusses the selection of an appropriate numerical simulator, the model construction and parameters for the various experiments, and the results from these experiments.

Selection of a Model

One method of modeling karst aquifers is the use of equivalent porous media models. This type of modeling is based developing a hydraulic conductivity (K) value for a fracture system that is equivalent to the K of a porous medium. An example of how to develop this value is to use the cubic law for modeling flow through discrete fractures. The equivalent hydraulic conductivity is based on the size of the fracture aperture.

After developing equivalent porous media values some types of analysis of the aquifer can be completed using Darcy's Law calculations. MODFLOW (Harbaugh, 1988) is a 3D finite-difference program that computes the flow of groundwater through porous media. This is accomplished by creating a representation of the subsurface with a cell-centered grid and assigning porous media properties to those grid cells. A finite-difference solution is developed using numerical solvers to estimate hydraulic head levels and fluxes through the simulated aquifer and boundary conditions.

Numerical modeling of karst aquifers using MODFLOW is generally accepted for regional modeling of water budgets. Scanlon et al. (2004), Froukh (2002) and Dufresne (1999) investigated the ability of MODFLOW to simulate spring discharge and reproduce head gradients across the BSEA, the Eastern Groundwater Basin in the West Bank (Israel), and the Floridan aquifer near Lake City, Florida, respectively. Each concluded the models were sufficient for spring discharge and head reproduction. However, Dufresne noted that the model is not well suited for modeling contaminant transport due to lack of discretization along fracture and conduits within the karst. Painter (2004) further investigated the ability of MODFLOW to model karst systems. He concluded that

classical MODFLOW needed additional functionality to estimate both heads in conduits and heads in the matrix simultaneously. While this apparent weakness in using MODFLOW is evident, the use of equivalent porous media is still acceptable for some problems. As is the case with Scanlon (2004) and Dufresne (1999) the purpose of this modeling is to look at spatial varying aquifer properties and their impact on spring discharge. Scanlon (2004) specifically noted that the use of MODFLOW produce reasonable results for modeling spring discharge from a karst aquifer. Therefore, MODFLOW was used as our numerical simulator. However, if this study were investigating contaminant transport levels or trying to estimate differences in the head in matrix flow versus conduit flow, standard MODFLOW may not be an acceptable modeling tool.

Model Construction and Parameters

In order to implement the conceptual framework for the different karst systems into a numerical groundwater model, the program MODFLOW was selected based on its ability to include each of the portions of the conceptual model and allow these properties to vary spatially. The MODFLOW grid consisted of 100 grid cells by 100 grid cells. Figure 4.4 shows a plan view map of the model domain with the associated boundary conditions. Each simulation had 1 year simulation time using either daily or hourly stress periods. Numerical experiments were conducted as sensitivity analyses rather than a single simulation with the exception of the experiment utilizing the equivalent K values taken from Halihan (2000). Sensitivity analyses were used to minimize the chance of missing important relationships that could possibly affect the results.

Aquifer Properties

The model is single layer defined as a confined/unconfined (laycon=3) layer. This required the definition of the hydraulic conductivity, specific storage, specific yield, and top and bottom elevations for each grid cell. Table 4.1 gives a summary of the values used for each of the numerical experiments conducted as part of this study. The top and bottom elevations and the specific yield remain constant throughout the experiments while the hydraulic conductivity and storativity were allowed to vary. Hence they are represented by ranges rather than absolute values in the table. By adjusting these aquifer properties each of the different conceptual models for the karst system were modeled.

Table 4.1 – Modeled aquifer properties for each simulation in

Aquifer Property	Units	Varied	Minimum	Maximum
Top Elevation	m	No	100	N/A
Bottom Elevation	m	No	0	N/A
Specific Yield	-	No	0.15	N/A
K (without conduit)	m/s	Yes	1.15E-05	5.7E-03
K (with conduit)	m/s	Yes	5.7E-03	1.15E-1
Storativity (without conduit)	m/m	No	1.00E-04	1.00E-02

Spring Discharge

In the southern portion of the model there is a single discharge location modeled using the Drain Package in MODFLOW. This model boundary condition represents a spring in

the aquifer. The drain package was selected to exclude the possibility of the boundary condition becoming a source of water. The drain was set to a constant elevation of 5 m with a conductance of 10,000 m/day. The conductance was high to allow water to flow out of the model without much head loss through the drain boundary condition.

Recharge

A uniform recharge rate is defined for the entire model domain to represent diffuse recharge into the aquifer. Additionally, the Well Package (Harbaugh, 1988) is used to simulate discrete recharge locations in the aquifer in two locations A and B. The wells were assigned a positive flux value to signify injection into the aquifer.

The time series data used for model inputs of precipitation data are shown in Figure 4.5. The time series were extracted from NEXRAD data near the Barton Springs portion of the Edwards Aquifer contributing zones. Each time series is the precipitation estimate of one cell of the Stage III NEXRAD data available from the National Weather Service. The cells were selected at random and processed to develop two input hyetographs for modeling purposes. Figure 4.6 shows the location of the NEXRAD cells selected as well A and B. The input precipitation time series data are similar to one another temporally. However, they vary slightly in terms of magnitude. Furthermore, the flux does not equal the precipitation volume taken from the NEXRAD time series. It is assumed the entire precipitation depth does not enter the groundwater system. Therefore, only a 32 percent of the precipitation volume was input into the Well Package as a flux. This is consistent with other studies converting precipitation to groundwater recharge totals in Texas(TWDB,2000).

The NEXRAD data has a temporal resolution of 1-hour time steps. For model simulations where a daily stress period was used the hourly data were summed for each day to create a daily time series.

Discussion of results

Several combinations of aquifer properties and boundary conditions were used to test the different conceptual models discussed above. Also, these combinations of aquifer properties are used to test whether heterogeneity of aquifer properties can be inferred from spatial cross-correlation analysis. The following is a list of the experiments that were conducted:

- Verification of Typical Responses
- Homogenous K field - Two Precipitation Inputs
- Conduit K Field - One Precipitation Input
- Conduit K Field - Two Precipitation Inputs
- Barton Springs K Ranges - Two Precipitation Inputs

Each of these numerical experiments and its results are discussed in the following sections.

Verification of Typical Responses

Experiment Description - The first step in conducting the numerical experiments was to reproduce the results of Padilla and Pulido-Bosch. In this case the hydraulic conductivity

and specific storage were homogenous throughout the entire model domain. High conductivity values and low storage numbers should produce correlograms that resemble the correlograms produced by Padilla and Pulido-Bosch for the conduit flow dominated karst system. As the conductivity decreases and the storage increases, the flux from the precipitation events should be increasingly muted resulting in the correlogram that resembles the correlogram of the matrix dominated karst system. This experiment is designed to show the ability of MODFLOW to simulate each of these conditions effectively.

Results - A set of correlograms is shown in Figure 4.7. The response curves range from showing a conduit-flow dominated system to a matrix-flow dominated system. The experiment is successful in showing that depending on the hydraulic conductivity used for the experiment, MODFLOW can reproduce the results of the Padilla and Pulido-Bosch experiments. However, MODFLOW gives us a more robust simulator of aquifer dynamics including the ability to alter hydraulic conductivity and storage values spatially throughout the aquifer and simulate the interaction of matrix and conduit domains.

Homogenous K field - Two Precipitation Inputs

Experiment Description - In this modeling scenario there are two precipitation input locations with only a single discharge location near the southern portion of the domain. This expands the previous modeling scenario to test whether cross-correlation analysis results differ between the two separate precipitation time series when only one discharge location exists in the model. One precipitation time series was placed in the location of

Well A and the second in the location of Well B and the resulting simulated discharge was used for calculating the correlogram with respect to each well location.

Result – Figure 4.8 shows the correlograms for Well A and Well B, respectively, when used with the discharge time series at the southern drain. Based on the location of the wells that were used the correlograms showed only slightly different characteristics. The change in distance should have been more distinct because of the travel times. There is not a great deal of difference in the lag to the maximum correlation for each of Well A and B. This was attributed to the similarity in of the input precipitation of the time series and the homogenous aquifer properties. There is not enough difference in these parameters to result in major differences in the correlograms.

Conduit K Field - One Precipitation Input

Experiment Description - This experiment involved using the same precipitation time series while altering the K field to resemble a double porosity scenario. Figure 4.4b shows the K field for the MODFLOW simulation for this simulation. Instead of having a homogenous K field there is a line of connected cells from the southern discharge location to Well A. These model cells were assigned a relatively higher hydraulic conductivity than the surrounding cells. The line of highly conductive MODFLOW cells represents a conduit flow path for the flux from Well A. Depending on the contrast in K and Storage between the two zones the response correlograms should differ.

Results - The correlograms shown in Figure 4.9 show similar response to the homogenous K experiments correlograms shown in Figure 4.7. However, in the maximum correlation

of the mixed system curve for Figure 4.9 is larger than the maximum correlation shown for the mixed system in Figure 4.7. This demonstrates the ability of the cross-correlation analysis to illustrate the differences in the modeled aquifer properties. Specifically, when the MODFLOW aquifer properties were designed to represent conduit flow, the correlogram showed the corresponding differences. In Figure 4.9, the correlogram results from a simulated aquifer with less diffusivity into the matrix portion of the model. Therefore, the simulated flow is concentrated into the conduit portion of the model and reaches the simulated spring discharge location more rapidly.

Conduit K Field - Two Precipitation Inputs

Experiment Description - In this experiment two separate conduit K flowpaths were added to the MODFLOW simulation. These flowpaths were modeled using relatively high hydraulic conductivity values with respect to the surrounding cells. Figure 4.4b shows the locations of these flow paths. The flow path for Well A is a much shorter distance from the southern discharge location than is the flow path at Well B. Separate precipitation time series were input at the locations of Well A and Well B. Both the difference in the flow path length and the differences in the precipitation time series should cause variations in the resulting correlograms.

Results - Figure 4.10 shows the correlogram for wells A and B for three separate K realizations. In each instance the maximum correlation for well B occurs at a lag greater than for well A. This is due to the longer flow path constructed into the hydraulic conductivity field for the MODFLOW simulation. These results indicate that given similar precipitation time series the correlogram of each time series to a single discharge

point will show effects of the flow path that the water travels through. The only difference between the modeling simulations shown in Figure 4.8 and 4.10 is the construction of the modeled hydraulic conductivity field. In Figure 4.10, the heterogenous K field results in a larger separation in the lag time to the maximum correlation than the correlograms shown in Figure 4.8. This result supports the concept that using the field data for a karst spring and separate rainfall measurements, the differences in flow path can be inferred by cross-correlation analysis. By developing these relationships over a region, a map of areas with similar properties may be developed.

Barton Springs K Field - Two Precipitation Inputs

Experiment Description - As discussed in Chapter 2, the BSEA is a karstic aquifer with a major discharge point in Barton Springs. Investigating the usefulness of spatial cross-correlation analysis of karst aquifers yielded encouraging results in the initial numerical experiments described in this paper. Therefore, one final numerical experiment was completed to investigate the usefulness of these methods for the BSEA. Halihan (2000) studied the equivalent porous media values for the BSEA. His work developed a set of equations that could be used for this area to develop hydraulic conductivity values that could be used to model the BSEA. As part of this work, historic values of K throughout the BSEA were compiled and mean values of K were developed for the conduits, fractures, and matrix of the BSEA. Using equations developed by Halihan (2000) equations for conduit K and non-conduit K and mean permeability values for conduits, fractures and matrix portions of the aquifer, the values of equivalent K (Table 4.2) were

estimated. Values used in regional models developed by Klemt (1979), Maclay and Land (1988), and Thorkildsen and McElhaney (1992) were 1473 m/day, 4726 m/day, and 711 m/day respectively. The values developed from Halihan (2000) fit nicely within this range.

The values for K that the Halihan equations estimated were input into the model for the conduit and non-conduit flow paths in the MODFLOW model. This modeling scenario is not intended to be a model of flow at Barton Springs. No attempt to calibrate the spring discharge to historic discharge was conducted. Using the range of K values typical for the BSEA was used to evaluate what to expect from applying cross-correlation to the field site.

Results - Running the model and completing the cross-correlation analysis on a daily time step resulted in the correlogram seen in Figure 4.11. The results are not physically consistent with the system because the highest correlation for both Well A and Well B occur at a negative lag time. This occurred because the daily time step is too long and allows aliasing of the signal. Therefore, the model simulations were completed a second time using an hourly time step. Figure 4.12 shows the correlograms for the hourly time step simulation. The maximum correlation for Well A occurs in hour 17 while the maximum correlation for Well B occurs in hour 20. This difference in correlation magnitude and time is consistent with the spatial location for both Well A and B (i.e. Well A is closer to the drain cell than Well B). However, the difference in time is on the magnitude of hours rather than days as in other simulations. This suggests that field experiments should lead to differences in correlation magnitudes and lags. Therefore, the

field analysis may need to be completed on an hourly time step rather than a daily time step to yield these results.

Table 4.2 -Equivalent Hyrdraulic Conductivity estimates for the BSEA based on Halihan (2000).

Model Cell	m/d	m/hr	m/s
Equivalent K (with conduit)	1.174E+03	4.89E+01	1.359E-02
Equivalent K (non-conduit)	2.055E-01	8.562E-03	2.378E-06

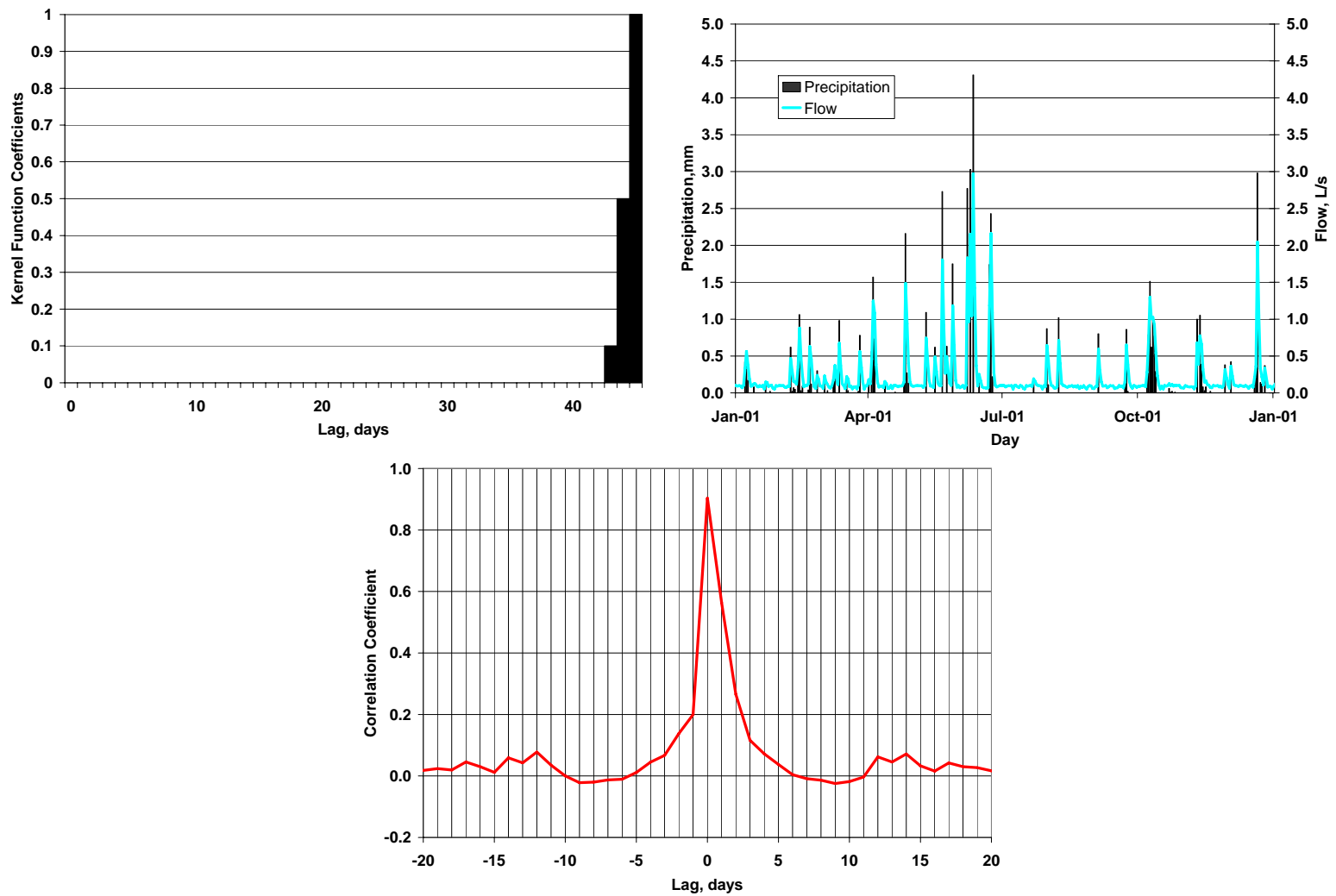


Figure 4.1 – Kernel function, precipitation and flow hydrograph, and corresponding correlogram used to model flow in a karst aquifer for conduit-controlled system.

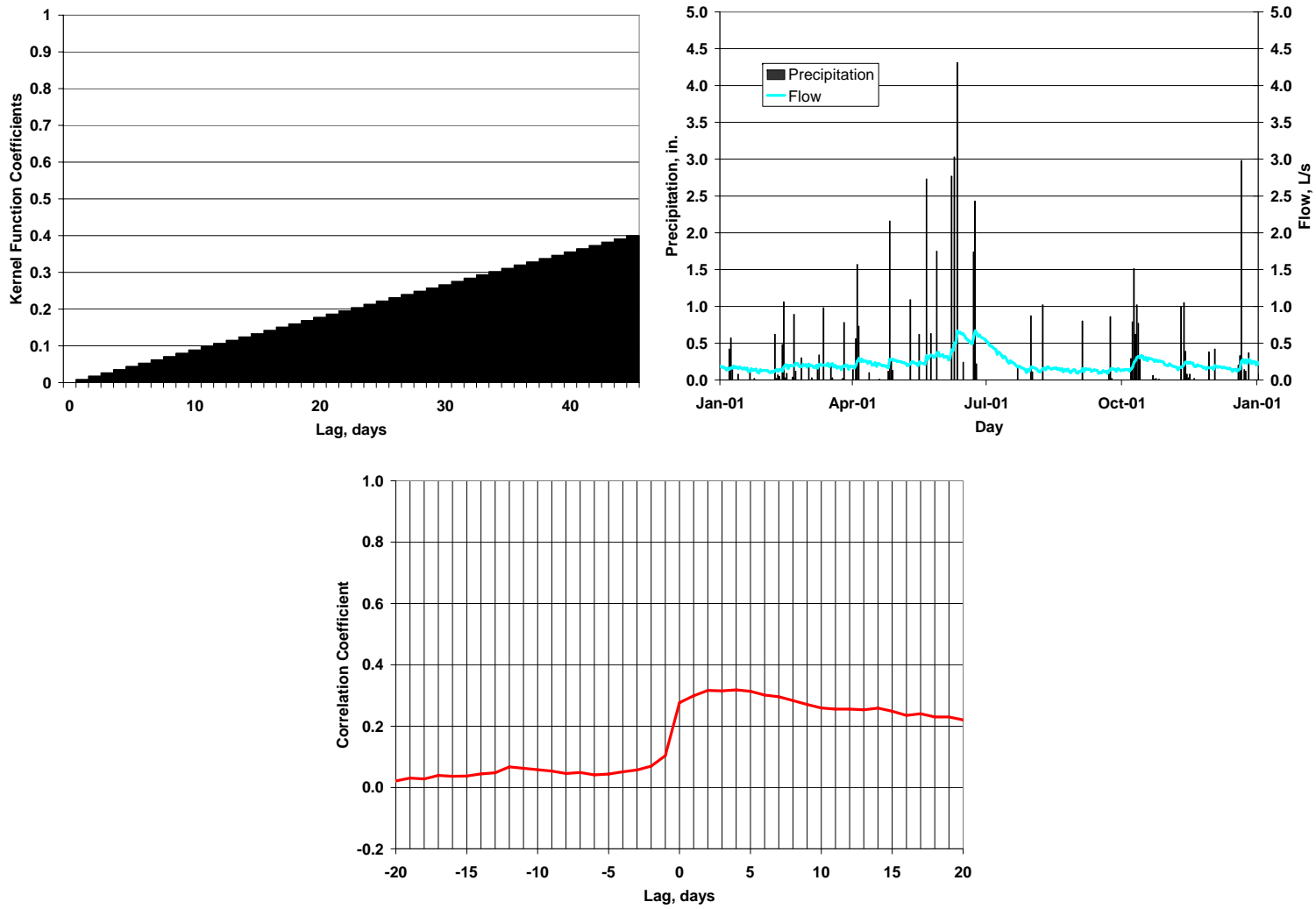


Figure 4.2 – Kernel function, precipitation and flow hydrograph, and corresponding correlagram used to model flow in a karst aquifer for matrix-controlled system.

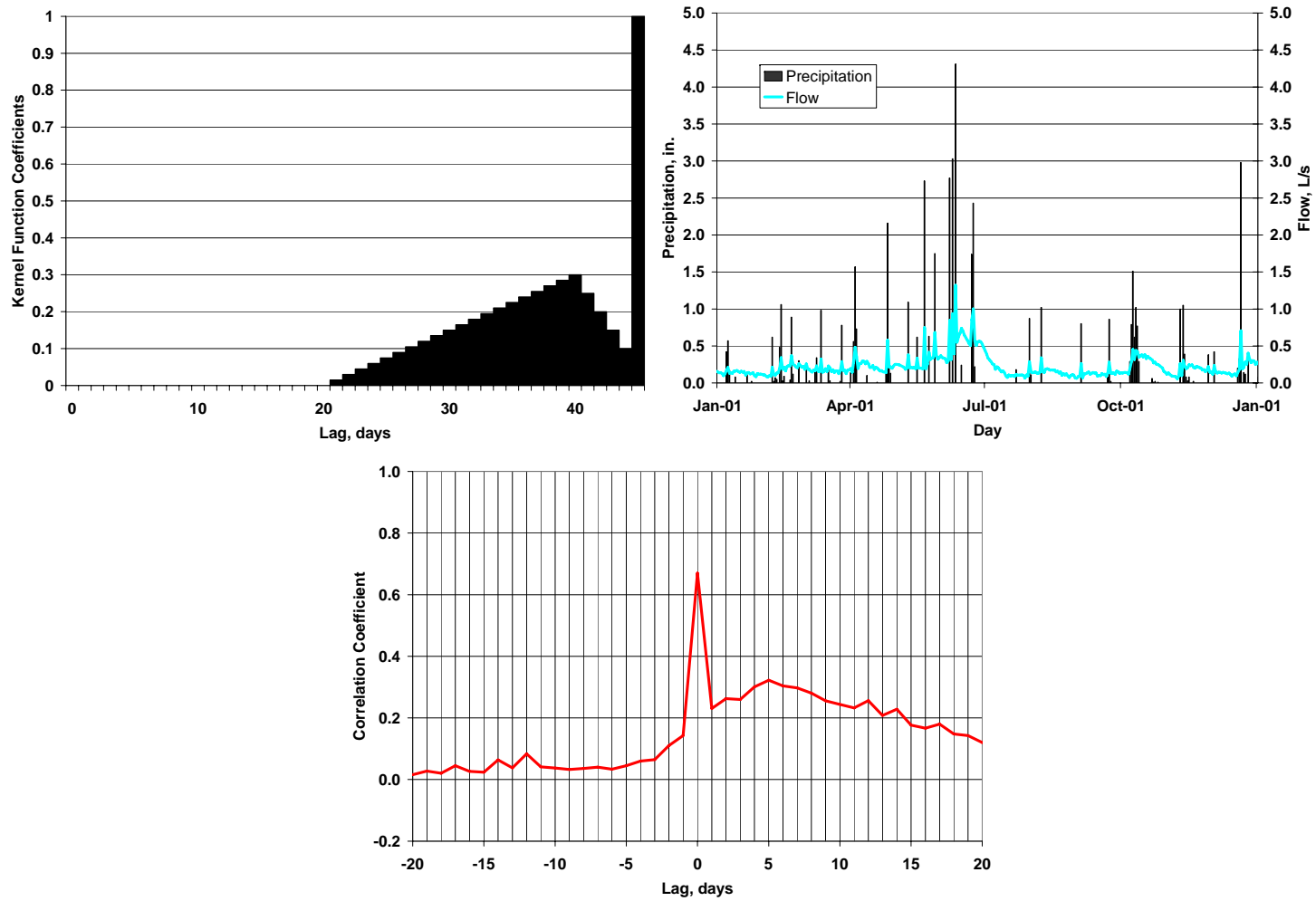


Figure 4.3 – Kernel function, precipitation and flow hydrograph, and corresponding correlogram used to model flow in a karst aquifer for mixed-control system.

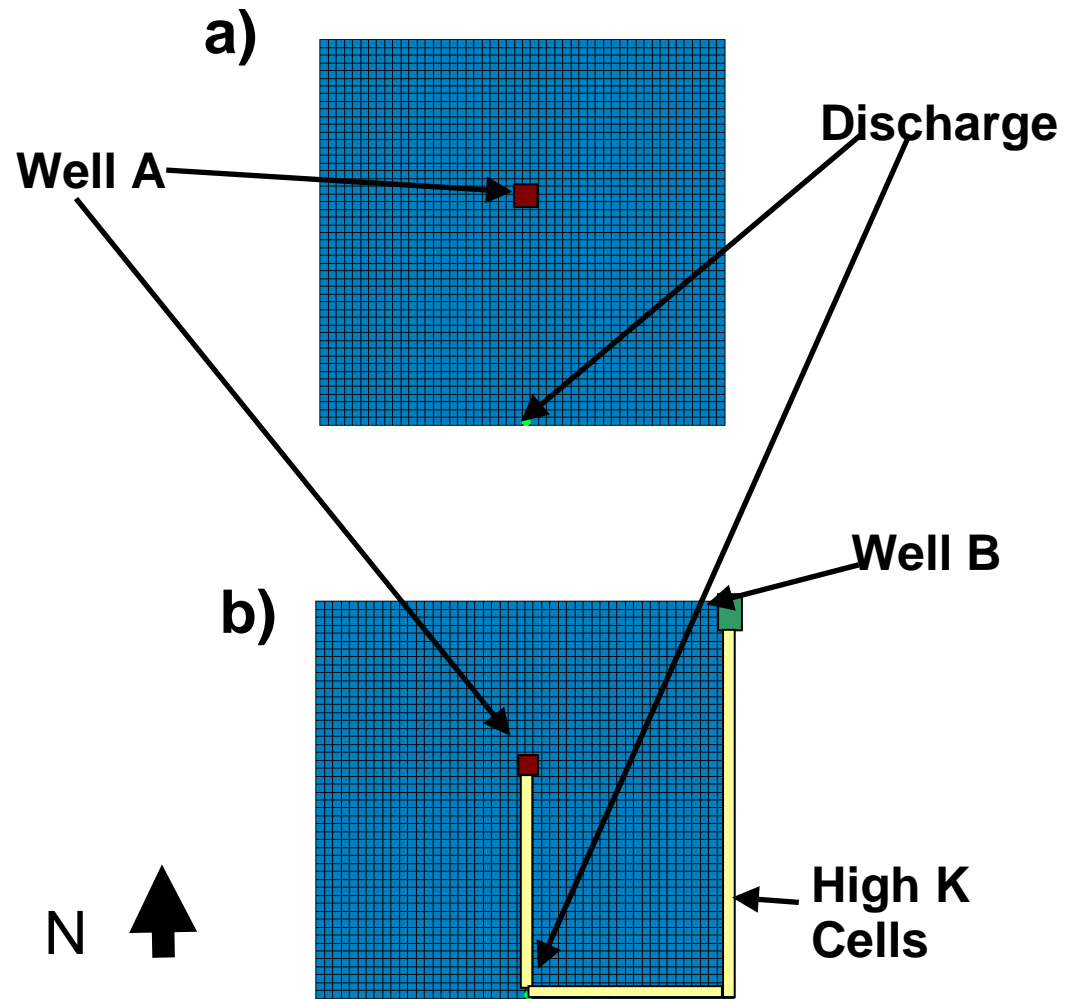


Figure 4.4 – Plan view map of the MODFLOW model domain with the associated boundary conditions.

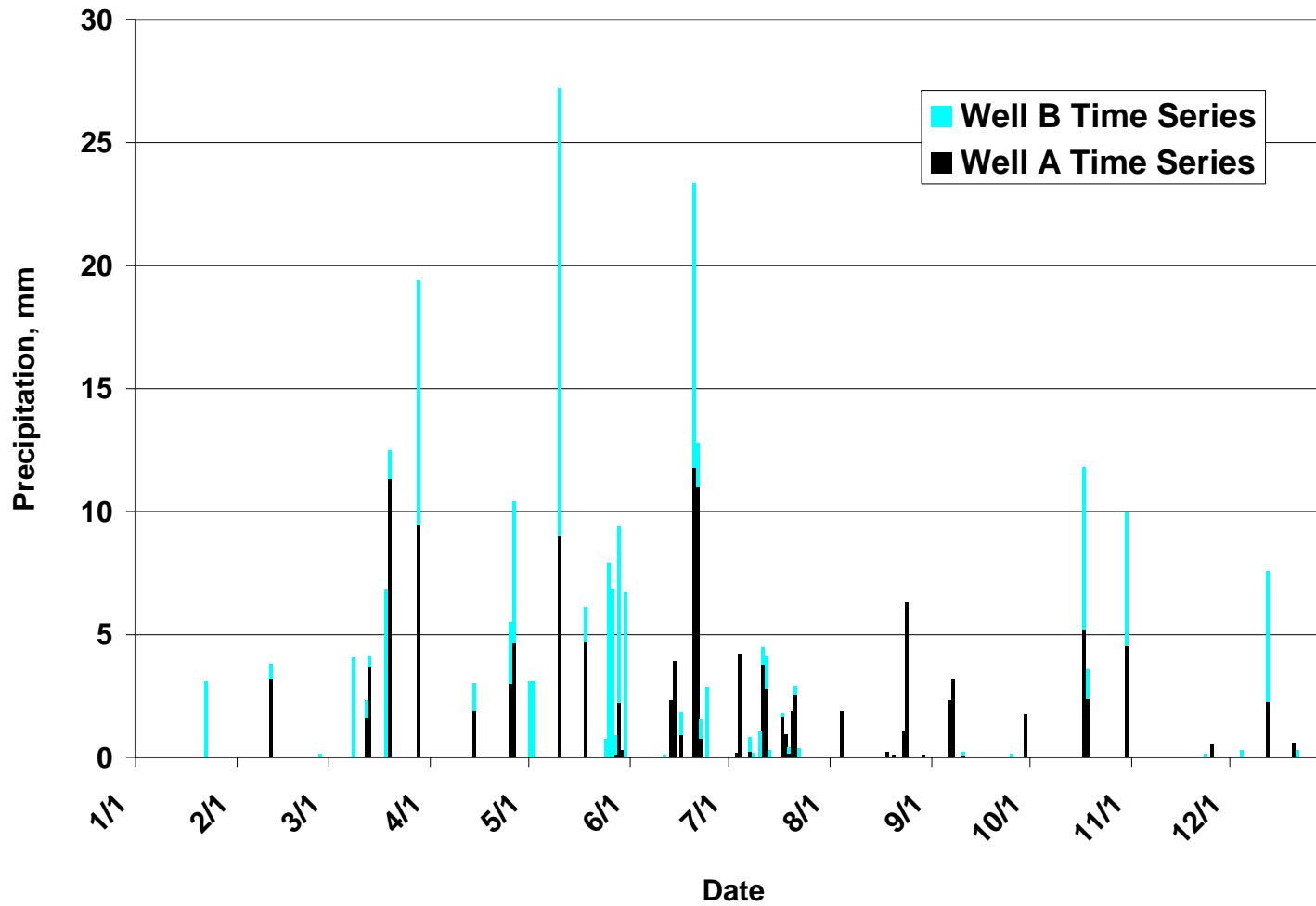


Figure 4.5 – The time series data used for precipitation events used to create discrete recharge for the MODFLOW model using the well package.

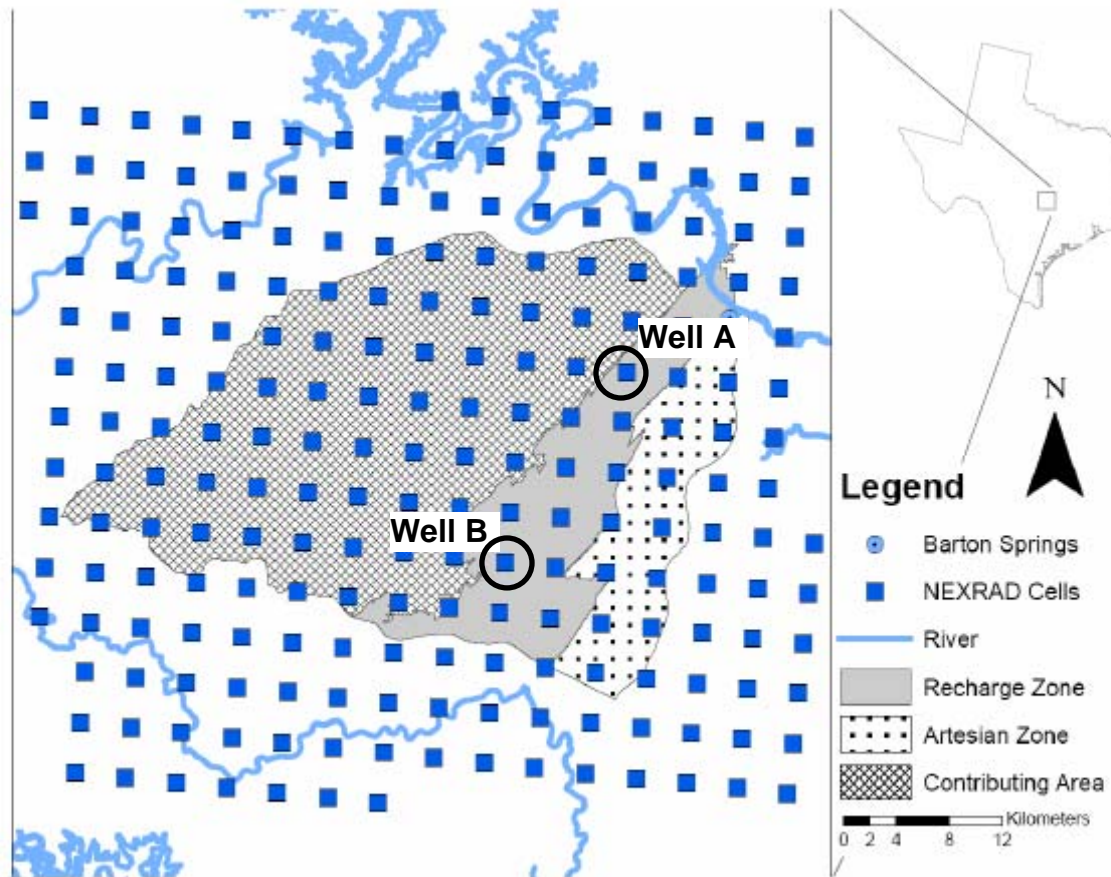


Figure 4.6 – The locations of the NEXRAD cells used for the precipitation input series used at location Well A and Well B.

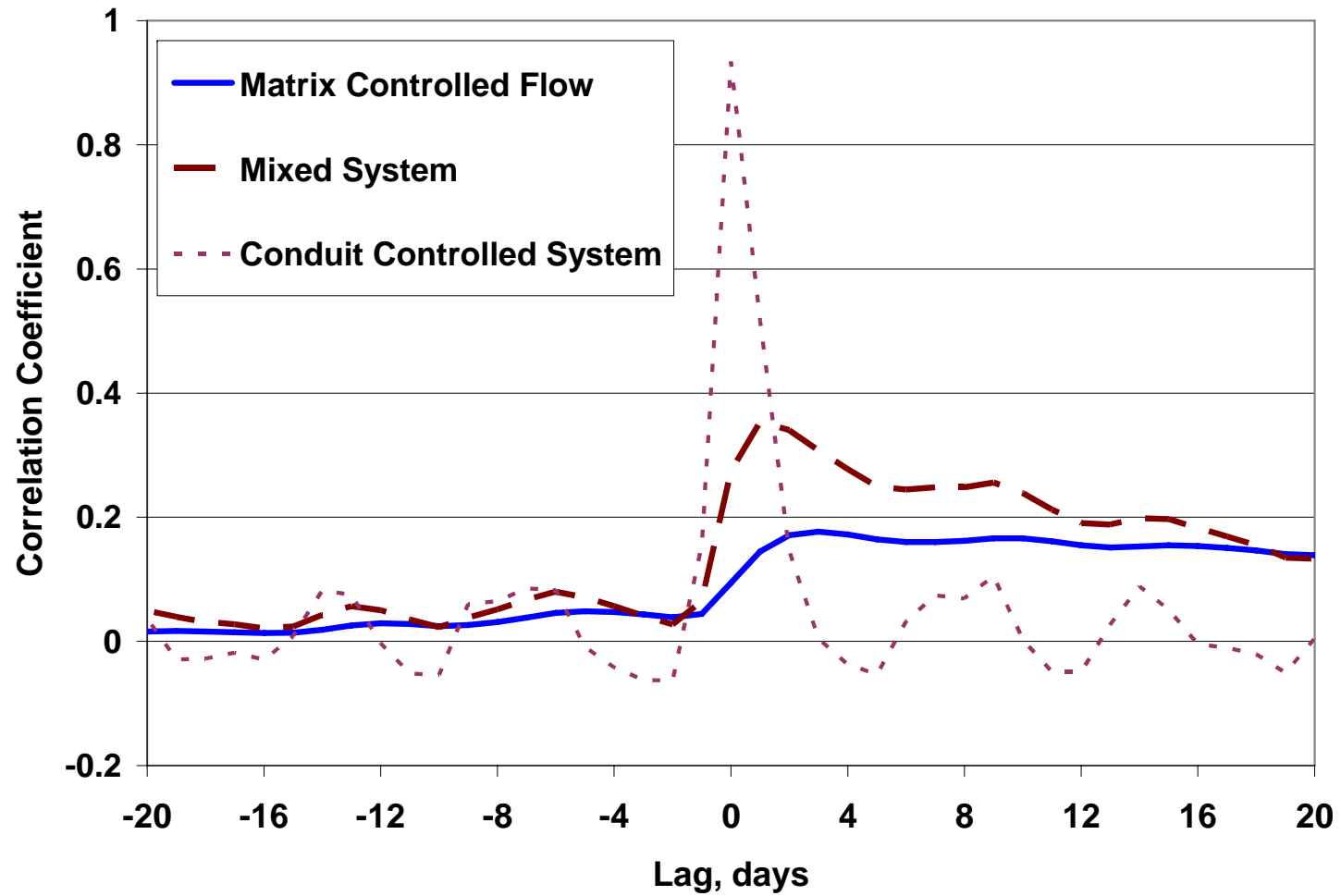


Figure 4.7 – A set of correlograms that reproduce the three numerical experiments presented by Padilla and Pulido-Bosch.

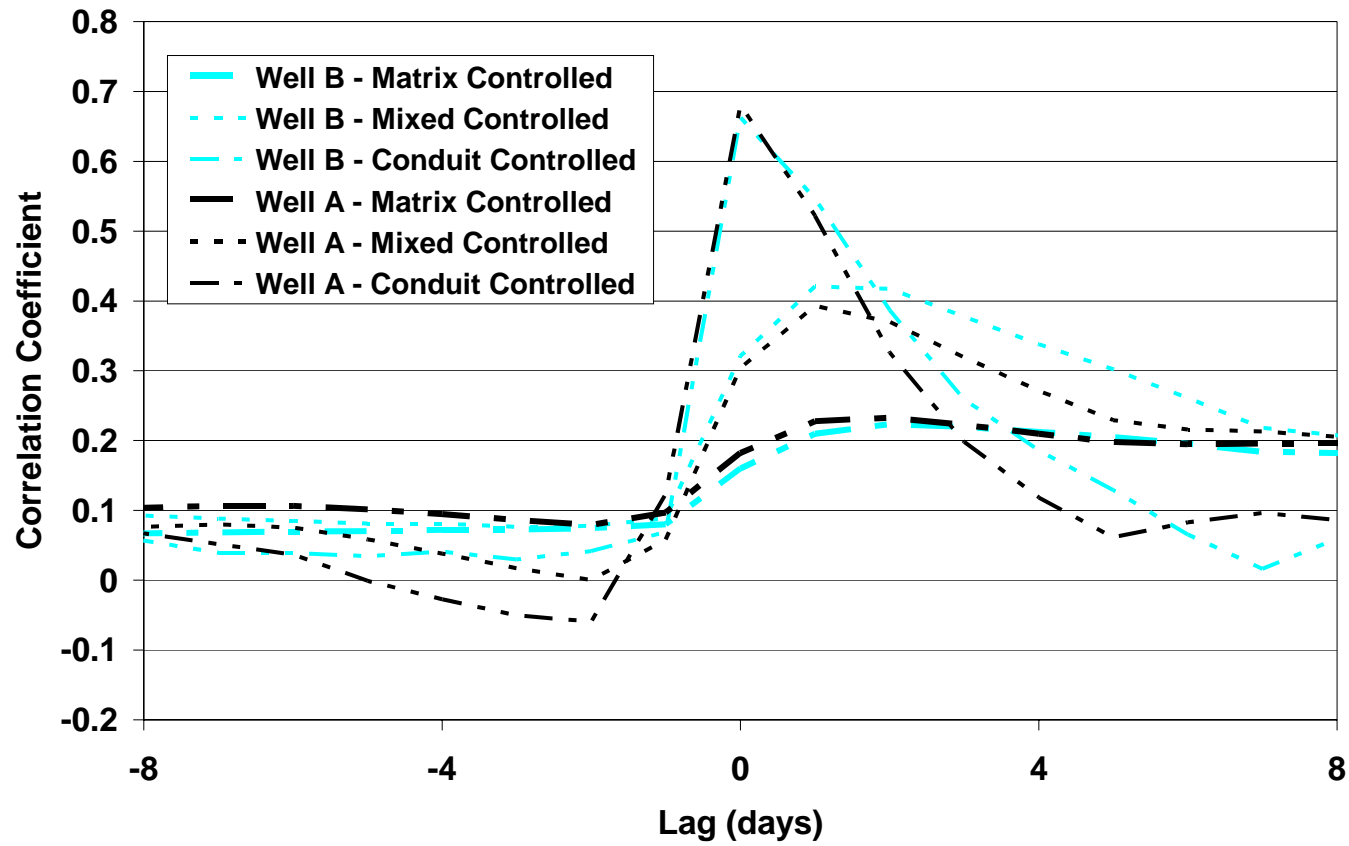


Figure 4.8 – Correlograms for Well A and Well B using a homogenous K field with two precipitation inputs. While differences in the correlogram can be seen, they are extreme.

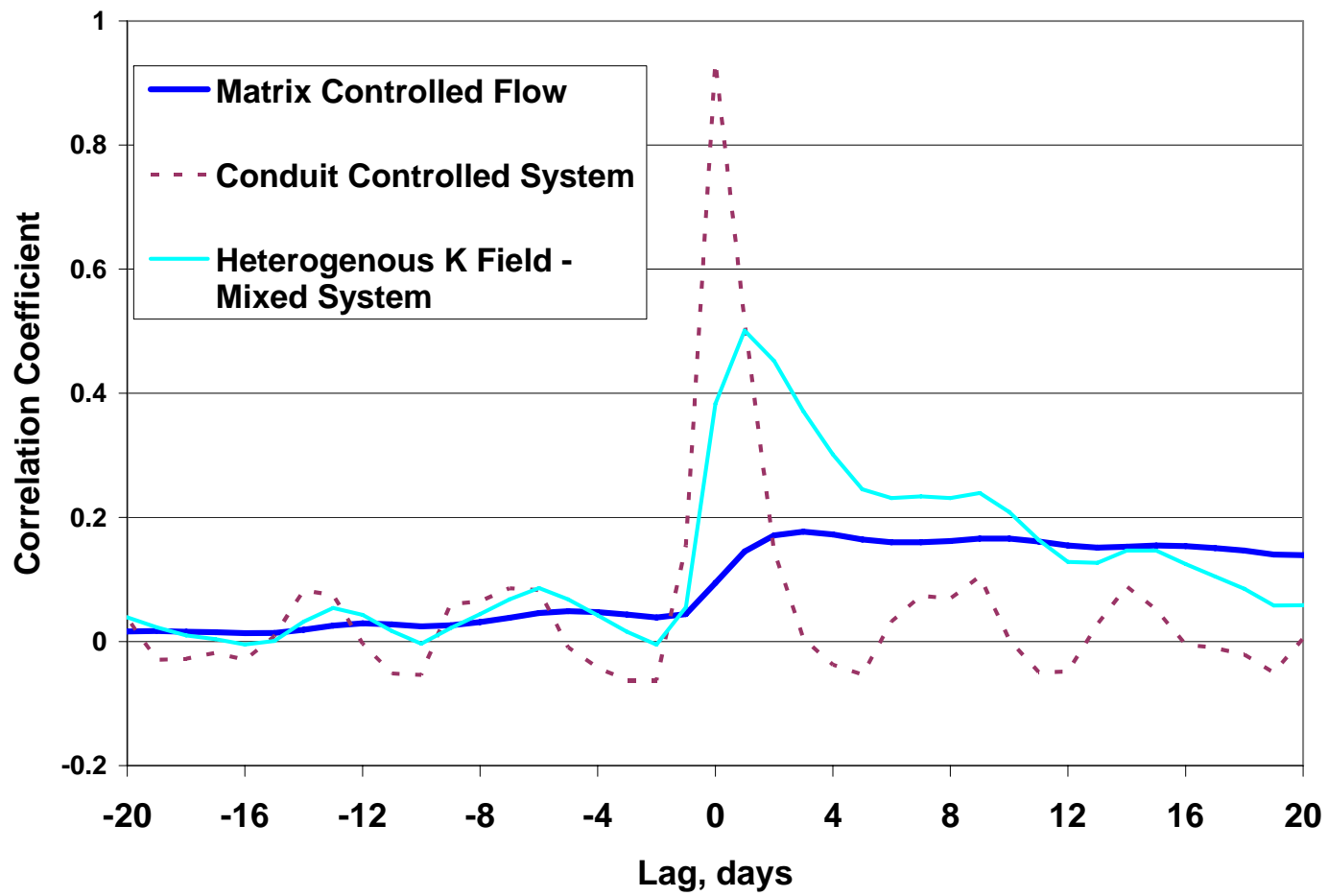


Figure 4.9 – Correlogram for numerical model with hydraulic properties for a conduit flow field.

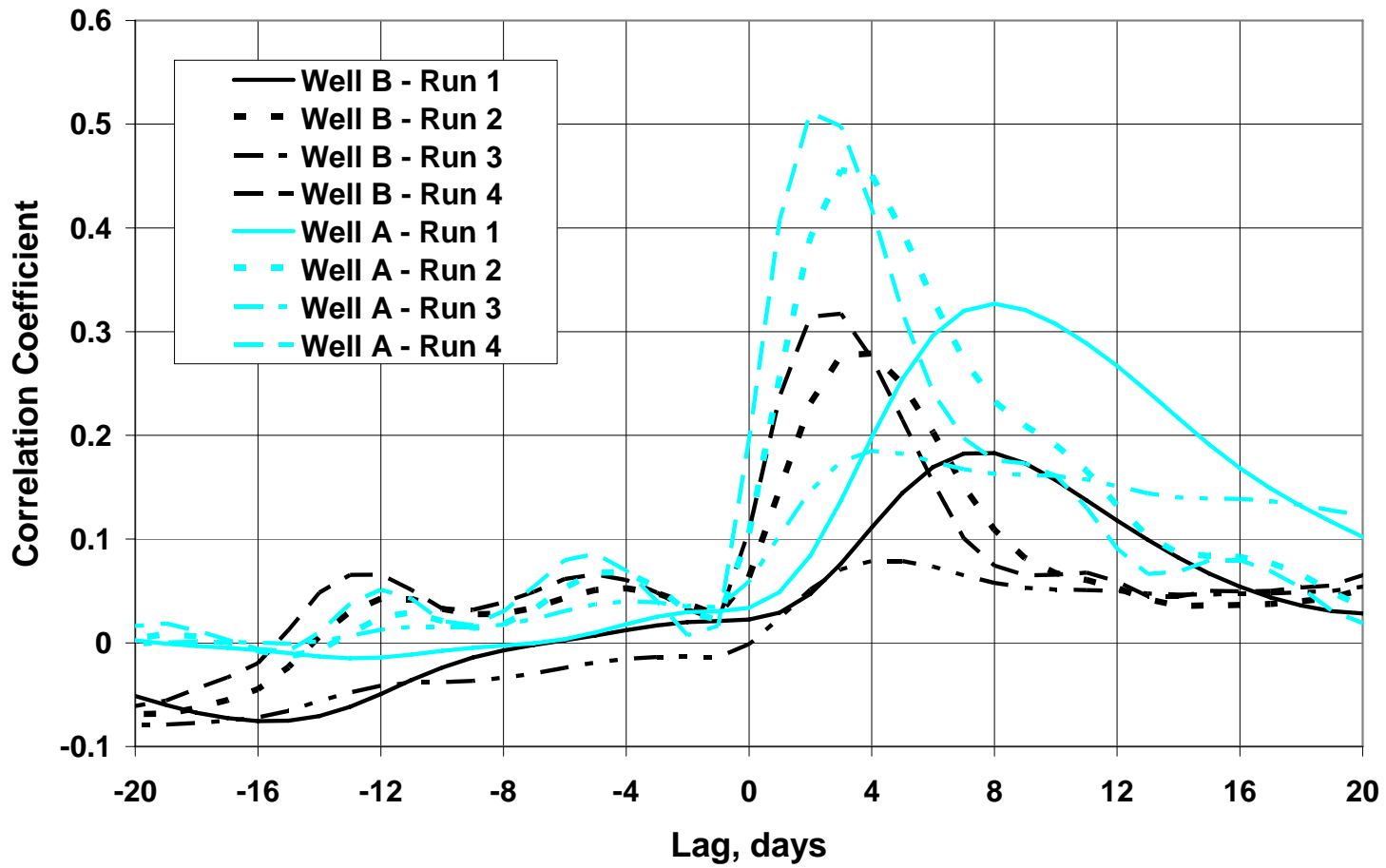


Figure 4.10 – Correlograms for several simulations using multiple precipitation inputs and the conduit flow MODFLOW simulation.

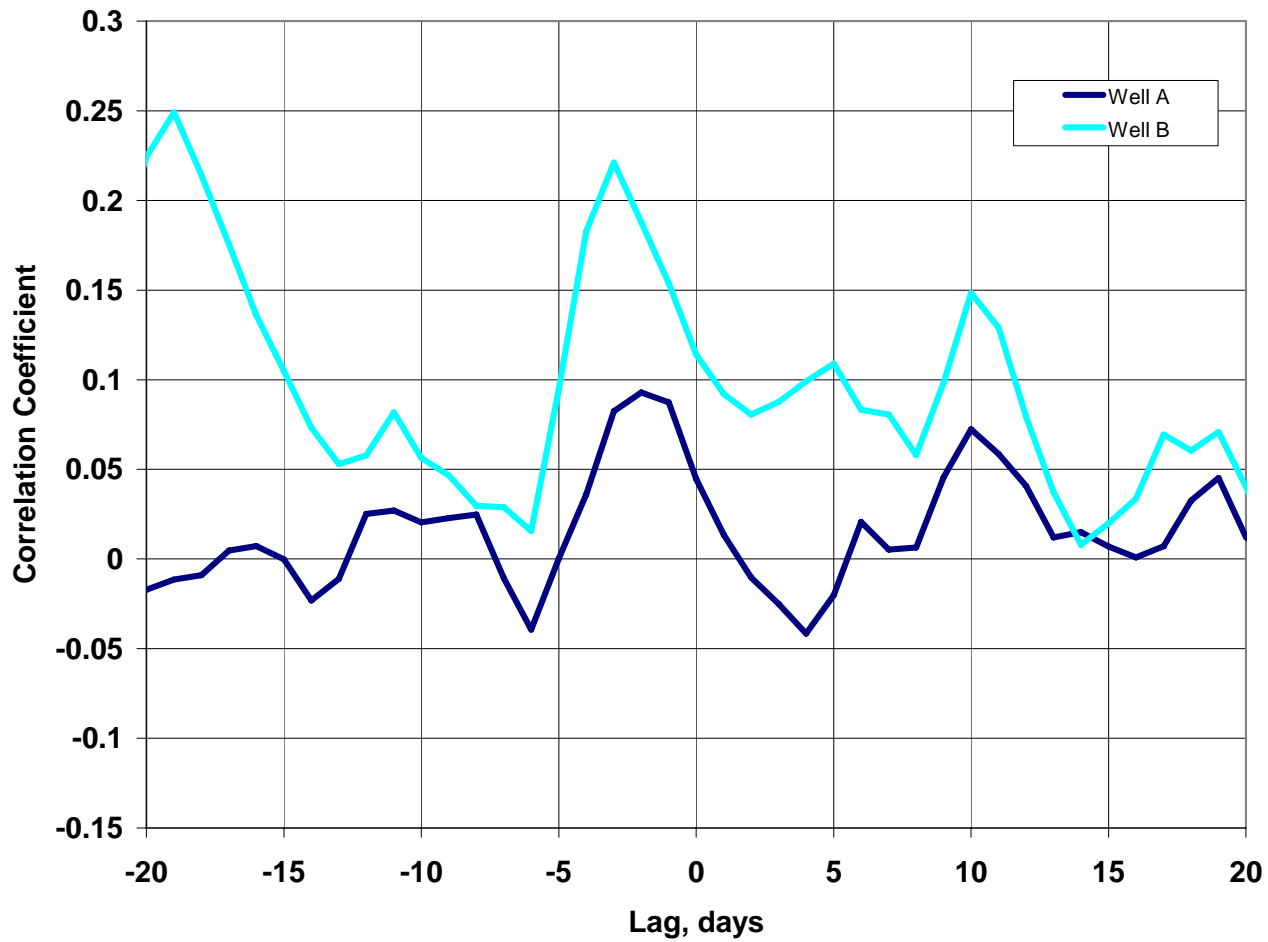


Figure 4.11 – Correlogram for Well A and B using a daily timestep in the model. Maximum correlation is found at a negative lag which is physically impossible.

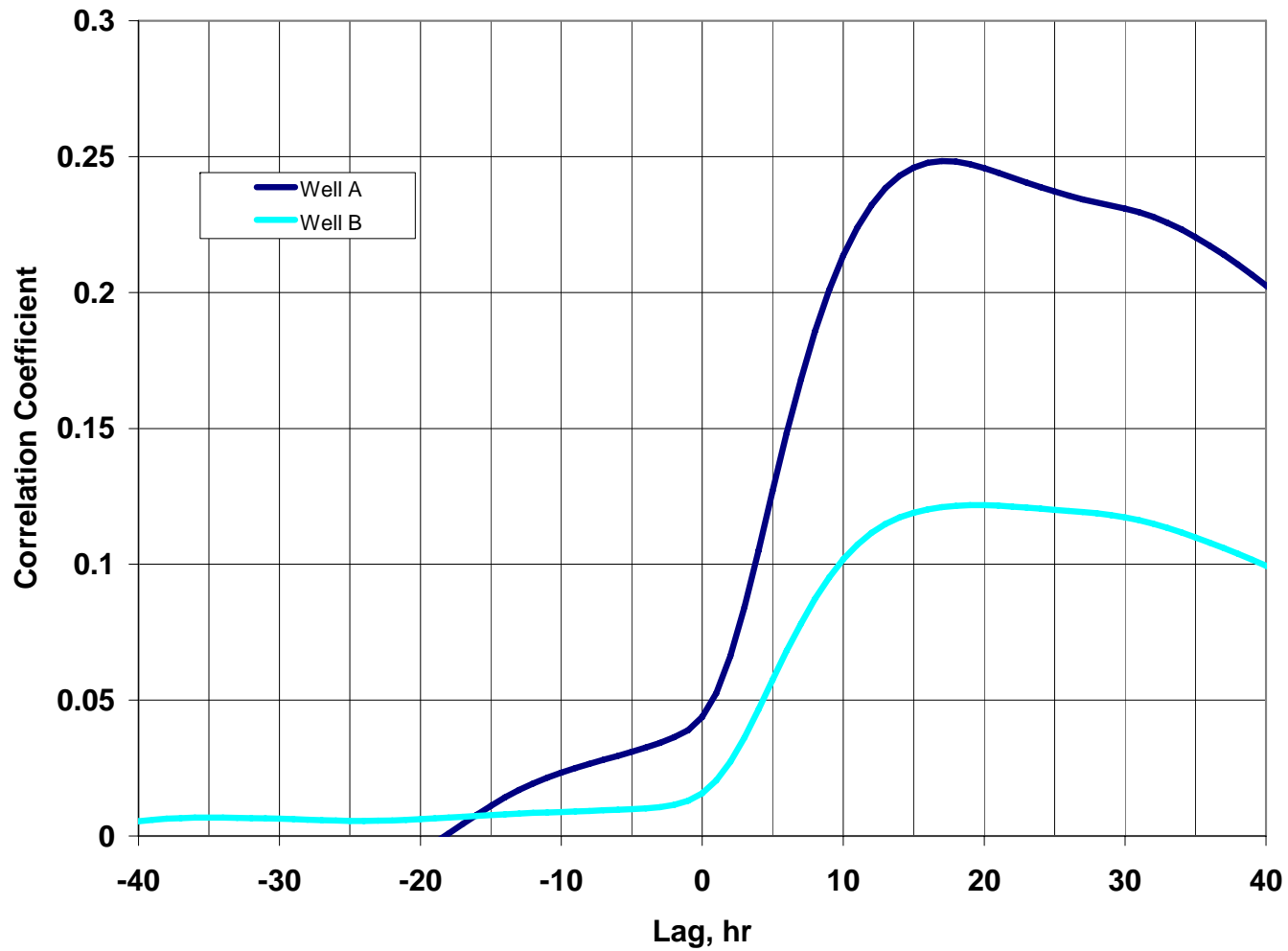


Figure 4.12 – Correlograms for Well A and B using the numerical model with aquifer properties equivalent to those in the BSEA. The lag for this correlogram is hours as opposed to days for other correlograms in this chapter.

Chapter 5. Field Applications

The application of cross-correlation analysis using spring discharge and NEXRAD data was carried out at two karst springs in Central Texas. Barton Springs near Austin and Jacob's Well near Wimberley (Figure 1.1) were selected as the locations for this application. The hydrogeology of these two spring systems was summarized in Chapter 2. In this chapter comparison of the relevant data available at the two springs and the cross-correlation analysis completed at each spring are discussed.

COMPARISON OF BARTON SPRINGS AND JACOB'S WELL

Barton springs and Jacob's well were selected based on several criteria. These include: 1) existing estimates of a recharge zone; 2) recorded spring discharge time series; and 3) previous dye tracing experiments. Each of these criteria are discussed below.

Existing Estimate of Recharge Zone

Both Barton Springs and Jacob's Well are springs discharging from Cretaceous limestone aquifers. Both are used as indicators of the health of their respective groundwater systems by the surrounding communities (BSEACD, 2007, WVMA,2007). Groundwater flow to Barton Springs has been the subject of many studies including a precise estimate of the geographic boundary of the recharge zone (Senger 1985, Slade, 1984, Hauwert, 1994, BSEACD, 2005). However, studies completed near Jacob's Mace et al. (2000), Scanlon (2001), Hanson and Small (1995), Bluntzer (1992), Ashworth (1983), and Grimshaw (1970)) have not produced a precise map of the contributing area.

Hence, Barton Springs was selected as a location to test whether or not cross-correlation using NEXRAD data could reproduce what is generally accepted as the recharge pattern in the aquifer. Conversely, due to the lack of an estimated recharge zone for Jacob's Well, applying the methodology to Jacob's Well may allow a first estimate of where recharge is most likely.

Recorded Spring Discharge

To conduct the cross-correlation analysis both the precipitation and spring discharge data are required. The period of record for Stage III NEXRAD data is 1994 to present. Barton Springs discharge has been recorded on a 15-minute time step for this entire period. Therefore, the period of record for NEXRAD data is the limiting data set. An analysis of Barton Springs can take place for any time period within the NEXRAD period of record. However, spring discharge at Jacob's Well only has a period of record from 2005 to present. In the case of Jacob's Well, the spring discharge period of record limits the range of dates usable for this analysis.

Previous Dye Tracing Experiments

Dye tracing experiments at each spring were key to selecting the sites used for the field application. This section contains a description of the previously conducted dye-tracing experiments at each of the springs.

Barton Springs

In the case of Barton Springs, the City of Austin, Texas and the Barton Springs/Edwards Aquifer Groundwater Conservation District (BSEACD) have conducted

over 20 dye-trace experiments in the delineated recharge zone for Barton Springs (shown in Figure 5.1). These dye tracing experiments provide supporting evidence that the delineated recharge zone for BSEA contribute to flow at Barton Springs. Therefore, if results of the cross-correlation analysis approximate the current estimate for groundwater recharge this supports the hypothesis that this method can be used to identify likely recharge locations for Barton Springs.

Jacob's Well

A single known dye tracing experiment was conducted in 2005 at Jacob's Well (UT, 2005). The experiment recovered no dye. Results from cross-correlation analysis were used to investigate possible reasons no dye was recovered from the test and to identify locations where further dye-tracing experiments might be conducted.

CROSS-CORRELATION ANALYSIS AT TWO SPRINGS

Cross-correlation analysis was completed at Barton Springs and Jacob's Well. NEXRAD data processing are discussed in Chapter 3. However, this section discusses a comparison of the NEXRAD dataset used in the cross-correlation analysis to rain gages in the study area. This is followed by a discussion of the results of cross-correlation analysis at both Barton Springs and Jacob's Well.

NEXRAD Data Comparison to Rain Gages

The NEXRAD dataset used for cross-correlation analysis with spring discharge data were compared to gage data within the study domain to make a quality assurance check on the NEXRAD data. Figure 5.2 gives the center locations of the NEXRAD data

cells used in both the the Barton Springs and Jacob's Well analyses along with the rain gage data available throughout the area. Out of the rain gage data shown, only five gages had a period of record that overlapped the period of record for the NEXRAD data. These rain gages were the Dripping Springs, Camp Mabry, Austin Bergstrom, Fischer Store, and Wimberley gages. The NEXRAD data that were compared to the rain gage data were taken from the NEXRAD cell where the rain gage resides geographically closest to the NEXRAD cell center. Where no data were available (meaning that the collecting agency did not have a value available for analysis, days where a zero was recorded for either the gage or NEXRAD data were included in the dataset) for individual dates in either the precipitation gage or the NEXRAD data, the date was removed from the comparison. . This eliminated collector bias in the analysis based on lack of coverage for one of the time-series versus the other. Plots of these data were created for comparative purposes on a cumulative period of record and on a cumulative record for each year.

The large period of record dictates the use of the cumulative precipitation depth plots. Otherwise, the information would be more difficult to visualize. An example of this is found in Figure 5.3. The cumulative precipitation depth plot for the Dripping Springs gage is shown along with a bar chart representing the depth of each individual rain event. The large period of record requires the bar chart have extremely small widths that make them difficult to decipher. However, the cumulative depth plot provides a means to see the incremental changes overtime and compare the cumulative change in volume of precipitation that has occurred. Hence, the cumulative depth plots are used to

compare the rain gage and Stage III data at this scale. These comparisons are discussed below.

Cumulative Precipitation Depth

The cumulative precipitation depth plot displays the incremental change in precipitation over time with respect to each precipitation event that is recorded at the rain gage and in the NEXRAD dataset. The plots for the Fischer Store, Wimberley, Dripping Springs, Austin Bergstrom, and Camp Mabry gages are shown in Figure 5.4 thru 5.8, respectively. At each gage the cumulative precipitation recorded by the rain gage is greater than that of the NEXRAD data over time.

The cumulative precipitation volume plots indicate good agreement between the rain gage and NEXRAD data with respect to the timing of precipitation events. The timing of rainfall events in the NEXRAD data set and in response in the spring discharge is the key parameter to getting reliable results from the cross-correlation analysis. The agreement of these two sets of data gives us confidence in using the Stage III NEXRAD data in this analysis. Furthermore, the NEXRAD data set presents a higher resolution of coverage over a larger region when compared to the five rain gage locations available.

Cumulative Precipitation By Year

In each of the cumulative precipitation plots rain gages recorded large volumes of precipitation over the period of record. It is possible that the difference in precipitation volume is caused by large discrepancies early in the period of record. This was evaluated using annual cumulative precipitation plots for each rain gage. These differ from

previous plots by re-initializing the precipitation volume to zero at the beginning of each year. Figures 5.9 thru 5.13 show the annual cumulative precipitation plots for each of the rain gages. By visual inspection the cumulative precipitation for the years after 1999 appear to match better than those before 1999. These figures also include a table showing the difference in precipitation volume at the end of each year and the average annual difference before and after 1999. At each gage, except the Austin Bergstrom gage where no gage data were available before 1999, there is a significant difference between the average annual difference in precipitation volume. The difference between the before and after 1999 values ranges between 12.3 in (312 mm) and 5.2 in (132 mm) at the Wimberley and Camp Mabry gages respectively. The decrease in precipitation volume discrepancy corresponds to an error discussed in a NWS report regarding Stage III data processing (Seo et al., 2000, NWS, 2002, Xie et al., 2006). The error caused the truncation of precipitation values caused by lack of precision in dimensioning variables in Fortran code used in the Stage II algorithm (see Chapter 2). This error may be the cause of underestimation of NEXRAD rainfall with respect to rain gage data prior to 1999. The algorithm was changed after 1999 and the precipitation volumes appear to match better after this time frame.

Barton Springs Analysis

Figure 5.14 shows an example correlogram from the cross-correlation analysis of Barton Springs discharge and precipitation. The response shows the maximum correlation at three days of lag. The value for maximum correlation is 0.27. The significant correlation value is represented by the dashed line at a value of 0.13. For this

correlogram the maximum correlation occurs at a sharp peak and well above the statistically significant threshold. The spatial variation in the maximum correlation is shown in Figure 5.15. The recharge zone as delineated by the BSEA is also shown in the figure. The highest values of maximum correlations generally follow the delineated recharge zone for the aquifer. Figure 5.16 shows the same region only the values represent the difference between the maximum correlation and the statistical significance threshold value. The average significance threshold is 0.15 with a standard deviation of 0.024. Again, the locations where the difference between the maximum correlation and the significance threshold are highest are located in and near the delineated recharge zone.

The locations of highest maximum correlation and the largest difference both follow the delineated boundary with exception of a various locations directly up-dip of the Mt. Bonnell Fault. While the Mt. Bonnell Fault is the recharge zone boundary, these correlation values suggest that precipitation occurring in this region recharges the aquifer. It is possible that precipitation in this region produces surface runoff that flows past the Mt. Bonnell Fault and recharges through stream beds over the recharge zone. However, it is also possible that there may be discrete recharge features on the up-dip side of the Mt. Bonnell Fault. In either case precipitation in this location has a high correlation with increased flow at Barton Springs.

Average Precipitation in Current Zones

Above the application cross-correlation analysis of NEXRAD data at individual NEXRAD cells was discussed. However, multiple NEXRAD cells can be grouped

together to investigate the recharge correlation within a larger area. Figure 5.17 shows the current estimate for the contributing area, recharge zone and artesian zone (USGS, 2007). The precipitation estimates from NEXRAD data were averaged over these areas to evaluate the relative contribution of precipitation within each zone to discharge at Barton Springs. If cross-correlation analysis between the NEXRAD data and the spring discharge are mimicking the accepted conceptual flow model of the aquifer, then the order of correlation from highest to lowest should be recharge zone, contributing zone, and artesian zone.

Average precipitation time series were developed from NEXRAD data over each of the aquifer zones shown in Figure 5.17. The average was calculated using an arithmetic average of all NEXRAD cells with a cell center located inside the polygon for each corresponding zone of the aquifer. Cross-correlation statistics were calculated for each of the zones with respect to discharge at Barton Springs. The results of this analysis are shown in Figure 5.17. The maximum correlation values are 0.24, 0.28, and 0.23 for the contributing, recharge, and artesian zones respectively. The difference above the statistically significant threshold was 0.15, 0.15, and 0.14 respectively. The recharge zone has a 40% larger value above the significant threshold than both the contributing and artesian zone. The order of correlation is in agreement with what would be expected based on the current conceptual understanding of discharge to Barton Springs.

MPE vs. Stage III

As discussed in Chapter 2, MPE NEXRAD is currently the product used for river forecasting operations by the NWS. Algorithms used for estimated MPE precipitation

provide more quality assurance procedures and more input datasets (Shelton, 2008, NWS, 2002). In previous discussions of the analysis of NEXRAD data and spring discharge at Barton Springs, the NEXRAD product used was Stage III data. In the case of Jacob's Well, MPE data were used. The period of record for MPE data and Stage III data used in this research overlap from 2001 to 2004. To compare differences in the results of cross-correlation analysis on the two sets of data, the cross-correlation analysis was carried out for both sets of data at BSEA for the overlapping time period.

Figure 5.18 shows a comparison of the values within the recharge zone of the BSEA. The MPE has a higher correlation than the Stage III data. However in both cases the higher values of maximum correlation reside over the recharge zone of the aquifer. In figure 5.19 a method for finding natural breaks, or Jenks method (Jenks and Caspall, 1971) was used to define the color coding for each of the analyses individually. Overall, the results using the Jenks method from both types of NEXRAD data show the agreement in where the most likely recharge locations occur. However, the MPE data show more contribution in the south western portion of the aquifer than the Stage III data.

Jacob's Well

Jacob's Well is a spring that produces water from a 30 m deep vertical cavern in Cretaceous age Glen Rose Limestone. This section discusses the data used and the results of the cross-correlation analysis of NEXRAD data with respect to spring discharge at Jacob's Well.

Data Collection

The USGS has collection spring discharge at Jacob's Well from 2005 to present. This limits the range of dates usable for this analysis. The public servers for downloading NEXRAD data discussed in previous sections do not have available data since 2005. The NWS West Gulf River Forecast Center provided MPE NEXRAD data that overlap the time period of spring discharge at Jacob's Well.

Results

The shape of the correlograms for calculated at Jacob's Well are similar to those for Barton Springs. An example correlogram is shown in Figure 5.20. The maximum correlation rises above the statistically significant threshold at a sharp peak. Figure 5.21 and 5.22 show spatial locations of the maximum correlation and correlation above the statistically significant threshold, respectively. In most cases the maximum correlation value was higher than the statistically significant threshold. However, there are several NEXRAD cells in the eastern portion of the study area (downdip from Jacob's well) that show a maximum correlation less than the statistically significant threshold. None of these values occur up-dip of Jacob's Well.

While there is no delineated recharge zone for this spring, the pattern highest maximum correlation is consistent with the general structure in the area. Figure 5.22 also contains the delineated surface water catchment zone for Cypress Creek above Jacob's Well based on the 30 m USGS DEM. For the most part the highest values of maximum correlation lie to the north west of the spring similar in location to the topographic catchment. This agrees with the assessment of Bluntzer (1992) that the majority of

recharge for Jacob's well would have originated locally in the Trinity Aquifer. To the south and east, values of maximum correlation are lower indicating that the likely recharge zone is the northwest of the spring.

The previously discussed dye-tracing experiment conducted at Jacob's Well was conducted at the site marked by the red box in Figure 5.21. The location resides just outside of the highest maximum correlation values. This suggests that one reason no dye was recovered was lack of hydraulic connection between the selected dye injection location and the spring. It would be more likely to recover dye if it were injected into the aquifer in a location further to the north and west of Jacob's Well.

LIMITATIONS OF CROSS-CORRELATION WITH NEXRAD

The purpose of this section is to discuss some of the limitations of the data and the algorithms that were observed in conducting this research. These observations include practices that increased or decreased the efficiency that this work can be done. These include the climate, the magnitude of the precipitation, and the size of the basin. These are discussed below.

Climate

Precipitation can include rain, hail, ice, and snow. Hail, ice, and snow in a cooler climate can cause problems with the cross-correlation analysis. If any of these fall in a location where they remain in a frozen state, the NEXRAD data will record a precipitation event with no increase in precipitation. While this is physically accurate, it does not help identify locations where recharge is occurring based on the precipitation record. Increased spring flow would be more sensitive to increasing temperature and the

melting snow pack than the timing and location of precipitation. Cross-correlation analysis with NEXRAD data would be less effective in this environment.

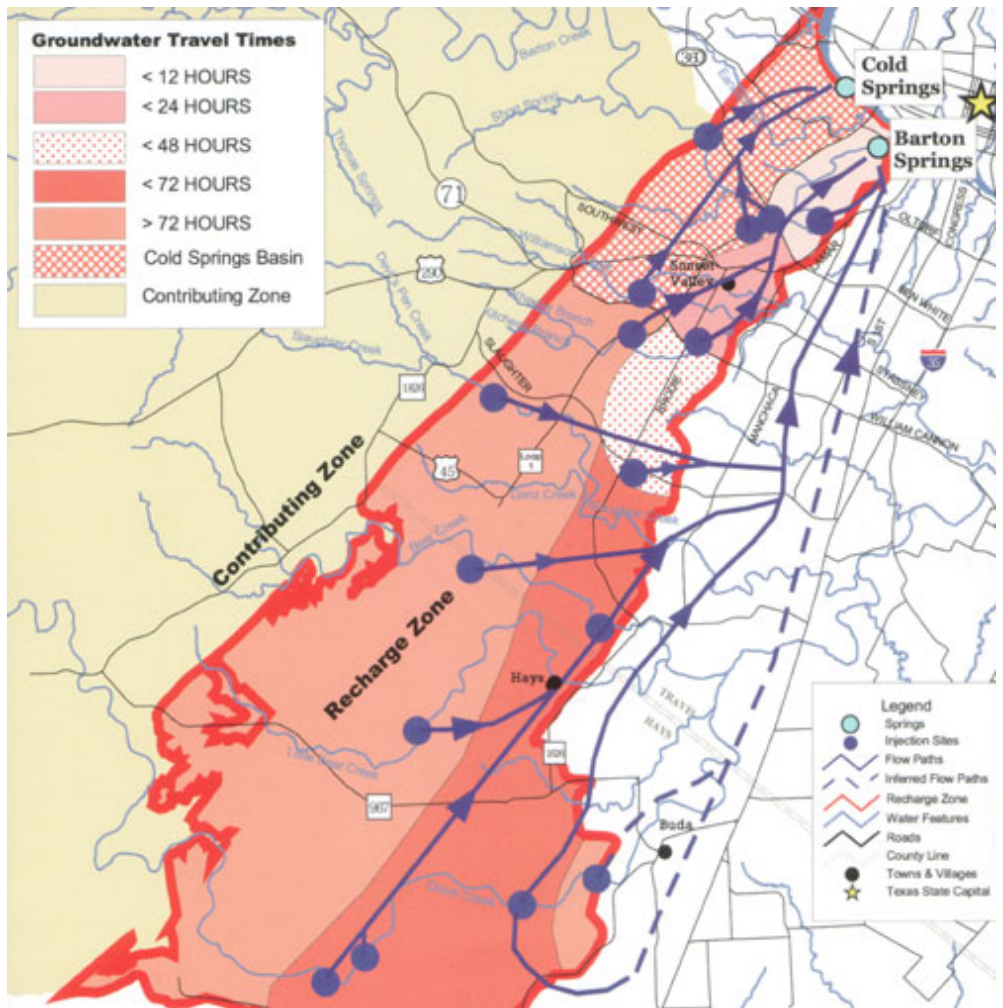
Magnitude of precipitation

The spring of 2007 in Texas was particularly wet. Several records for total precipitation were set during this time period. Before early 2007 the Central Texas had experienced several years of drought. The cross-correlation analysis conducted at Jacob's well initially included the months of March to July 2007. However, the map of likely recharge locations produced by the analysis showed the most likely locations of recharge occurred in the center of the BSEA contributing zone. This resulted from the fact that the volume of precipitation in 2007 dwarfed that of the previous two years. Furthermore, the extent of precipitation during that time was regional in nature and occurred simultaneously in the BSEA and Jacob's Well contributing zones. The results of the initial cross-correlation analysis reflected these regional rainfall events. To remove the bias in the NEXRAD record caused by these regional events the analysis was run from January 2005 to February 2007. The results discussed previously reflect this time period. While, this caused a problem over a relatively short period of record (2 years) it is expected that if data were available over a longer period such as at the BSEA, these regional precipitation events would bias the data less.

Size of Basin

Barton Springs has a contributing zone of approximately 670 km². At this size it was necessary to remove the large scale temporal pattern in the spring discharge in order to produce reasonable results from the analysis. Increasing the catchment size for the

spring would further mute the response of flow to single precipitation events. If individual springs derive their discharge from extremely large catchments, the analysis may not produce a valid map of likely recharge locations.



(BSEACD, 2003)

Figure 5.1 – Map of dye trace studies completed by the BSEACD and the City of Austin near Barton Springs.

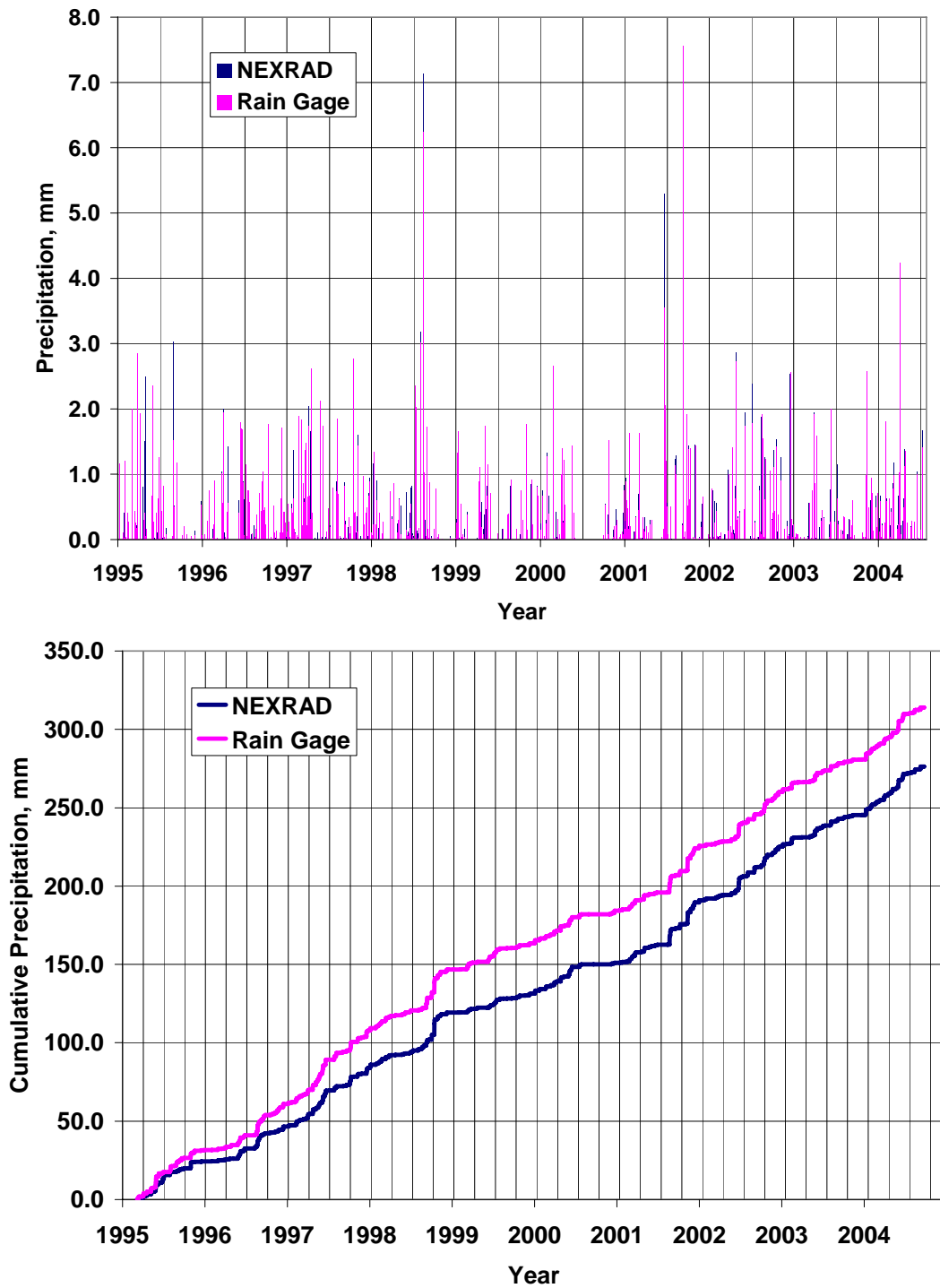


Figure 5.3 – Bar chart and cumulative precipitation chart for the Camp Mabry gauge. Due to the large time scale the bar chart is not as useful in comparing precipitation depths because the width of the bars is so small.

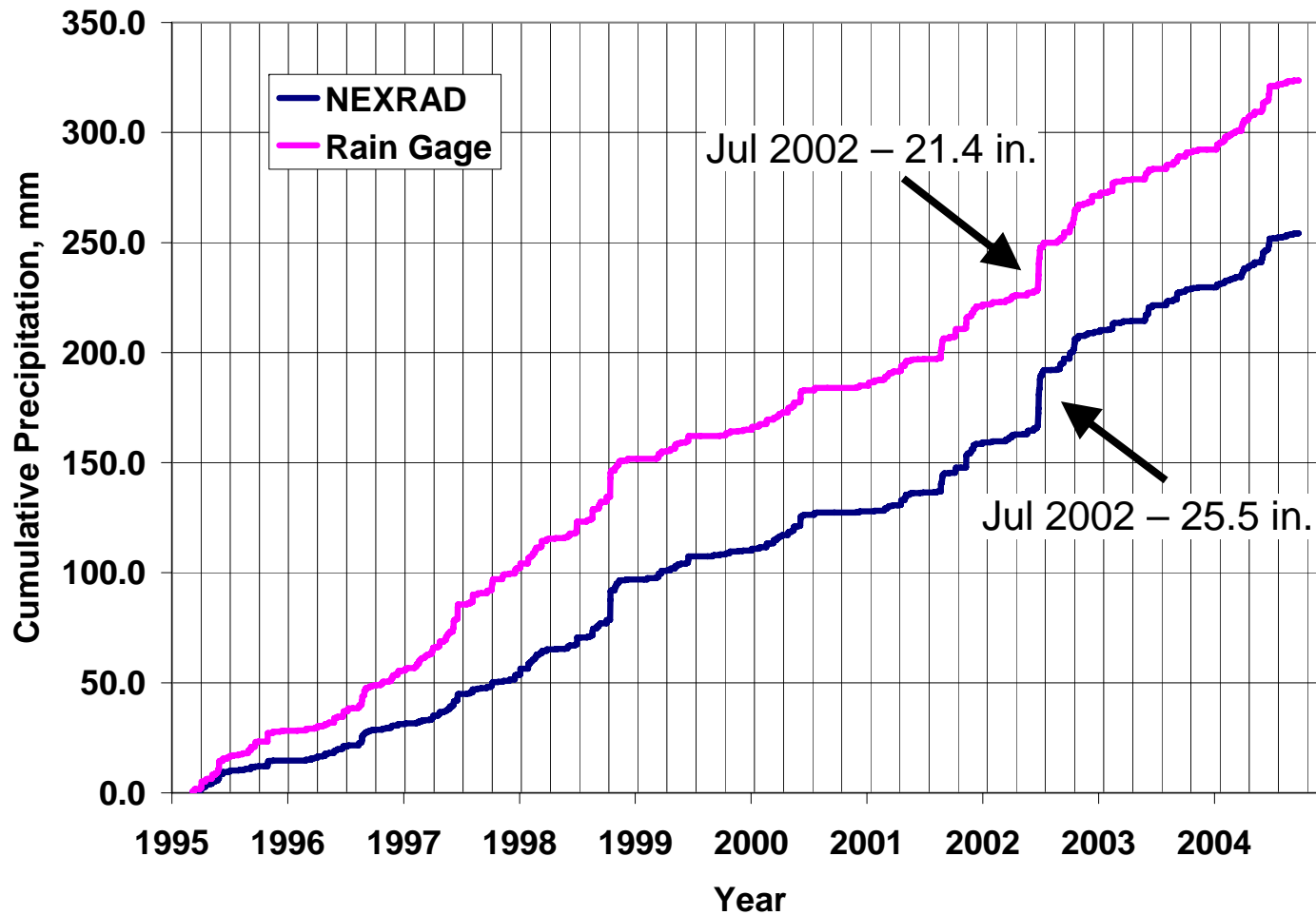


Figure 5.4 – Cumulative precipitation plot of Fischer’s Store gage and NEXRAD data for the corresponding NEXRAD cell.

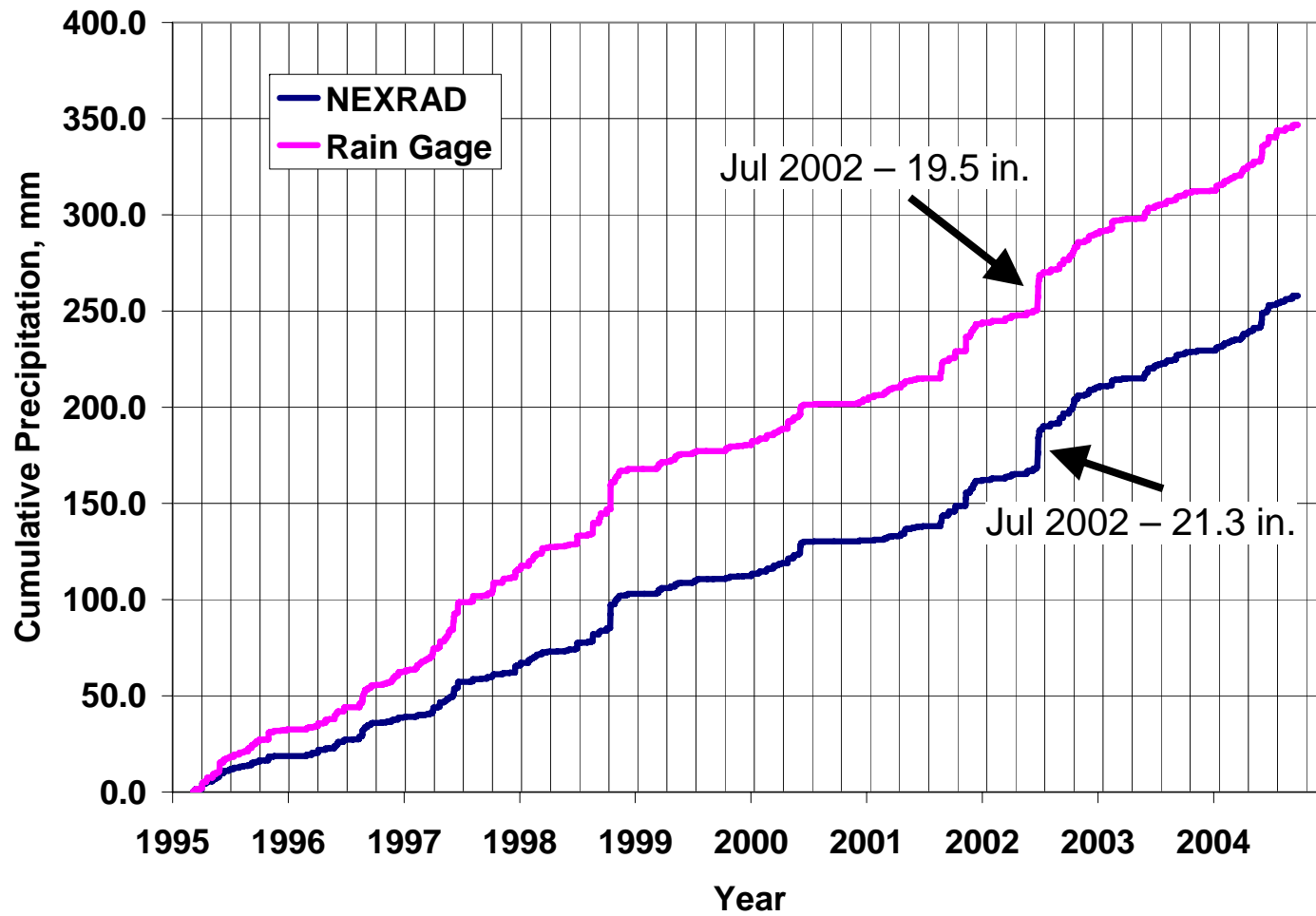


Figure 5.5 – Cumulative precipitation plot of Wimberley gage and NEXRAD data for the corresponding NEXRAD cell.

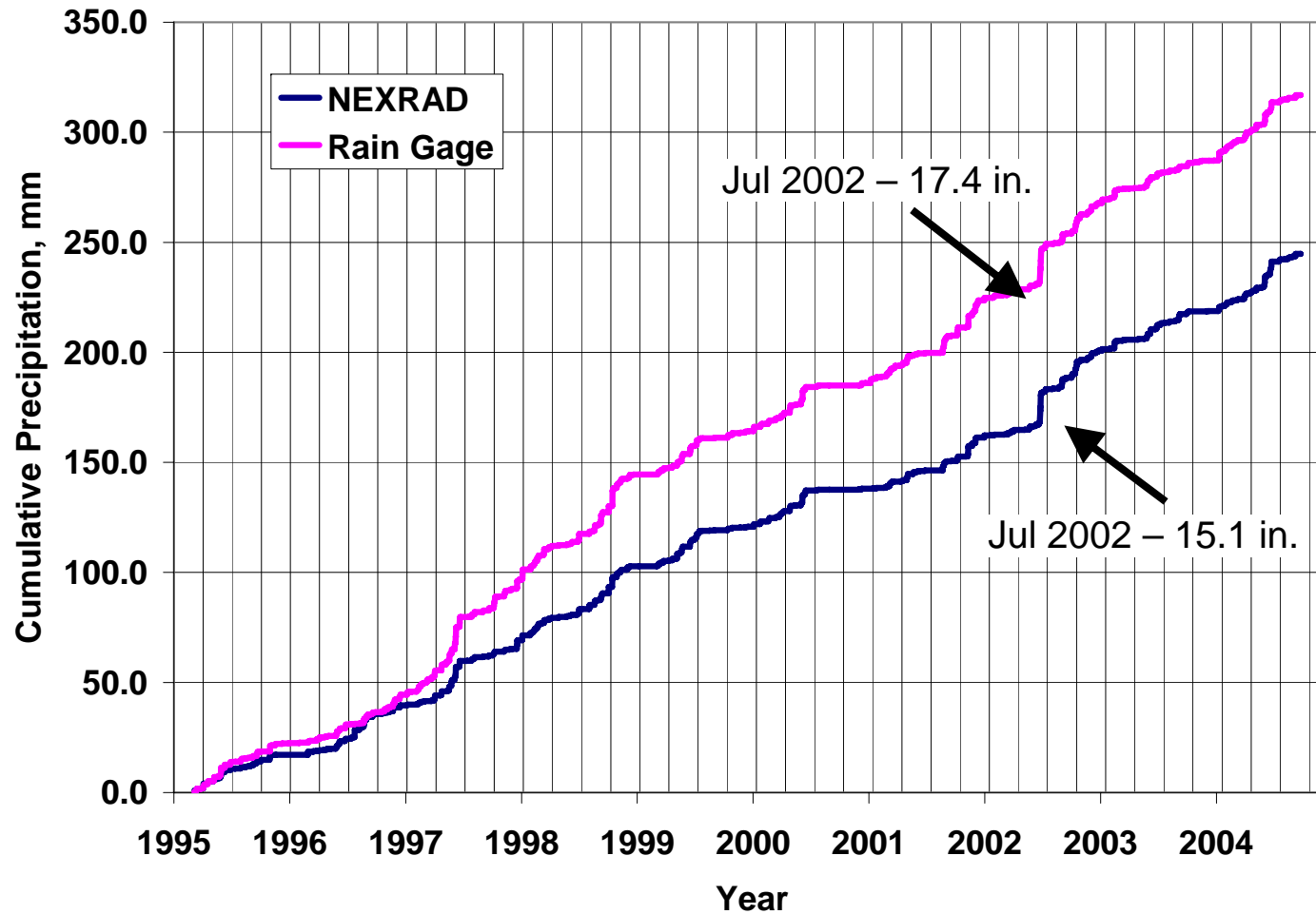


Figure 5.6 – Cumulative precipitation plot of Dripping Springs gage and NEXRAD data for the corresponding NEXRAD cell.

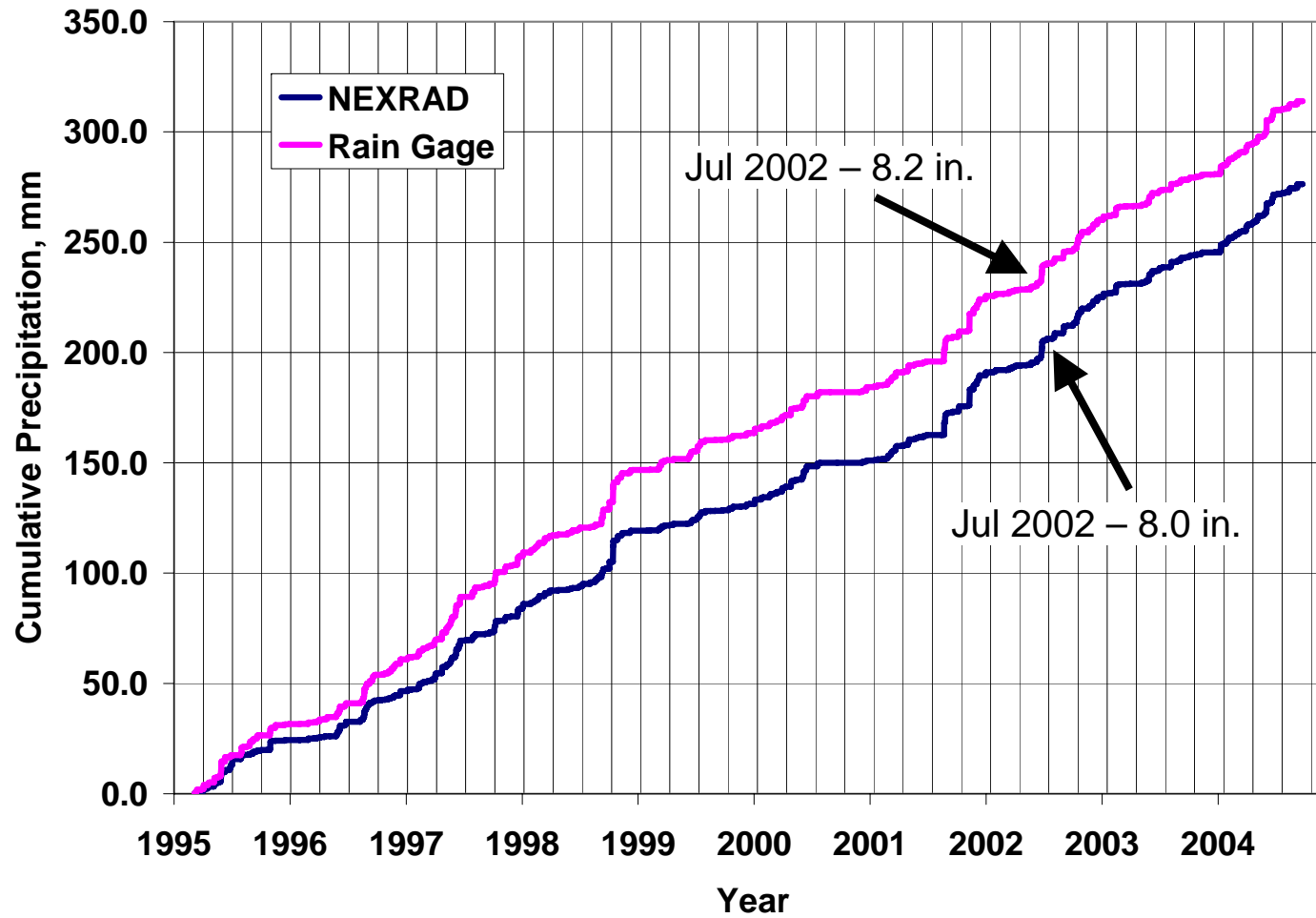


Figure 5.7 – Cumulative precipitation plot of Camp Mabry gage and NEXRAD data for the corresponding NEXRAD cell.

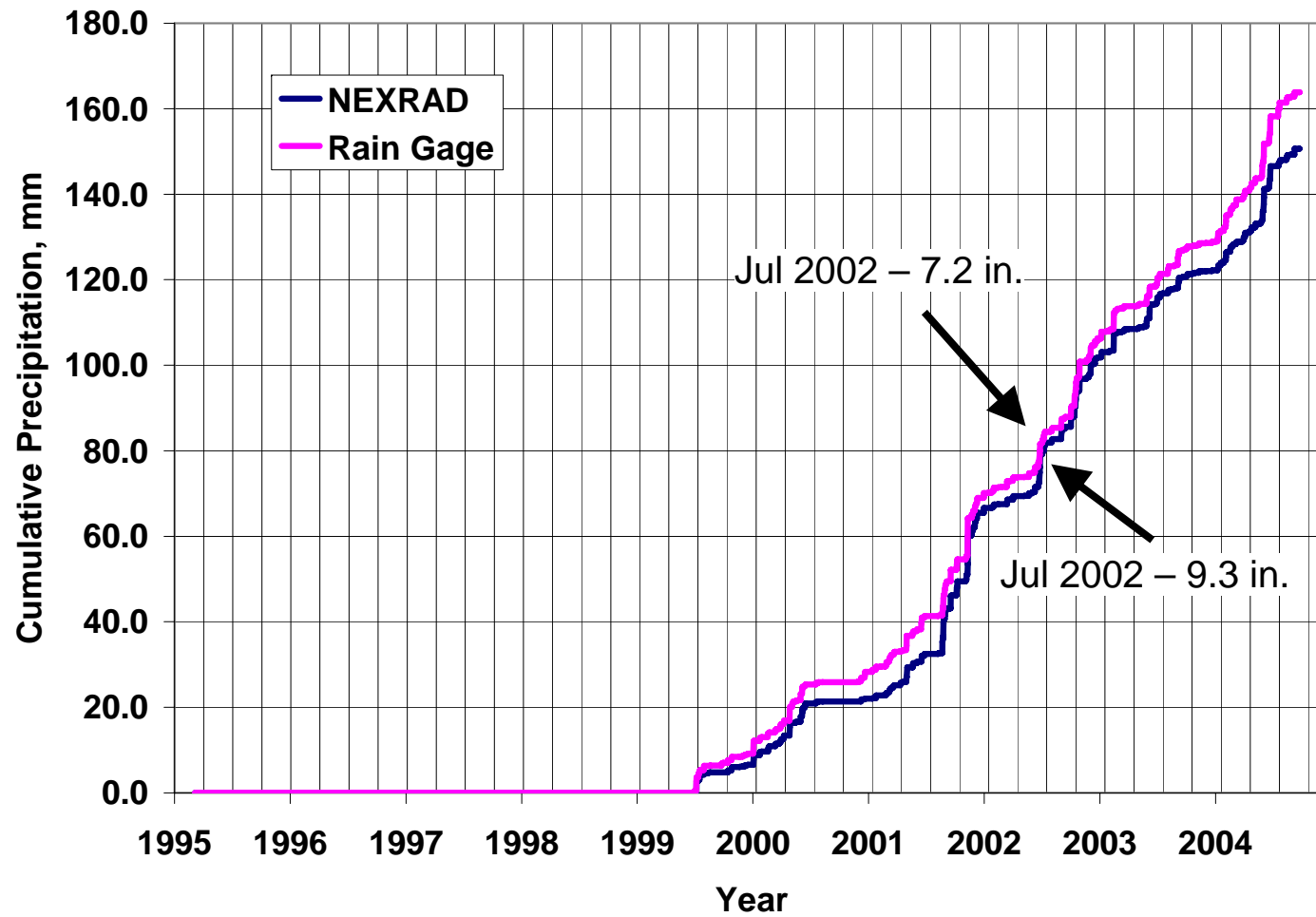


Figure 5.8 – Cumulative precipitation plot of Austin Bergstrom gage and NEXRAD data for the corresponding NEXRAD cell.

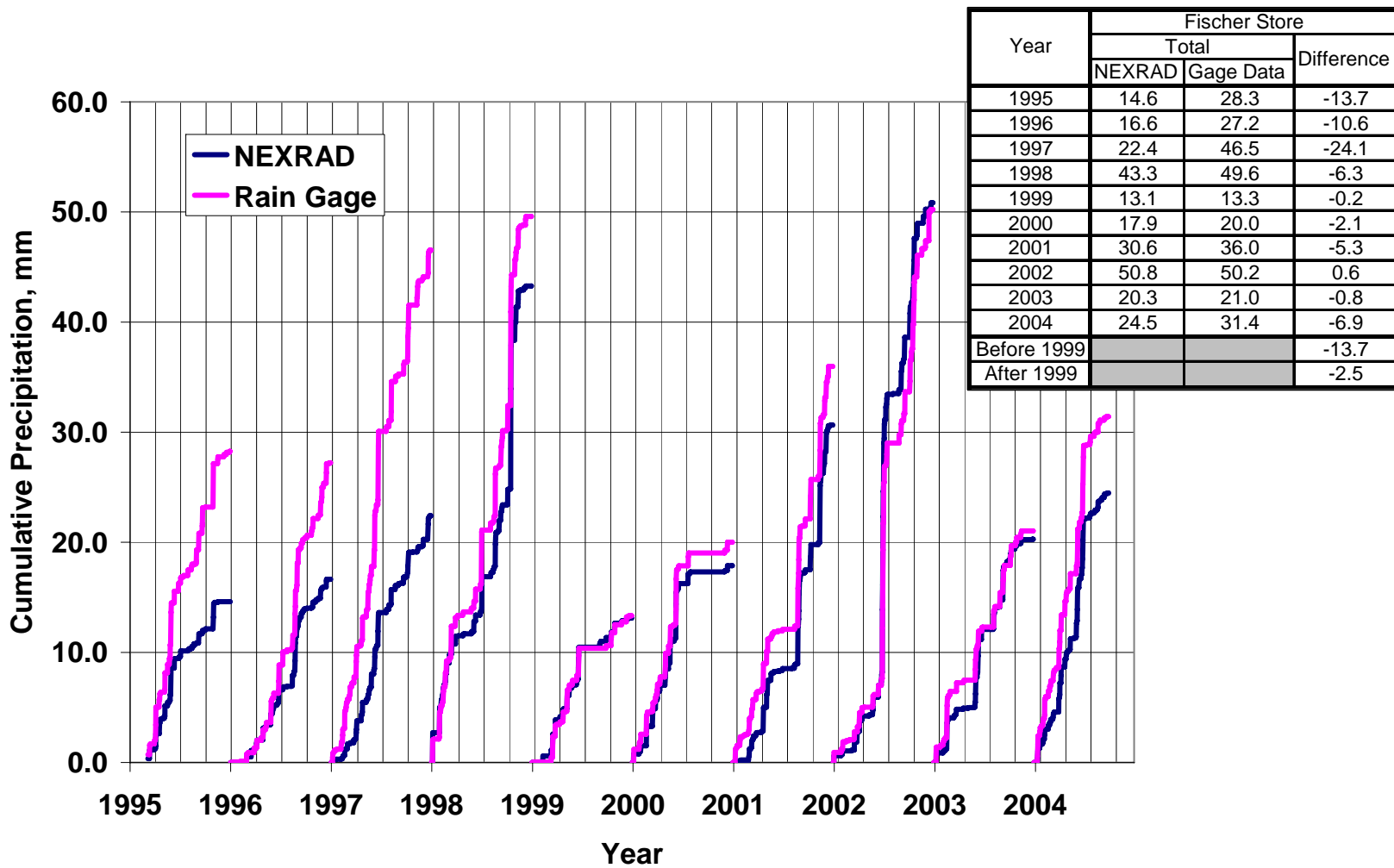


Figure 5.9 – Cumulative precipitation plot of Fischer’s Store gage and NEXRAD data for the corresponding NEXRAD cell.

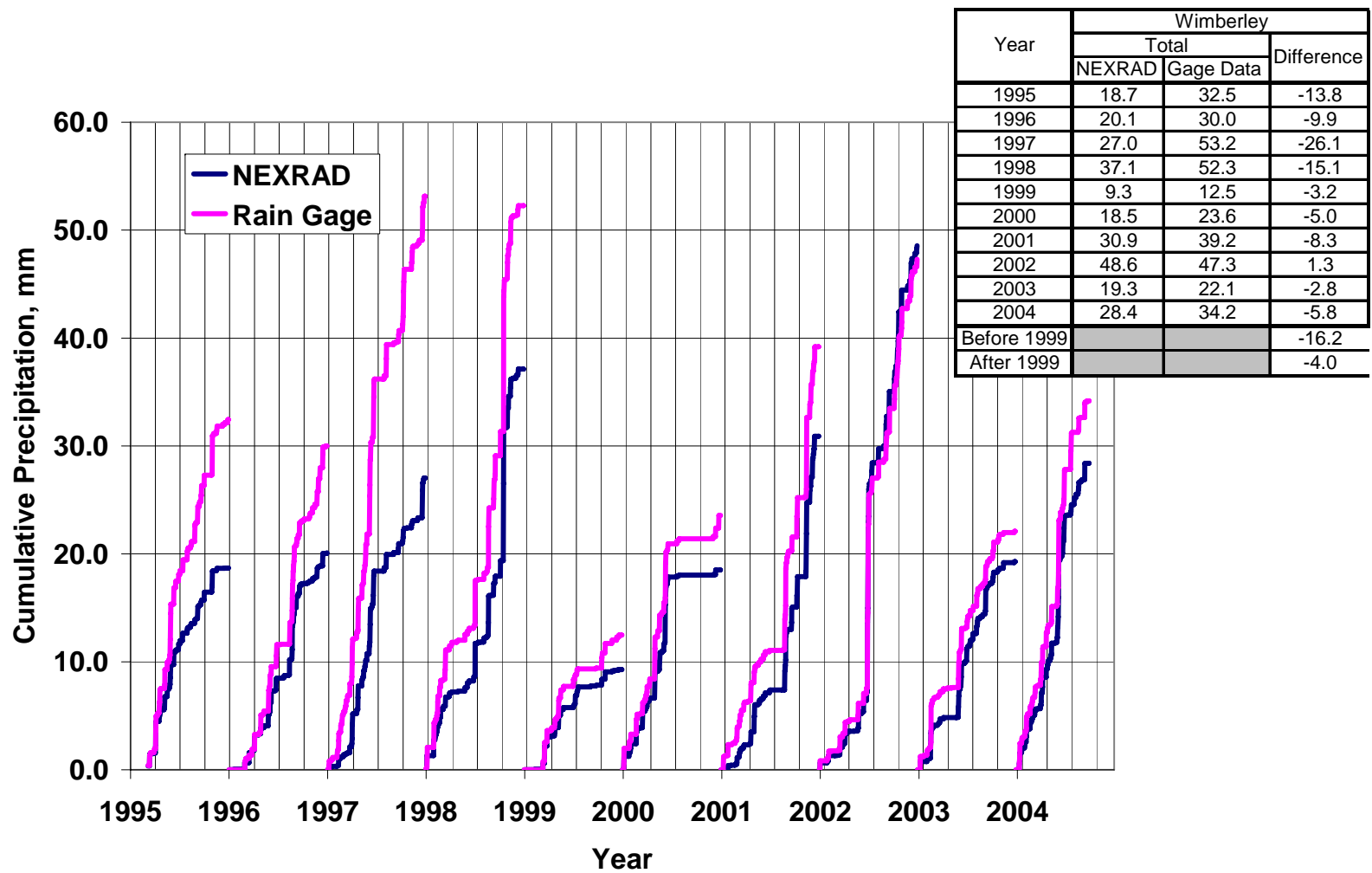


Figure 5.10 – Cumulative precipitation plot of Wimberley gage and NEXRAD data for the corresponding NEXRAD cell.

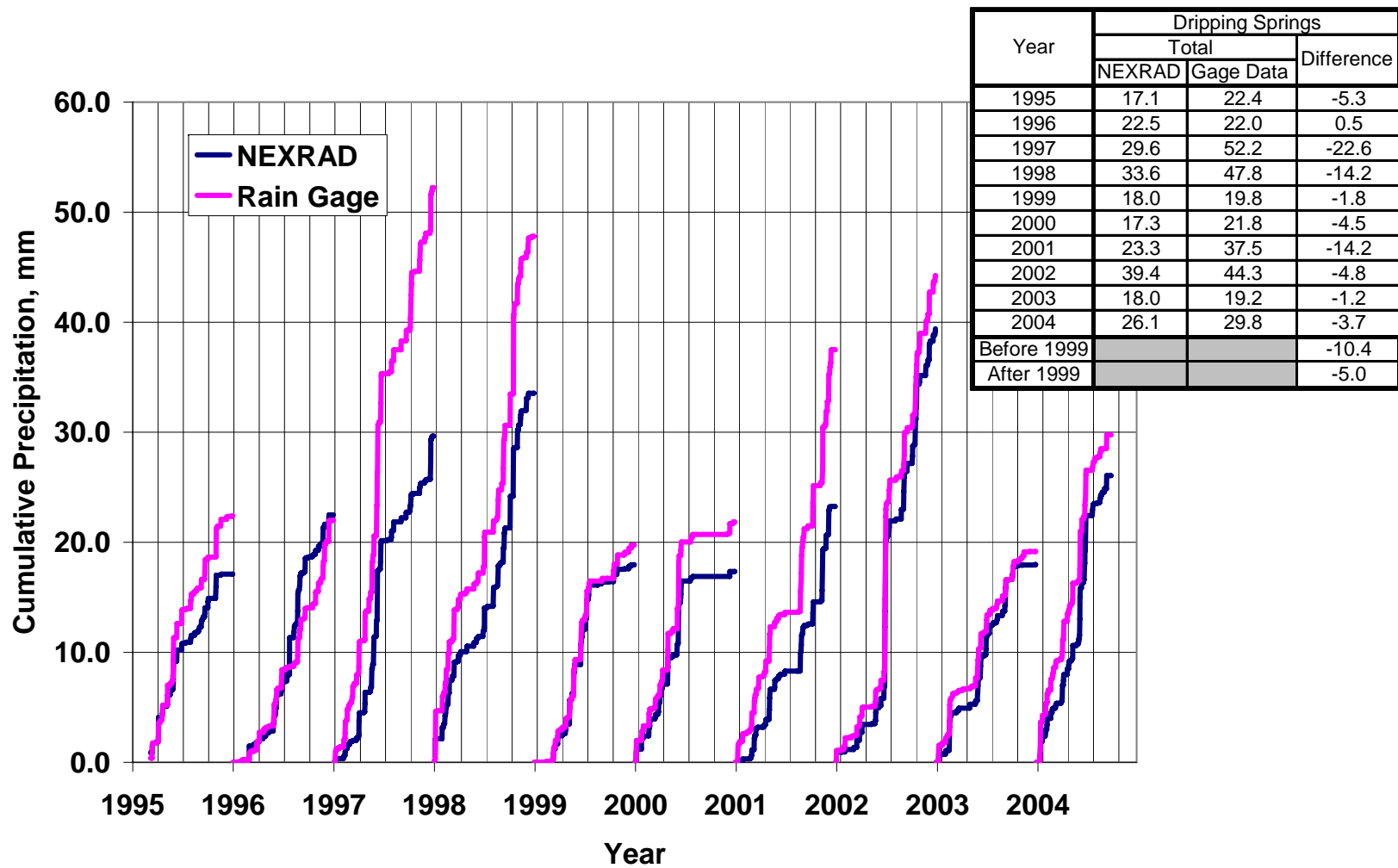


Figure 5.11 – Cumulative precipitation plot of Dripping Springs gage and NEXRAD data for the corresponding NEXRAD cell.

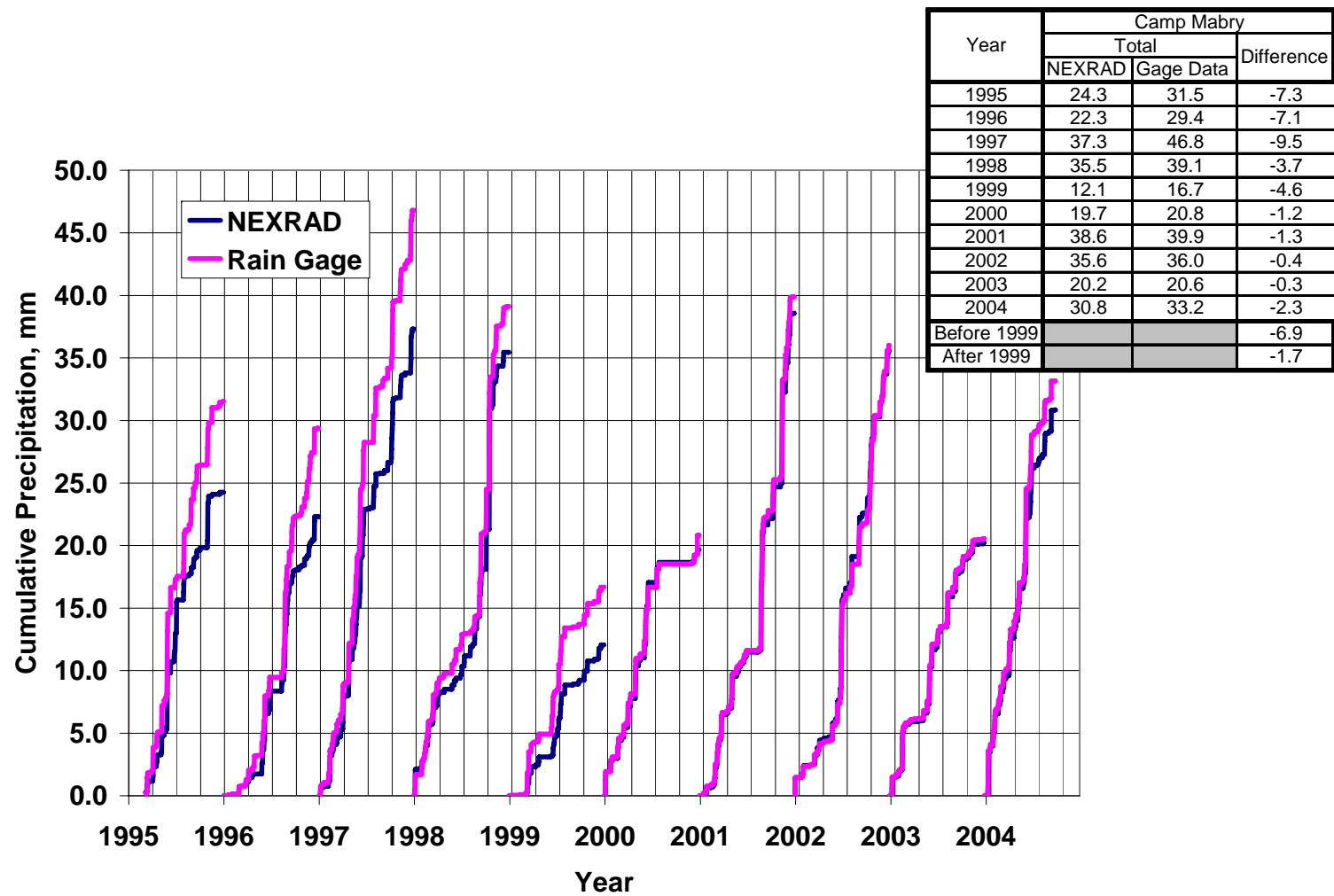


Figure 5.12 – Cumulative precipitation plot of Camp Mabry gage and NEXRAD data for the corresponding NEXRAD cell.

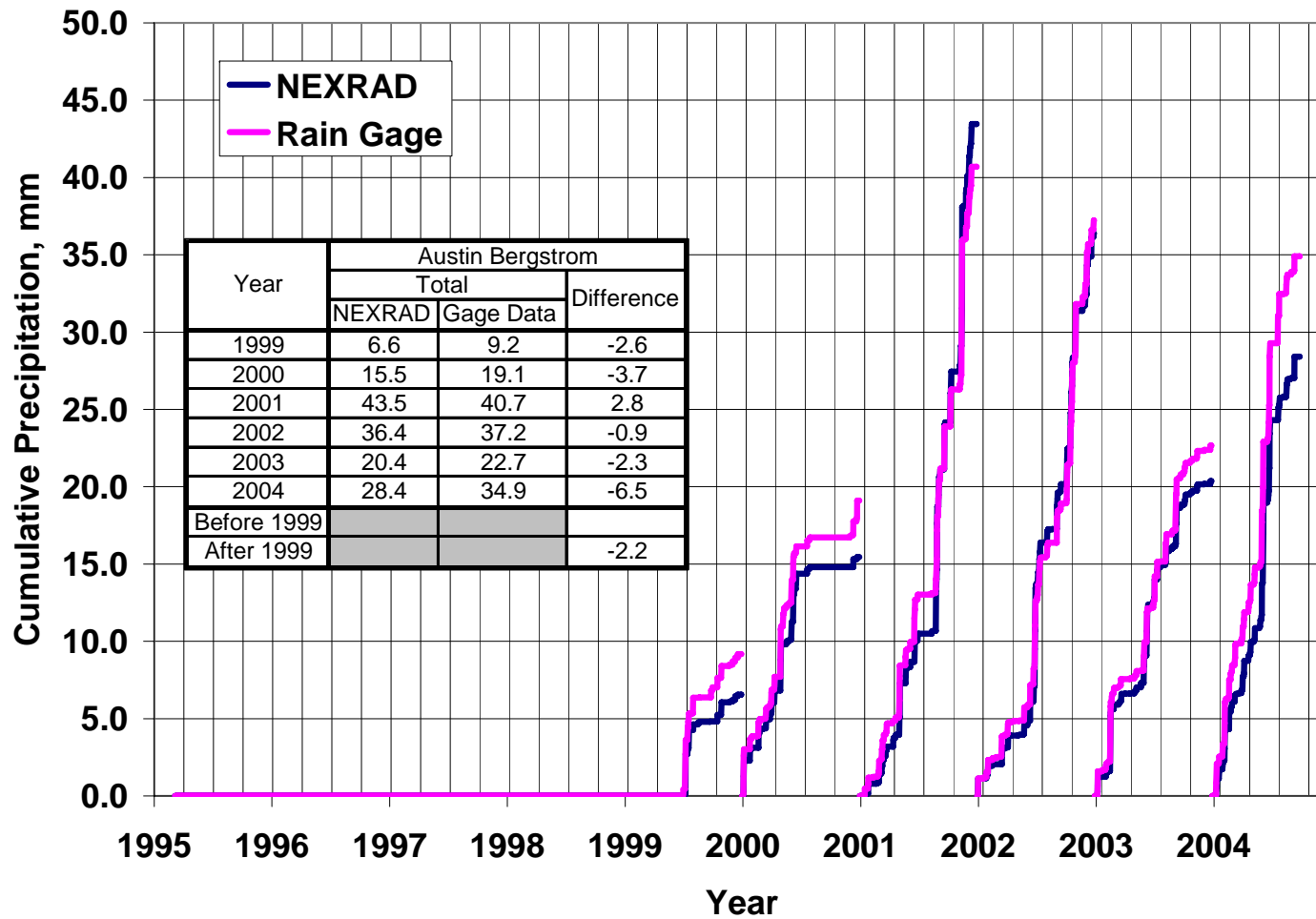


Figure 5.13 – Cumulative precipitation plot of Austin Bergstrom gage and NEXRAD data for the corresponding NEXRAD cell.

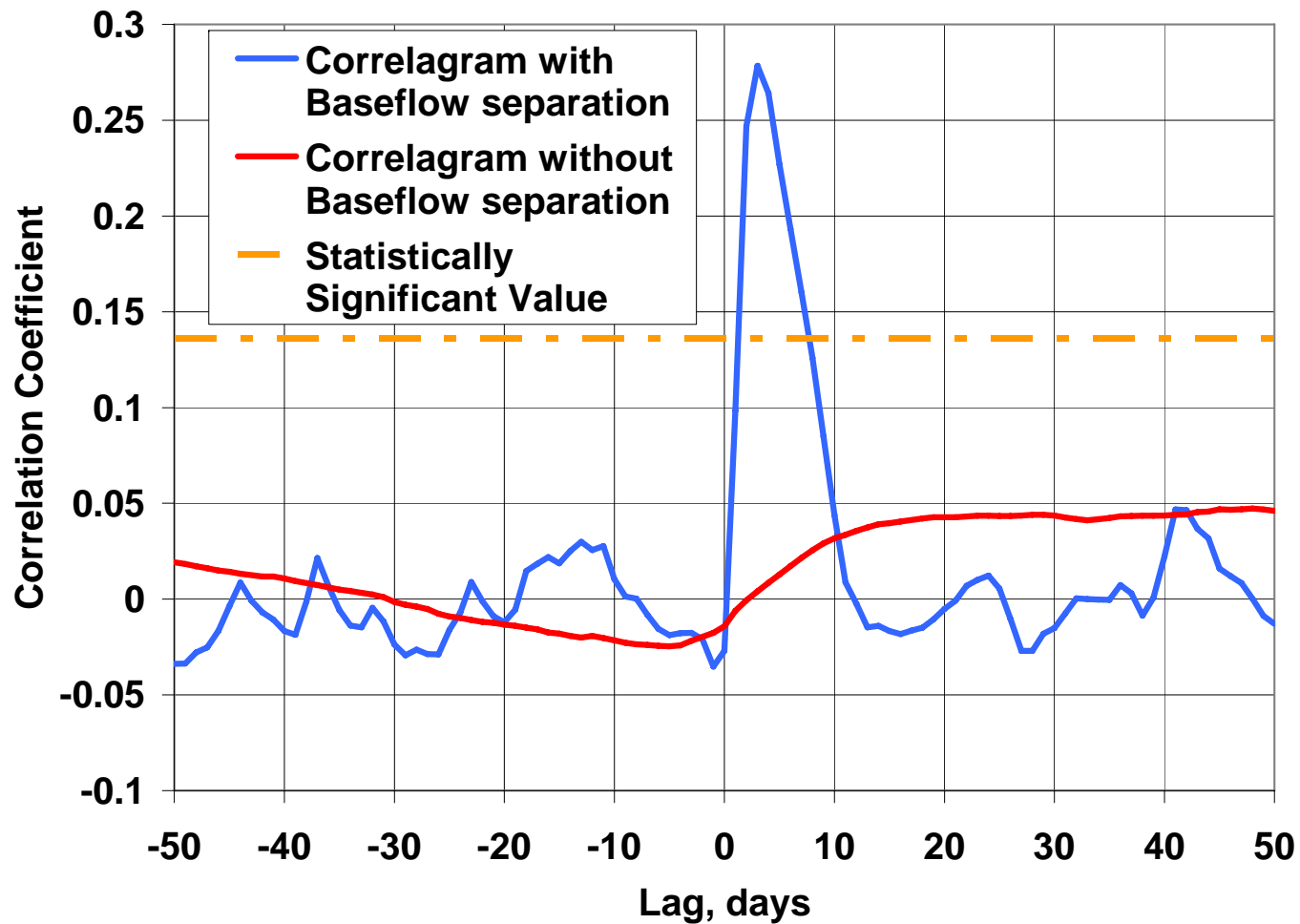


Figure 5.14 – Correlograms from a NEXRAD cell in the recharge zone of Barton Springs. The Blue Correlogram is derived using the baseflow separated discharge at Barton Springs and the red correlogram results when the baseflow is not separated. The orange dashed line is the statistically significant line.

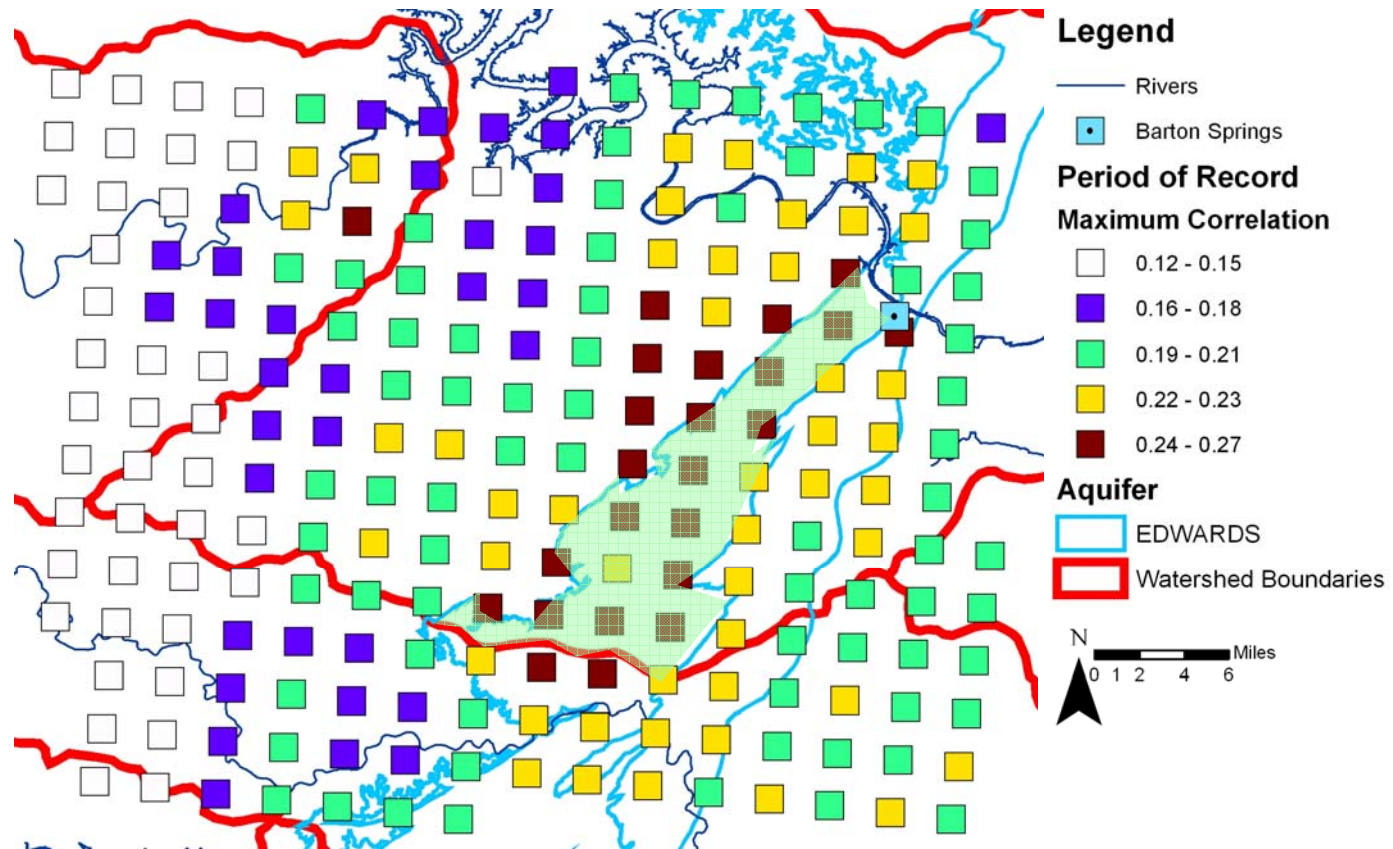


Figure 5.15 – The spatial variation in maximum correlation superimposed over recharge zone of the BSEA. The recharge zone is color-filled in light green.

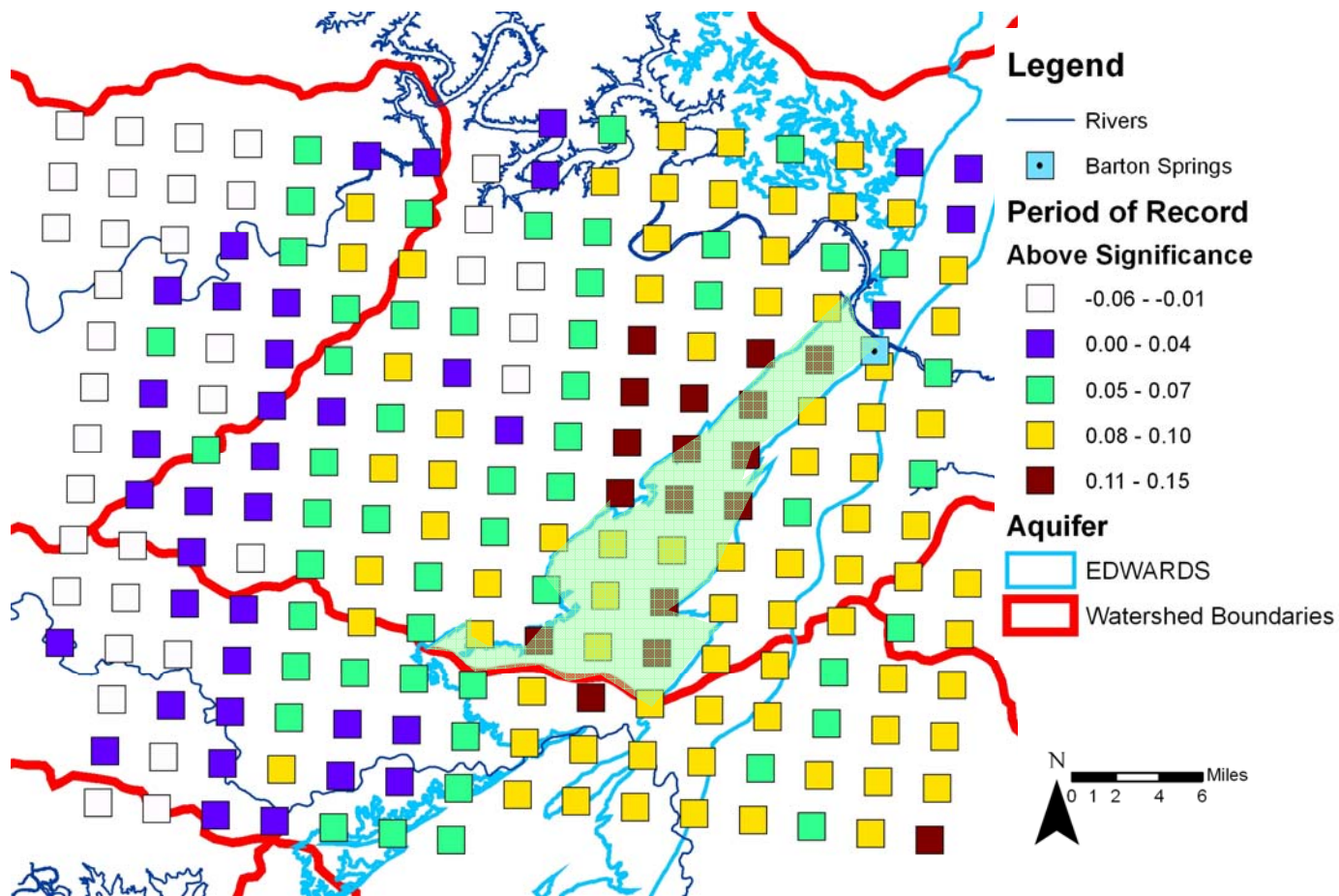


Figure 5.16 – The spatial variation in difference between the maximum correlation and the statistically significant threshold superimposed over recharge zone of the BSEA. The recharge zone is color-filled in light green

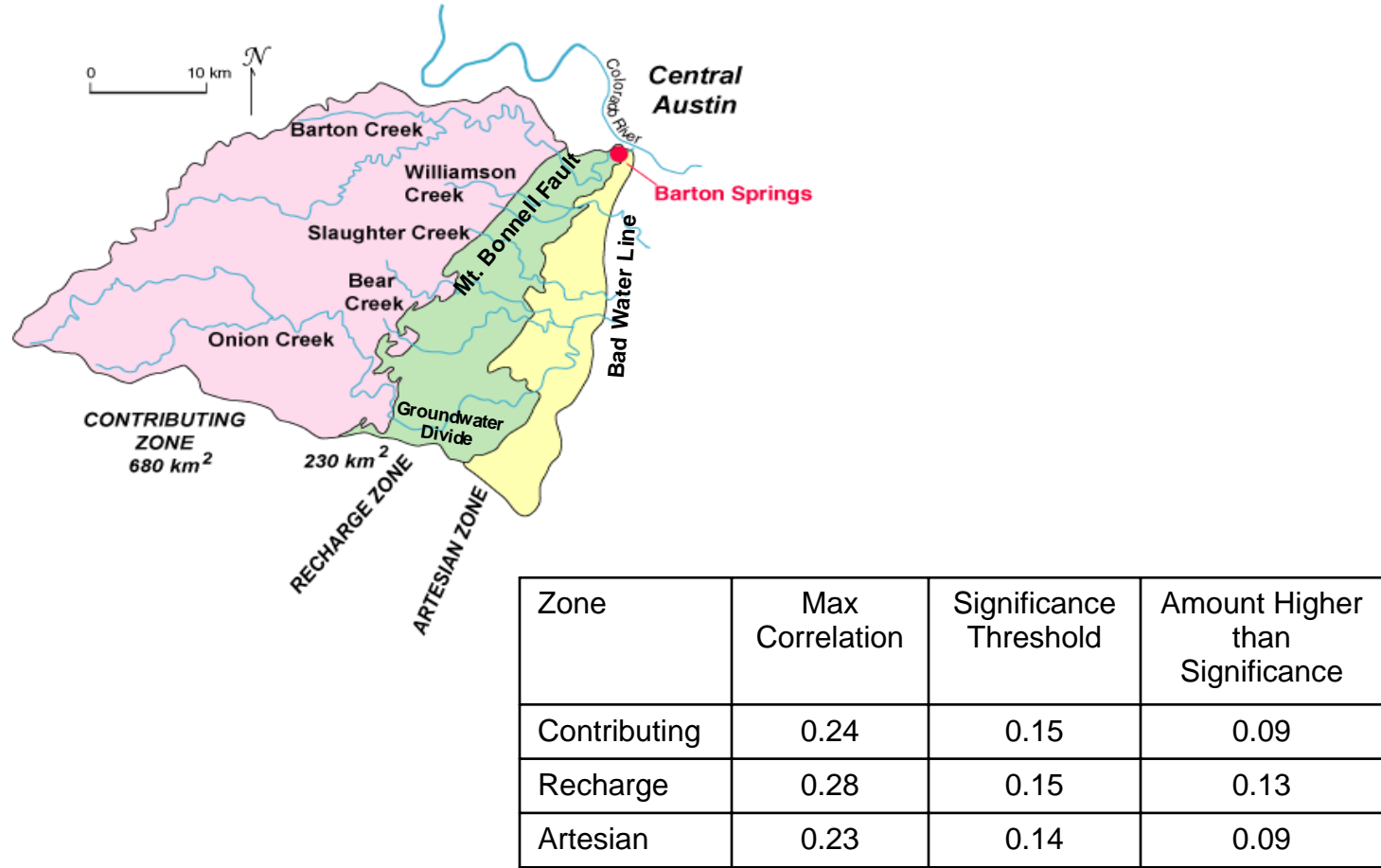


Figure 5.17 – The boundaries of the Barton Springs Aquifer with left to right: the contributing zone, the recharge zone, and the confined or artesian zone (USGS, 2008). The table contains the results from cross-correlation analysis based on averaging precipitation time series over each of these zones.

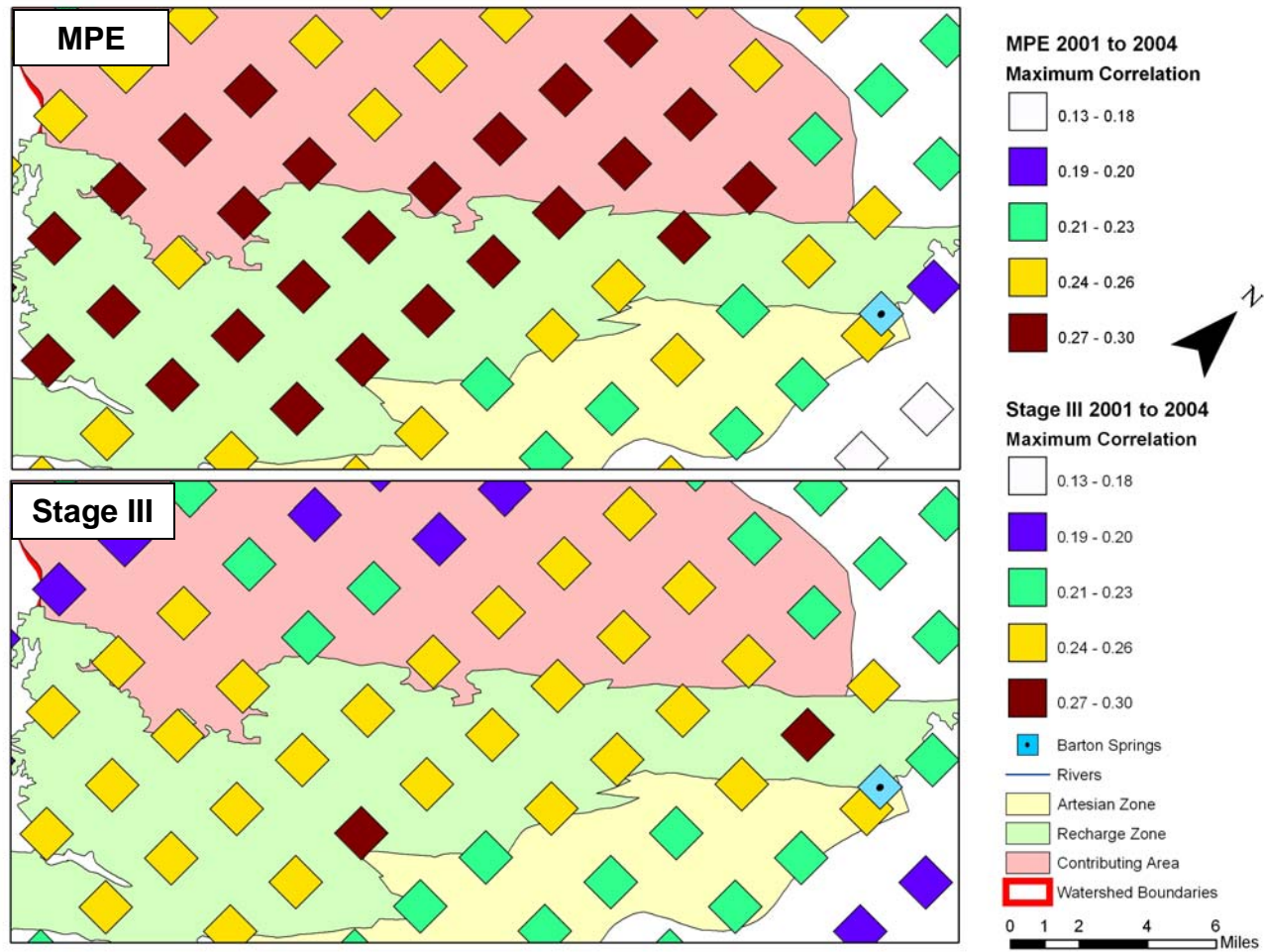


Figure 5.18 – Comparison of cross-correlation analysis using MPE and Stage III data over the BSEA recharge zone using the same color ramp for maximum correlation.

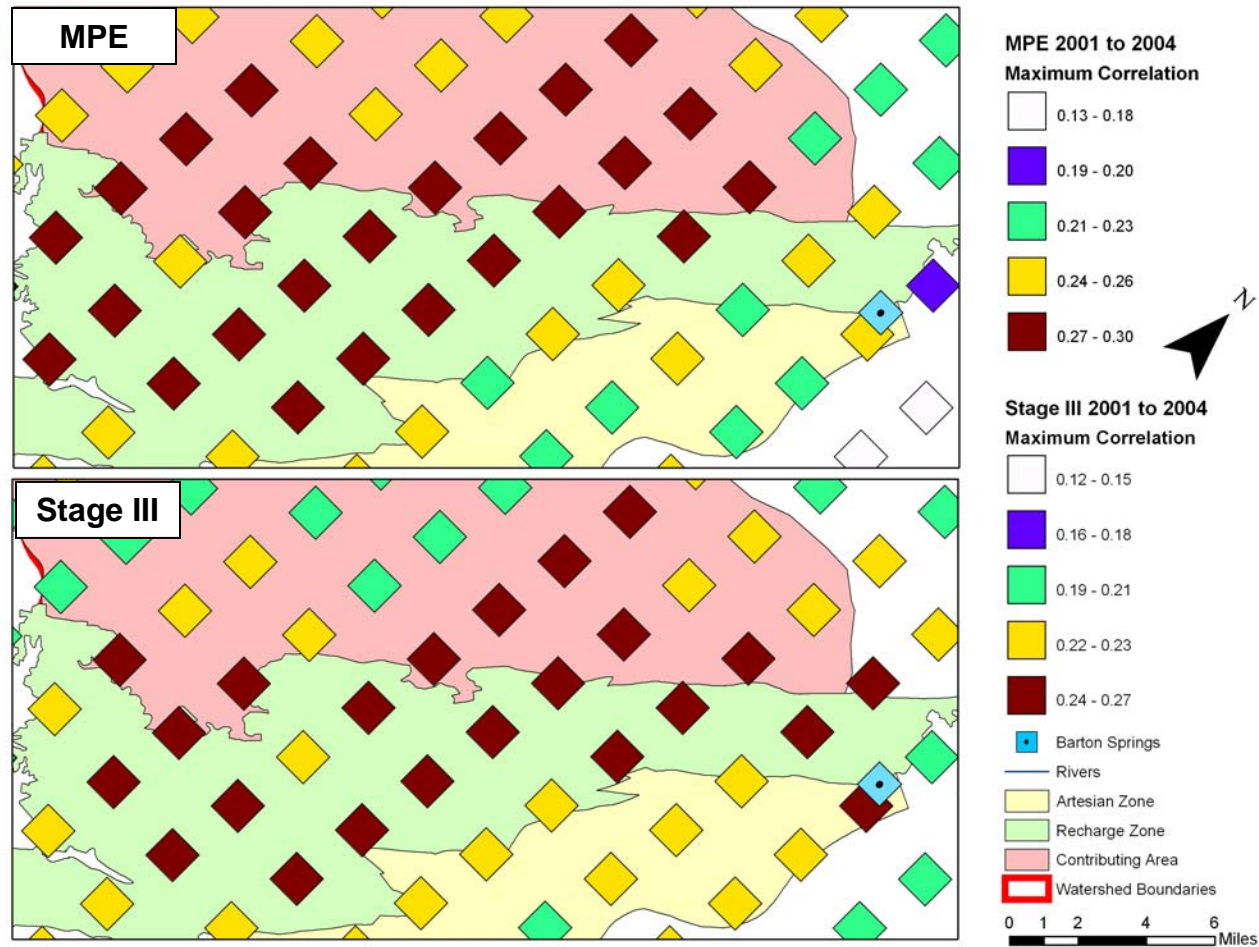


Figure 5.19 – Comparison of cross-correlation analysis using MPE and Stage III data over the BSEA recharge zone using the natural breaks (Jenks) method for color coding maximum correlation.

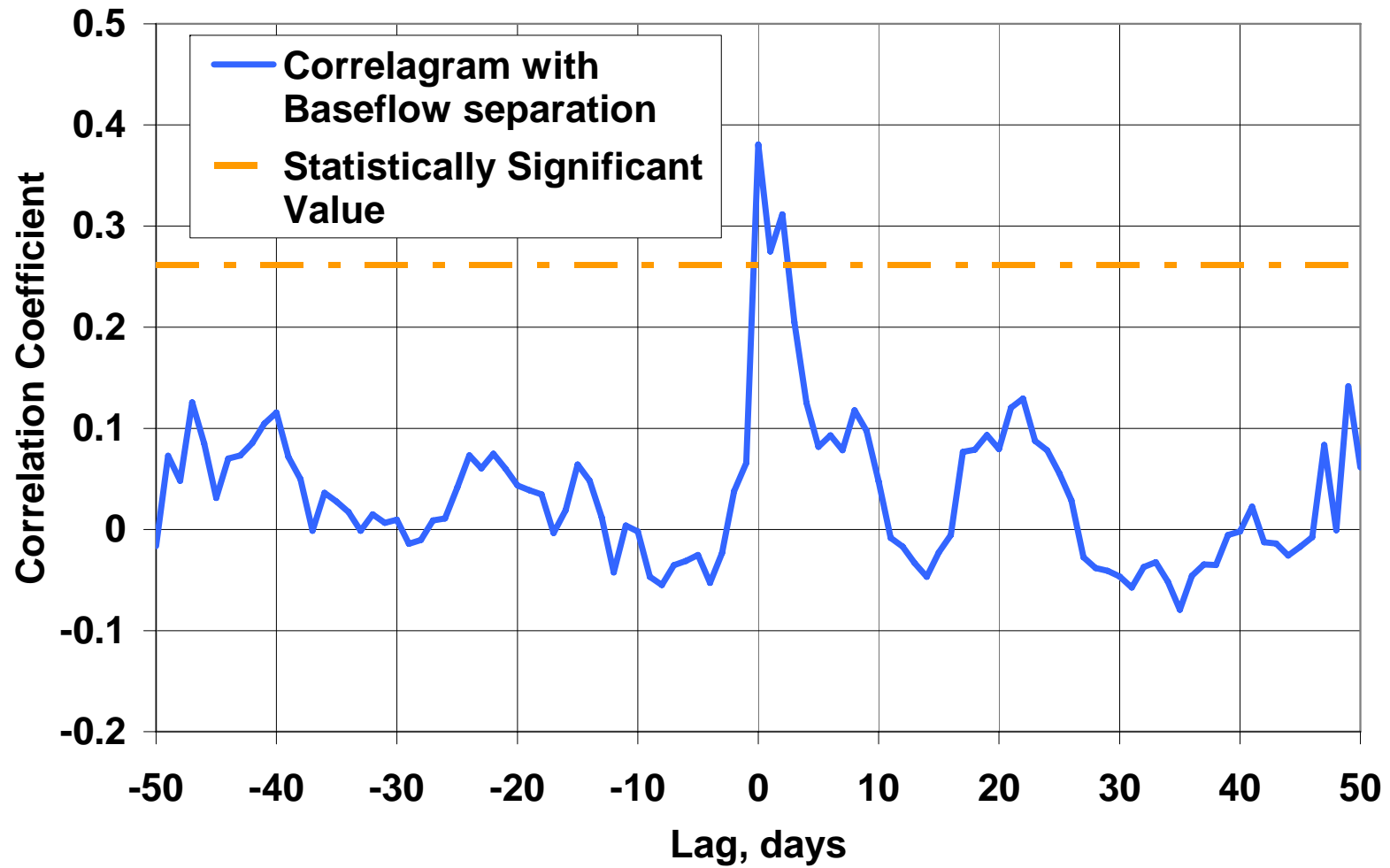


Figure 5.20 – Example of a typical correlogram of a NEXRAD cell near Jacob’s Well.

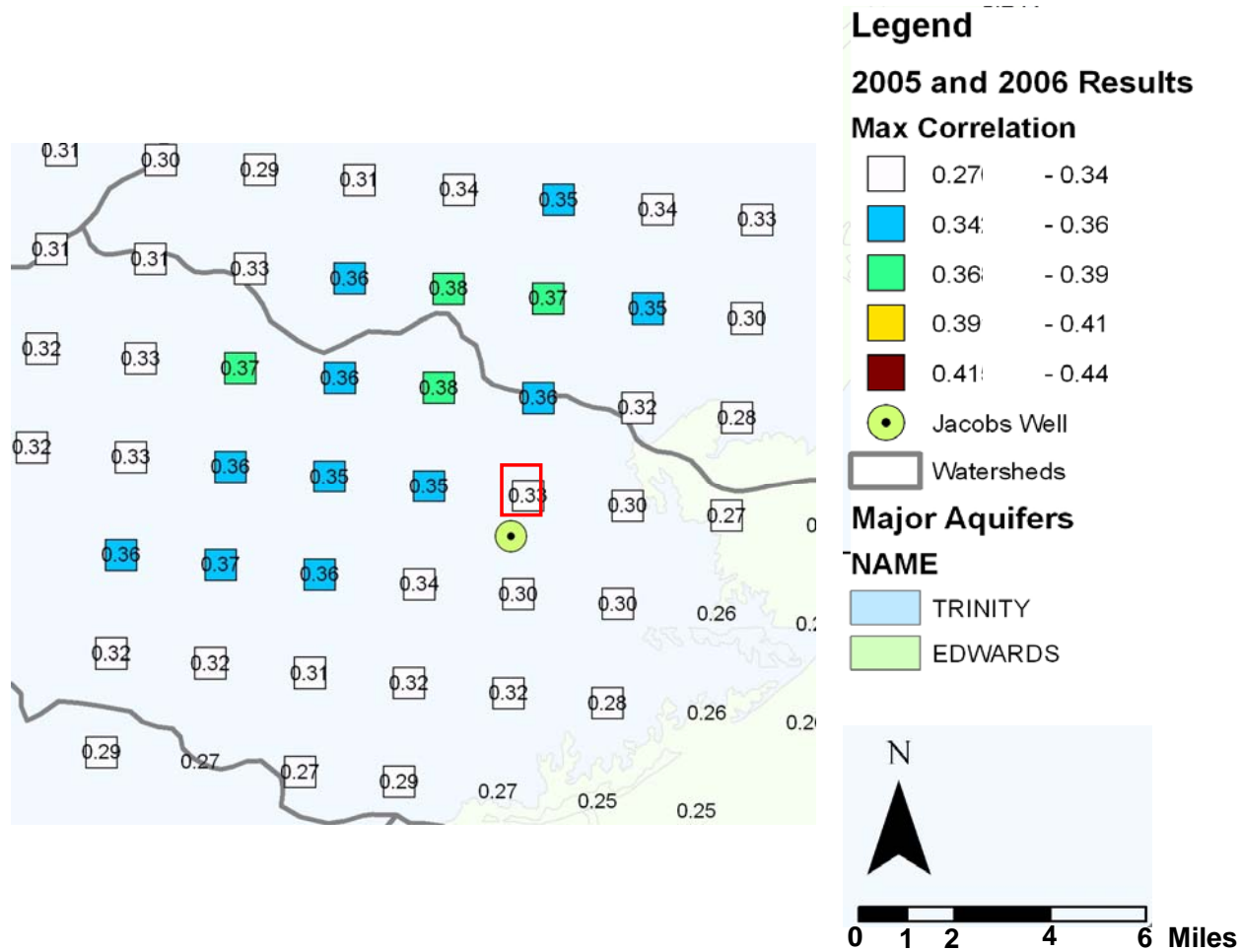


Figure 5.21 – Maximum correlation plot near Jacob’s well for data from 2005 and 2006. The red square indicates the location of a previously conducted dye-trace study.

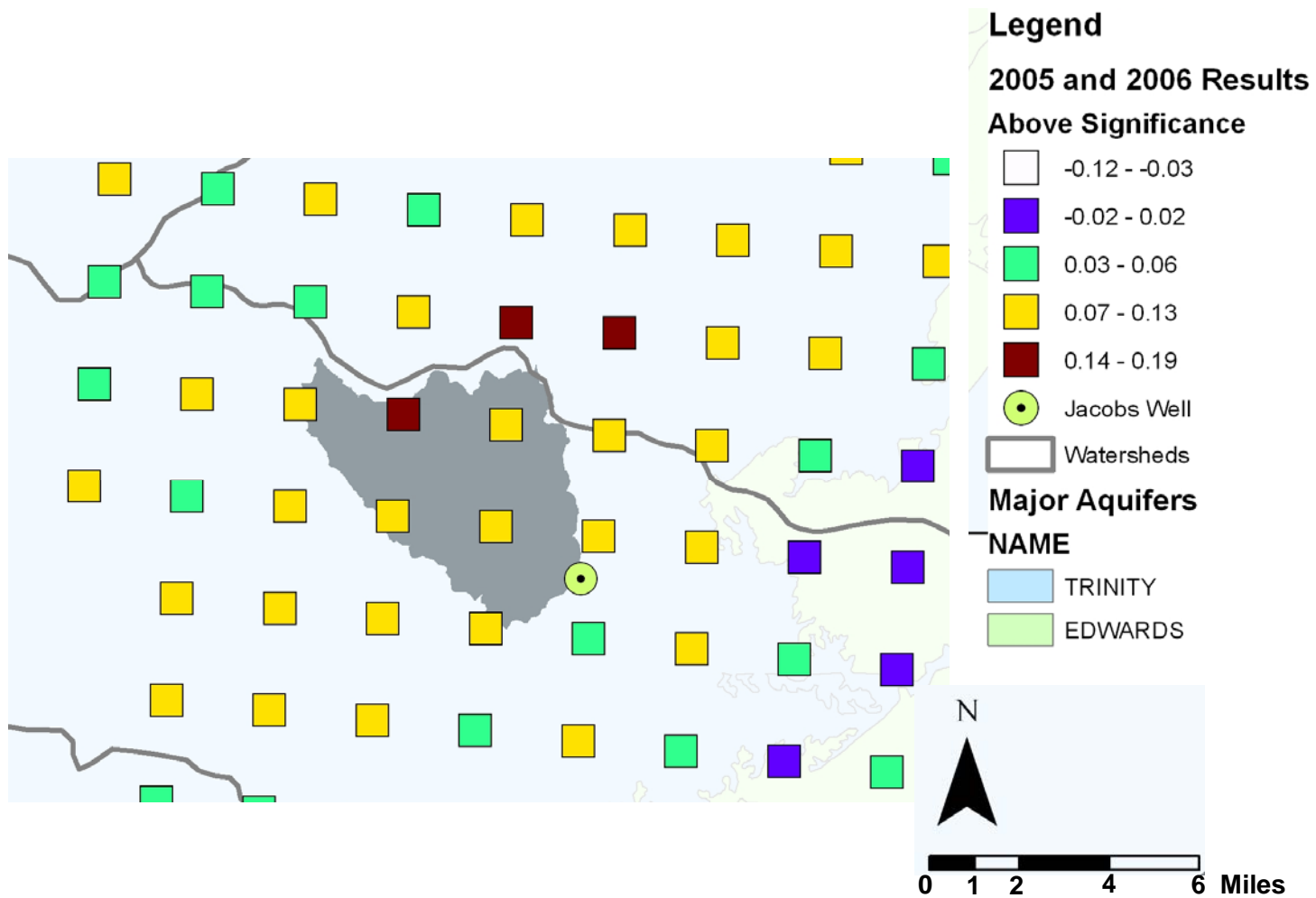


Figure 5.22 Plot of amount above the statistically significant value NEXRAD cells near Jacob's well. The darkened area is the surface water catchment above Jacob's well derived from the 10 m

Chapter 6. Application to GAM

Previous chapters demonstrated the ability to use spatial cross-correlation (SCC) to investigate likely locations of recharge in a karst aquifer. This represents one application of this methodology. Recent investigations (Hunt, 2007, Massei and Mahler, 2007) have shown that during different aquifer conditions, flow to Barton Springs follows varying flow paths. SCC of NEXRAD data and spring discharge can be applied at during high and low aquifer levels to evaluate patterns in recharge during each of the aquifer conditions. The resulting cross-correlation maps are then used for constraining the recharge patterns used in a regional groundwater availability model (GAM) of the BSEA.

First, the cross-correlation analysis at Barton Springs under different aquifer conditions is discussed. This is followed by a discussion of existing models of the BSEA and selection of an appropriate model for applying SCC to constrain model recharge input. Finally, the results of the SCC and the numerical modeling are compared with each other.

APPLYING SCC UNDER DIFFERENT AQUIFER CONDITIONS

The Barton Springs Edwards Aquifer Groundwater Conservation District (BSEACD) is the regulatory agency tasked with managing the groundwater resources in the BSEA. Their duties include monitoring aquifer levels, permitting new wells, and managing the resources during times of drought. This may include restricting use of the groundwater in times of drought or overuse. The BSEACD operates under a management plan that addresses the methods and rules for extracting groundwater from

the aquifer (BSEACD, 2008). As part of its management plan the BSEACD monitors hydraulic head and spring discharge levels to determine allowable pumping rates at permitted wells within the district. There are three status conditions defined by the BSEACD that determine pumping rates for permitted wells in the district, they are: Normal, Alarm, and Critical stage. Figure 6.1 shows a flyer produced by the BSEACD that shows both of these locations and gives the current drought status of the aquifer. When the discharge at Barton Springs drops below 38 cfs ($1.08 \text{ m}^3/\text{s}$) and 20 cfs ($0.56 \text{ m}^3/\text{s}$) the aquifer is classified as in “Alarm” and “Critical” stage, respectively. At this point the management plan calls for conservation measures possibly including a decrease in allowable pumping rate for some users. The status condition of drought is determined by the amount of discharge at Barton Springs and the hydraulic head level at Lovelady well (see Figure 6.2).

Figure 6.3 shows discharge at Barton Springs from 1994 to 2004 including the alarm stage threshold at 38 cfs. Discharge at Barton springs dips below this threshold several times for the given time period. The time-series data for the both discharge and precipitation were divided into two separate sets time-series data. One set of time series data representing the precipitation and discharge when Barton Springs was discharging above alarm stage and the other for when it was discharging below alarm stage. The same algorithms described in previous chapters were applied to these separate time series. Figures 6.4 and 6.5 show the resulting maximum correlation plots for BSEA for above and below alarm stage respectively.

The comparison of each of the plots indicate that there are likely differences in how and where groundwater enters the aquifer at different flow regimes. The maximum

correlations within the contributing and recharge area are located in the unconfined portion of the aquifer when the aquifer is classified as above alarm stage. There is a small section in the northwest corner of Figure 6.4 where highest correlations in the plot exist. However, the NEXRAD cells where these correlations occur are located outside of the accepted boundary of the aquifer and the contributing area. In fact many of the cells are on the opposite side of the Colorado River flowing through Austin, Texas. Also, the value of the correlations are lower (0.18 – 0.20) than those shown in the below alarm stage plot (0.38 – 0.50). This indicates that overall the aquifer is more sensitive to precipitation when the aquifer is classified as below alarm stage. The increased correlation during low aquifer levels also shows a shift in the locations most sensitive to recharge. When the discharge at Barton Springs falls below alarm stage the maximum correlations are located to the southern portion of the aquifer. There are several reasons why these changes in the recharge pattern occur. These are: 1) recharge by-pass when the aquifer is above alarm stage, 2) decreased pumping in the aquifer during the alarm stage and 3) a change in the amount of available storage in the unconfined portion of the aquifer during alarm stage. Each of these is discussed below.

Recharge By-Pass

The majority of recharge to the BSEA occurs through discrete features including sinkholes and creek beds (Slade, 1985, Hauwert, 2006). These mechanisms are discussed in more detail in Chapter 2. However, there is an upper threshold for the amount of recharge that can enter the aquifer (Scanlon, 2004). When the aquifer levels are high it is more likely that precipitation in the recharge and contributing area could by-pass the

discrete recharge features. This would one reason why cross-correlation values are dramatically lower when the flow at Barton Springs is classified as above alarm stage.

Decreased Pumping

Figure 6.6 illustrates a typical distribution of pumping found in the BSEA as included in the regional groundwater model developed by Scanlon et al. (2001). The majority of the large scale pumping occurs in the southern portion of the aquifer. When the aquifer is in alarm stage and pumping restrictions are enforced, pumping is limited in the southern section. Discussions with the Brian Smith, senior hydrogeologist with BSEACD, revealed that when pumping rates are reduced during alarm stage, the majority of reductions are made to wells in the southern portion of the aquifer (Smith, 2006). The apparent change in recharge pattern can be partially attributed to this reduction of pumping volume in the southern portion of the aquifer. The reduction in pumping would allow the recharge to by-pass extraction wells and flow northward toward the spring.

Unconfined Storage

Another factor in the change in location of recharge patterns may have to do with aquifer storage. Figure 6.7 shows a hypothetical depiction of a typical karst aquifer. When the average hydraulic head is decreased, as is observed during alarm stage, there is more available storage in the unconfined portion of the aquifer. Precipitation entering the aquifer as recharge may remain in the unconfined portion of the aquifer for an extended period of time as it travels toward the spring. This can reduce the observed response in the discharge hydrograph, reducing the correlation value obtained from cross-correlation analysis. However, this does not mean that the unconfined portion of the aquifer does not

add recharge to the aquifer, it only suggests that the affect of this recharge does not show a response in the Barton Springs hydrograph over the short-term. Massei and Mahler (2007) also indicated this as a possibility with their statistical analysis of specific conductance data at Barton Springs. They showed that the low hydraulic head levels allowed the water to have an increased residence time in the unconfined portion of the aquifer resulting in increased mineralization of the outflow.

CONSTRAINING BSEA GAM

SCC indicated different recharge patterns for flow at Barton Springs under different aquifer conditions. This agrees with the findings of Massei and Mahler (2007) and with information received from BSEACD (Smith, 2006). These types of data can be useful in constraining groundwater models. Using an available regional groundwater model, an analysis of the recharge rate and pattern was conducted to compare with the results of the SCC. An analysis was conducted using semi-automatic calibration methods in the software package PEST to look at what changes could be made to the input recharge pattern that would decrease model residuals with respect to spring discharge. This section is divided into subsections that discuss how the analysis was completed. First, the available models of BSEA are discussed. Then, a description of the model selected for this application is presented. Next, an overview of the semi-automatic calibration methods using PEST is given. Finally, results of the analysis are presented with a comparison to the SCC analysis at Barton Springs.

Previous Models of BSEA

Three models have been developed for the BSEA. Each of these was developed for different purposes and using different numerical codes. This section gives a brief overview of the three models, discusses which of the three was selected for this application, and gives more details on the selected model.

Three models

Slade and others (1985), Barrett and Charbeneau (1996) and Scanlon and others (2004) have all developed models of the BSEA. Slade and others built a two-dimensional finite-difference model using a numerical code developed by the USGS (1976). The main focus of the Slade and others model was to develop hydraulic parameter values across the aquifer. The model had a total of 318 cells across the entirety of the BSEA with two zones of hydraulic conductivity. Barrett and Charbeneau developed a lumped parameter model as a prediction tool for water quality and quantity at Barton Springs. The model contained only five computational cells and greatly simplified the heterogeneities of the aquifer. In 2001 Scanlon and others completed a MODFLOW96 model of the BSEA. The model contained one model layer with 14,400 model cells (120 columns and 120 rows). The purpose of the modeling was to predict changes in groundwater levels and spring discharge due to increased pumpage and droughts.

Selected model

Of all the available models of BSEA, Scanlon and others contained the most refined model grid and described the heterogeneities in the aquifer with the greatest detail. The purpose of this study is to investigate recharge patterns in the aquifer with

respect to analyses conducted using cross-correlation analysis. Therefore, the ability of the model utilize variable patterns of recharge is important. This model provides the best means to conduct this investigation because of the relatively fine grid resolution. Furthermore, in 2001 the model was adopted into the Groundwater Availability Model program for the State of Texas. It is used by the state to aid policy decisions with respect to the aquifer. The details of this model is discussed further in the following sections. The sections include a discussion of the GAM program in Texas, a more detailed discussion of the boundary conditions and hydraulic properties assigned to the model, and a detailed discussion of how recharge was input in the model.

Texas GAMs

In 2000 the State of Texas embarked on the development of groundwater availability models for groundwater resources within the state. Using the numerical groundwater modeling software MODFLOW96, funds to create numerical models for all major aquifers and some minor aquifers within the state were allocated through the Texas Water Development Board. To date, 20 models have been developed through the GAM program. Seventeen models represent the nine major aquifers found in Texas, while the remaining three were created model several of the minor aquifers within the state. These models represent 95% of the total groundwater resources available within the State (TWDB, 2000). The GAM program is designed to use the best available scientific data to create numerical groundwater models that provide quantitative estimates of the amount and possible use of groundwater resources of a given aquifer. The GAMs provide management entities with powerful tools for regulating the state's groundwater resources.

Groundwater districts and planning agencies are required to use GAM simulations for development of management plans and district rules. The regional model of the BSEA developed by Scanlon et al. (2001) has been accepted as the State sanctioned GAM for the BSEA.

BSEA GAM

The BSEA GAM is a one-layer MODFLOW96 model. The purpose of the model is to predict changes in spring discharge and groundwater level in response to variable pumping rates and changes in recharge. Figure 6.8 and 6.9 show the aquifer domain along with the hydraulic conductivity pattern and the major faults (horizontal flow barrier package) used in the model. Constant values were used for specific yield (0.05) and specific storage (0.0005). Springs were modeled using MODFLOW drain cells in the locations shown in Figure 6.9. The model was calibrated in steady state and transient mode to both hydraulic head and spring discharge data. Figure 6.10 shows cross-plots for hydraulic head measurements for the steady state calibration. Figure 6.11 shows the transient calibration of spring discharge on a one-month time interval at Barton Springs. For the most part the model reproduces the hydrograph reasonably well. The overall RMS of the hydrograph is 12 cfs. This represents 10 percent of the range of discharge values at the site.

Model Recharge

The recharge input for the BSEA GAM was organized using a zonal approach to discretization. A zonal approach means that sets of computational grid cells were assigned an equal value of recharge that differed from a group of adjacent cells. In the

BSEA GAM six zones were established (see Figure 6.12). Five of these zones represent recharge entering the system through stream beds as they flow across the recharge zone. The other zone represents diffuse recharge outside of the stream beds. The recharge rates were based on a mass balance of USGS stream gage data. The methodology for calculating the recharge rates was developed by Slade and others (1985) for the development of their BSEA model. They estimated that up to 80% of the recharge came through the stream beds. However, recent research by Hauwert (2007) indicates that this percent may be high and that more of the recharge enters through sinkholes and caves outside of the five main stream channels.

PEST Summary

PEST, short for Parameter ESTimation, is a software package used to aid in the calibration and uncertainty analysis of numerical models. Figure 6.13 shows a schematic of how PEST can be utilized in numerical modeling. A control input file is created by the user that interprets the inputs and outputs from any computer application. Based on the information provided in the control file, model input parameters are incrementally changed and simulated while the output of the model is compared to the observed data provided by the user. PEST compares the output to the observed data and calculates an objective function. PEST continues altering the specified input parameters until the value of the objective function falls below a user specified threshold or until PEST cannot lower the objective function further. PEST can be used to calibrate numerical models semi-automatically and determine uncertainty in model parameters. It has become increasingly popular as noted by the recent technical session in the last Geological

Society of America (GSA) conference being dedicated to applications of inverse models including PEST (GSA, 2007). This application utilizes the semi-automatic calibration features of PEST (PEST,2007).

Recently development of PEST has centered on the use of pilot points (Doherty, 2003). Pilot points allow flexibility in the spatial value of input parameters. Traditionally, parameter estimation of hydraulic properties in groundwater model consisted of dividing the computational grid into zones of constant values. This method is called zonation. Figure 6.8 illustrates the zones used for the BSEA GAM for hydraulic conductivity. Pilot points can also represent values for any model input parameter. However, in the case of pilot points the values are assigned to the computational grid through interpolation. Values in each grid cell may differ depending on the interpolation methods used. This adds flexibility in parameter values assigned to the computational grid and can also reduce the number of parameters that are estimated (Doherty, 2003). Furthermore, pilot points are not only used to assign raw hydraulic properties, they can also be used to alter existing property fields in a model. Figure 6.14 shows an example of pilot points that range in value from 0.0 to 3.0. When these pilot points are interpolated the result is a grid of values that can be multiplied with a grid of zonal values the multiplication results in new values that vary spatially. An example of a multiplier grid is shown in Figure 6.15. The multiplier grid is commonly referred to as a “warping grid” because it alters or warps existing model parameter values. Warping an existing field is a common method for conducting a sensitivity analysis on existing models (PEST, 2007, URS,2005). Altering the recharge field with a warping surface the PEST simulation is identifying regions in the aquifer where recharge is more likely to occur or not. A higher

value for the warping surface indicates the location where recharge is more likely and a lower value indicates a location where recharge is less likely.

Application of PEST to the BSEA GAM

PEST was used to alter the recharge of the BSEA GAM to evaluate how changes in the recharge field affect the spring discharge calibration. The BSEA GAM was designed estimate changes in spring discharge resulting from changes in future pumping and recharge conditions. The pumping rates in the transient model will not be changed because they are derived from field observed values. The recharge rates and pattern will be altered in order to decrease the objective function with respect to Barton Springs. If changes in model recharge that decrease the objective function are similar to changes suggested by the SCC application, this indicates that the SCC application can be an important tool for constraining recharge conceptual models for regional groundwater model calibration.

The application of PEST was completed by altering the recharge field using two sets of pilot points. The first set represents the warping surface of the recharge field when the aquifer is above alarm stage, and the second represents the warping surface when the aquifer is below alarm stage. The spatial location of the pilot points was the same in each of the aquifer conditions. However, the above alarm stage pilot points were used to warp the model recharge only when spring discharge was above alarm stage and vice versa for the pilot point warping surface for the below alarm stage. PEST was allowed to adjust the warping values of each of the pilot point locations within the range of 0.5 to 3.0 in order to decrease the objective function with respect to discharge at

Barton Springs. In order for PEST to run the BSEA GAM several custom pieces of software were developed. One code translated the warping surfaces created by pilot point interpolation into a valid MODFLOW96 package. Another was needed to change binary output from MODFLOW96 into an ASCII format usable by PEST.

Overall, PEST was able to reduce the objective function of simulated versus observed spring discharge at Barton Springs by 15%. Figures 6.15 and 6.16 show the final warping surfaces created by PEST for above and below alarm stage respectively. The magnitude of change in the below alarm stage averaged 1.5 while the values of the warping surface above alarm stage averaged 1.1. Further, there were evident differences in the spatial pattern of the warping surfaces. The highest values of the above alarm stage condition are closer to Barton Springs, while the highest values for below alarm stage are in the southwest portion of the aquifer.

COMPARISON OF RESULTS FROM SCC AND GAM APPLICATIONS

The results from both the SCC and GAM applications show similar trends in where recharge is focused. For below alarm stage, the southern portion has increased values for both applications. This indicates that more recharge enters in this portion of the aquifer when the hydraulic head in the aquifer is low. For the above alarm stage condition, the warping surface shows some variations in the aquifer. However, the magnitude of change is less than what was determined in the below stage condition. The location of the high value is close to the location of Barton Springs which is consistent with higher correlation values from the SCC when the spring discharge above alarm stage seen in Figure 6.4.

The application shows how SCC can be utilized to constrain model recharge input during construction and calibration of regional groundwater models. By using the relationships shown from SCC analysis conceptual model design could have included the understanding of different recharge patterns for different aquifer conditions within the recharge package of the model.


Drought Status: No Drought

Barton Springs/Edwards Aquifer Conservation District
 January 24, 2008



Barton Springs Discharge
(cubic feet per second)



Lovelady Monitor Well Depth to water level
(feet)

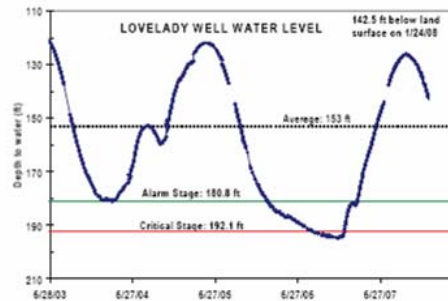
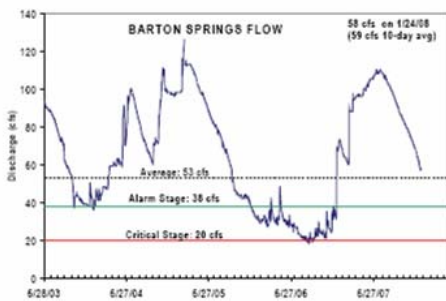
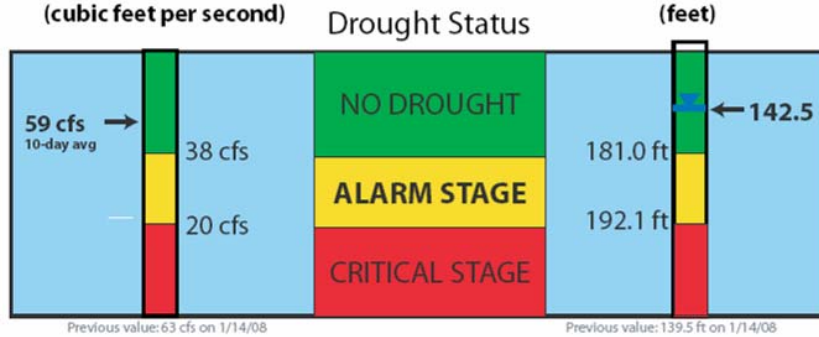


Figure 6.1 – Flyer produced by the BSEACD that shows both of these locations and gives the current drought status of the aquifer.



Figure 6.2 – Location of the Lovelady Well and Barton Springs with respect to the BSEA.

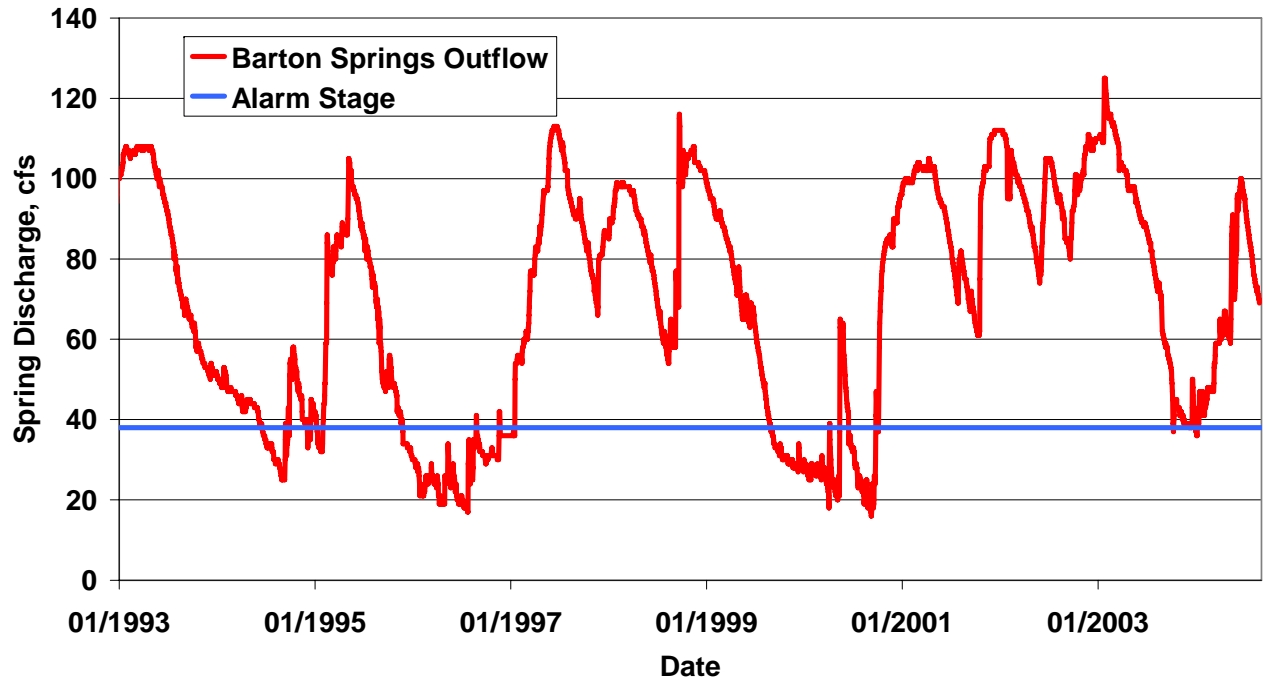


Figure 6.3 – Discharge hydrograph at Barton Springs from 1994 to 2004 including the alarm stage threshold at 38 cfs.

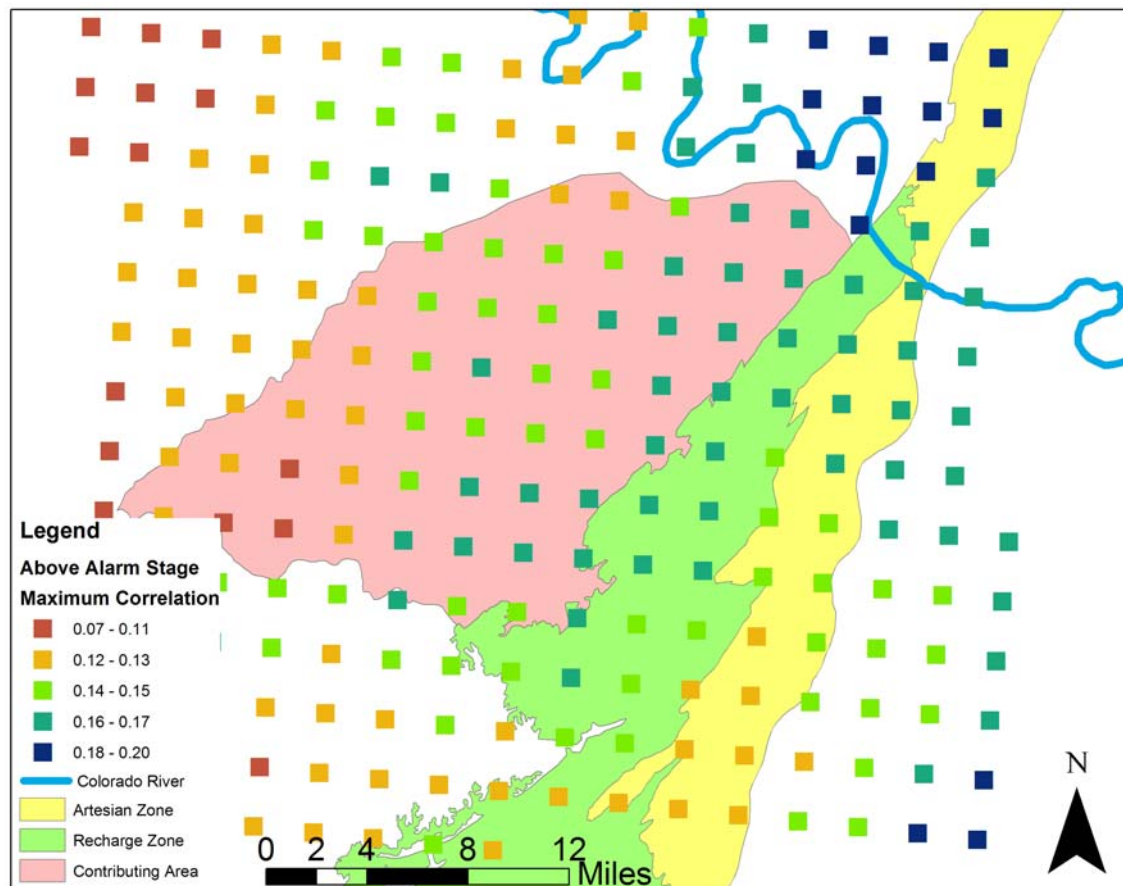


Figure 6.4 – Maximum correlation plot for BSEA when aquifer conditions were above alarm stage.

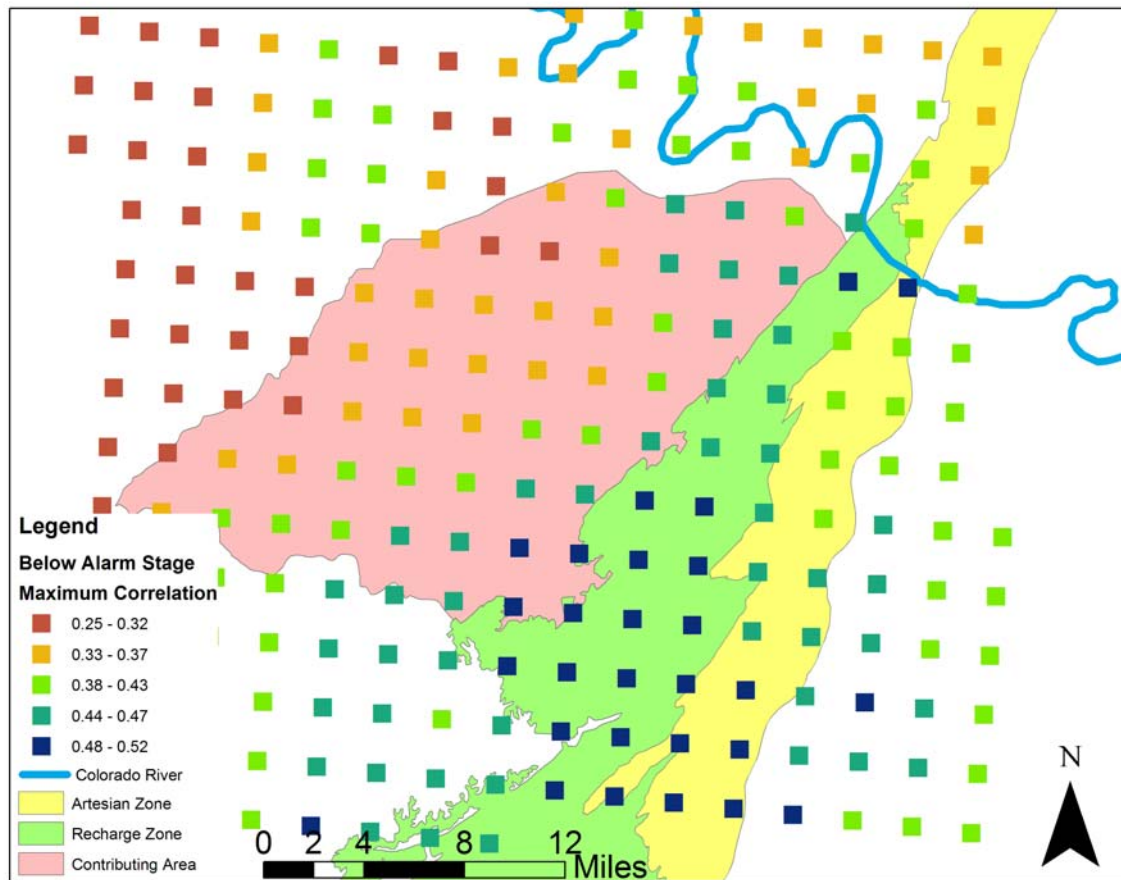


Figure 6.5 – Maximum correlation plot for BSEA when aquifer conditions were below alarm stage.

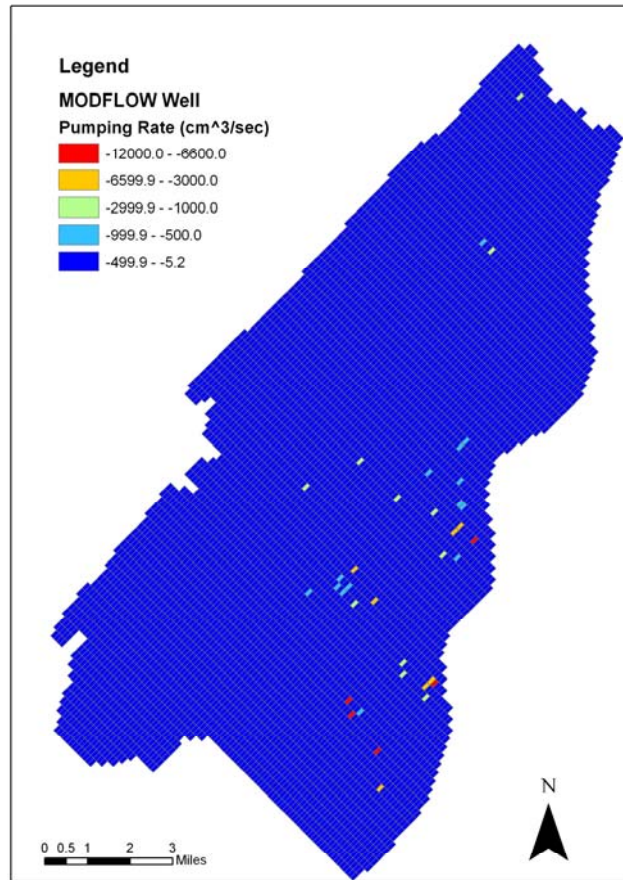
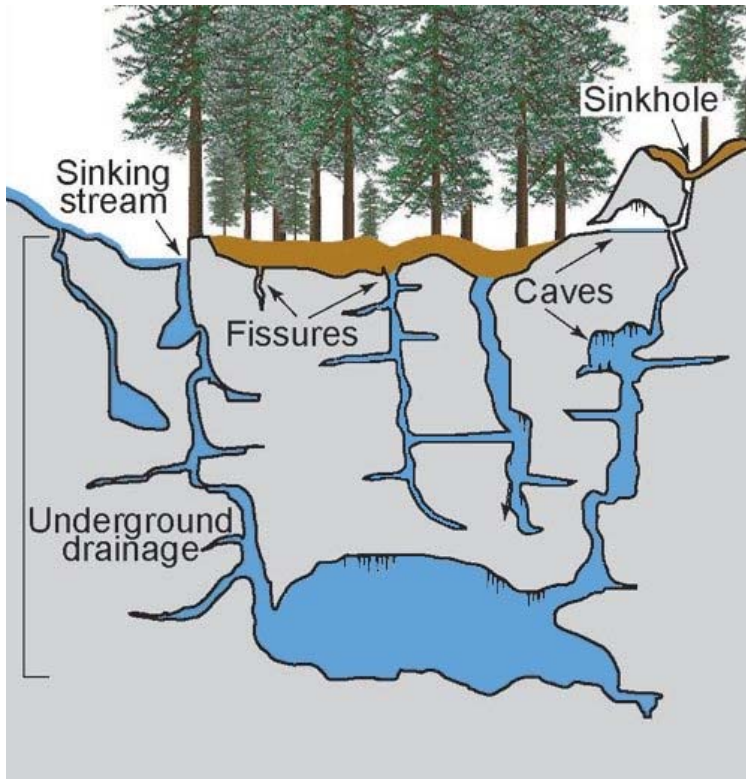


Figure 6.6 – Pumping distribution used for calibration of the BSEA GAM. Based on pumping rates received from BSEACD. The majority of the pumping occurs in the southern portion of the aquifer.

a) High Conditions



b) Low Conditions

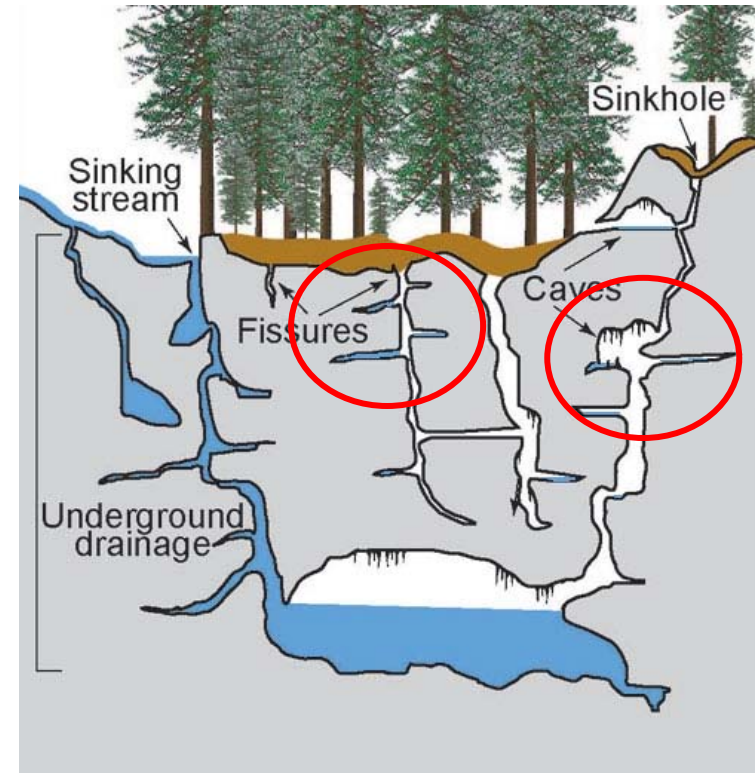


Figure 6.7 – Karst aquifer under different hydraulic conditions. Red circles show locations where during low conditions water may be stored in areas in perched locations that are not hydraulically connected to other locations of the aquifer. (Altered from ESI, 2007)

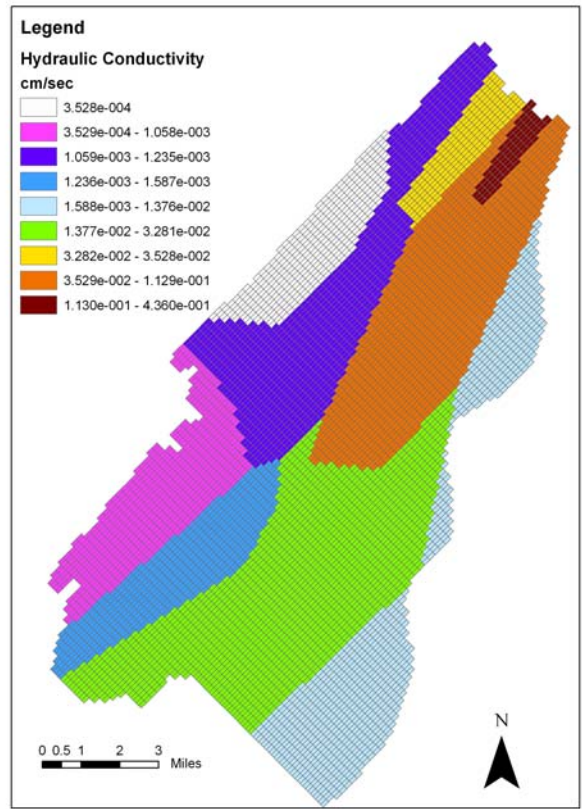


Figure 6.8 – Hydraulic conductivity used in the calibrated BSEA GAM.

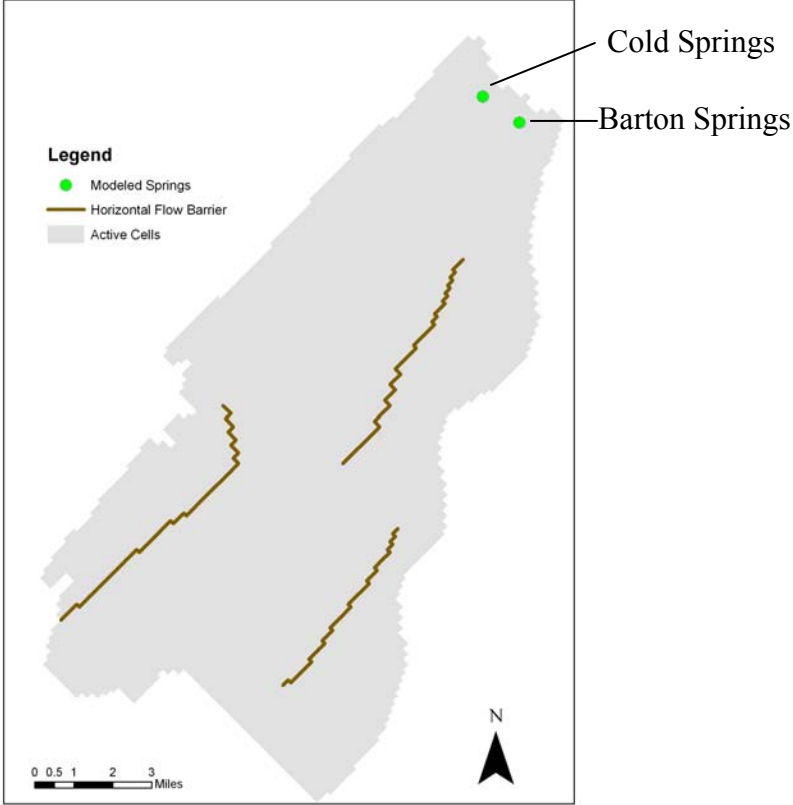


Figure 6.9 – Locations of springs (modeled using drain cells) and horizontal flow barrier representing major faults in the BSEA GAM.

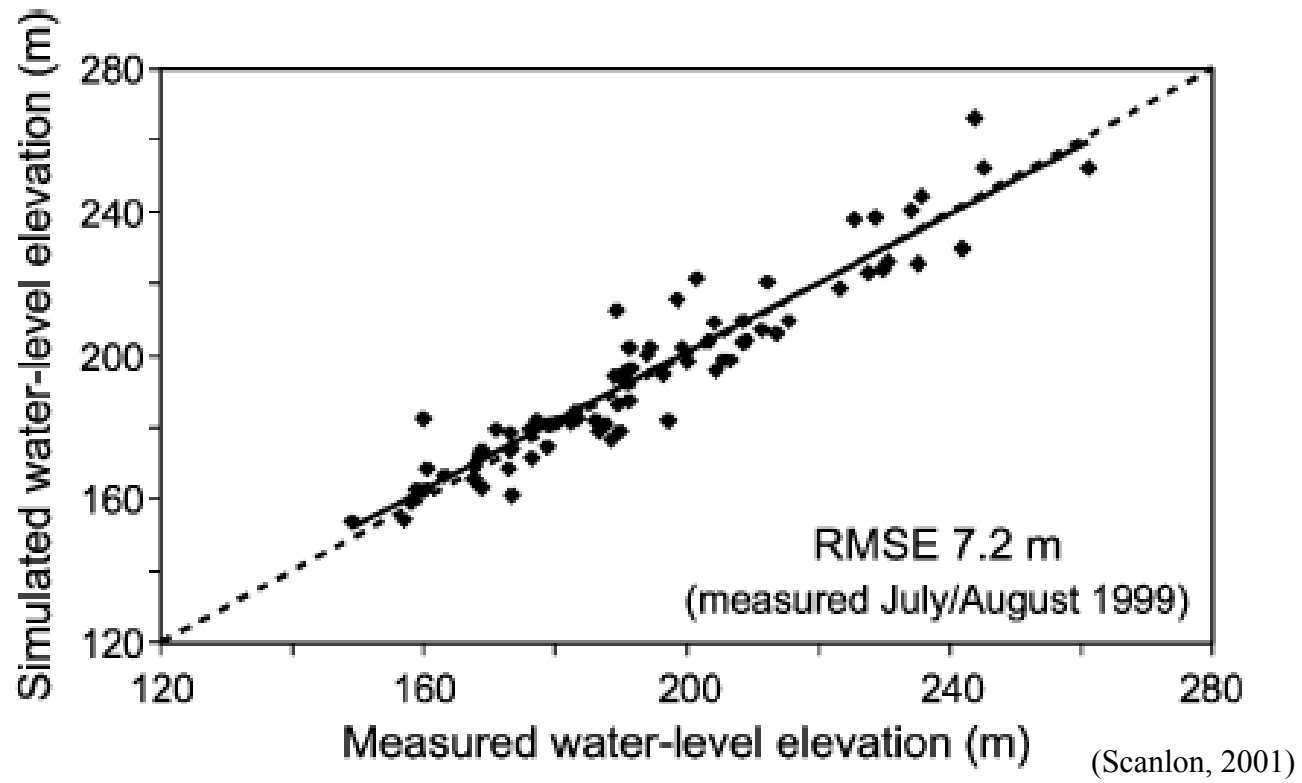


Figure 6.10 – Cross-plots for hydraulic head measurements for both the steady state calibration of the BSEA GAM.

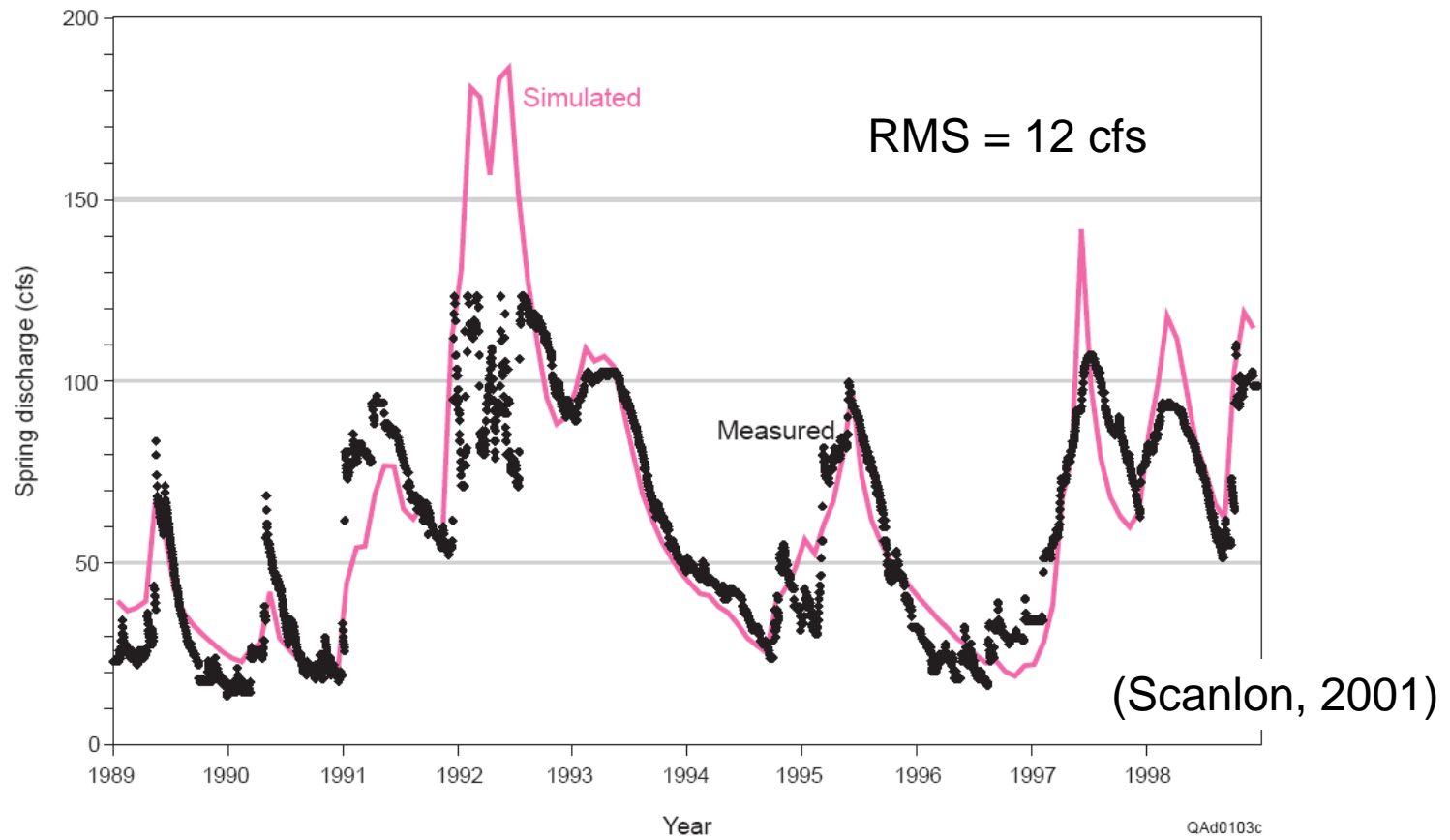


Figure 6.11 – Transient calibration of spring discharge hydrograph on a one-month time interval at Barton Springs

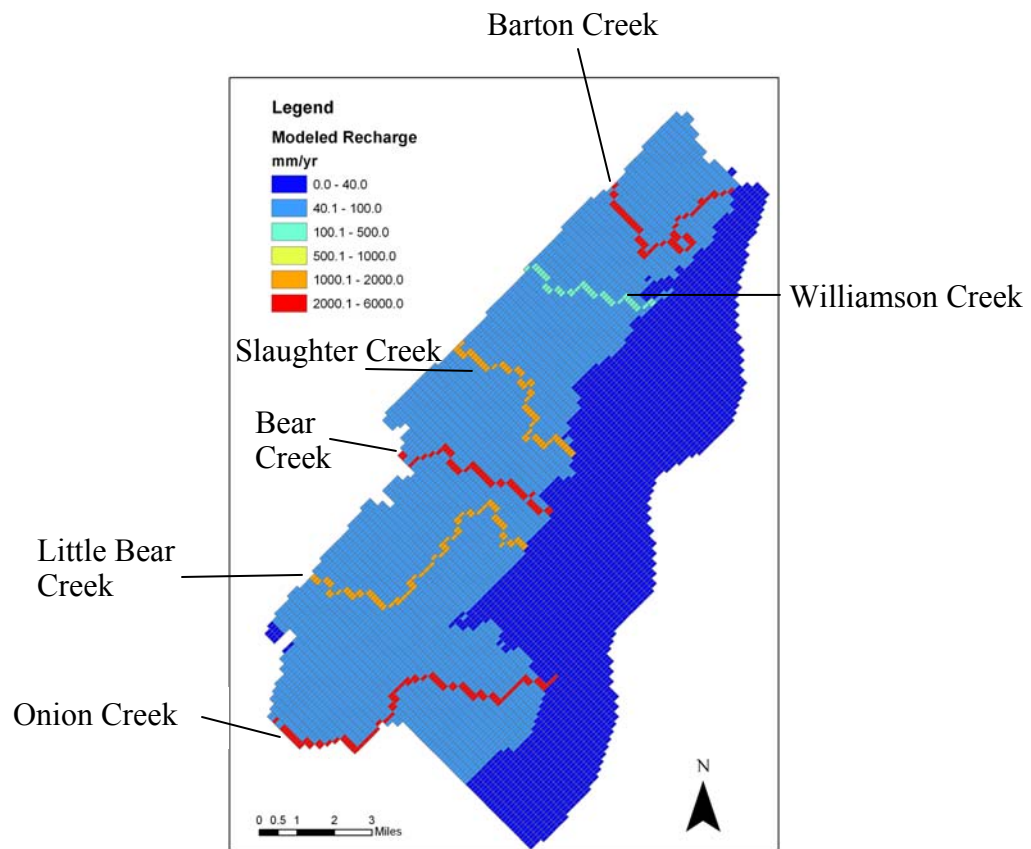


Figure 6.12 – Calibrated recharge pattern for the BSEA GAM. The pattern is a constant rate within each zone showed in the Figure.

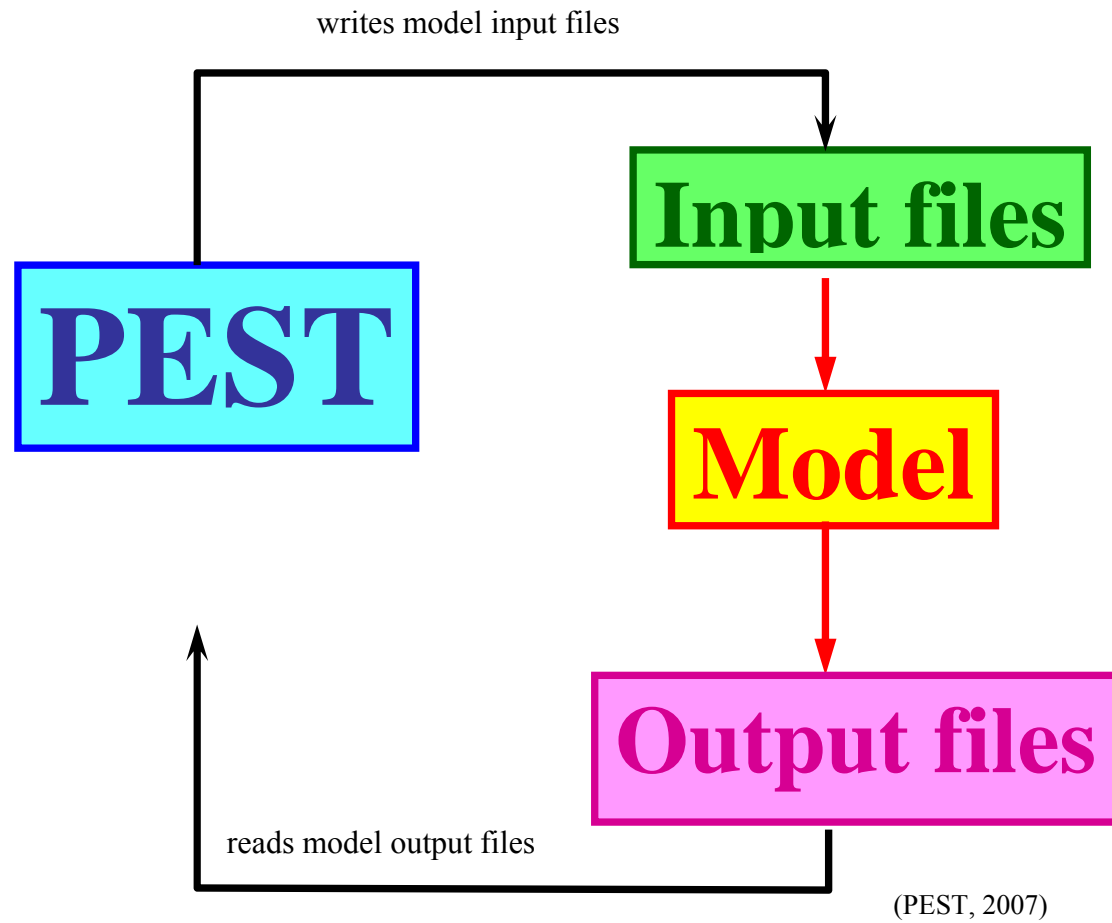


Figure 6.13 – PEST optimization can be used along with any numerical model that is based on command line arguments.

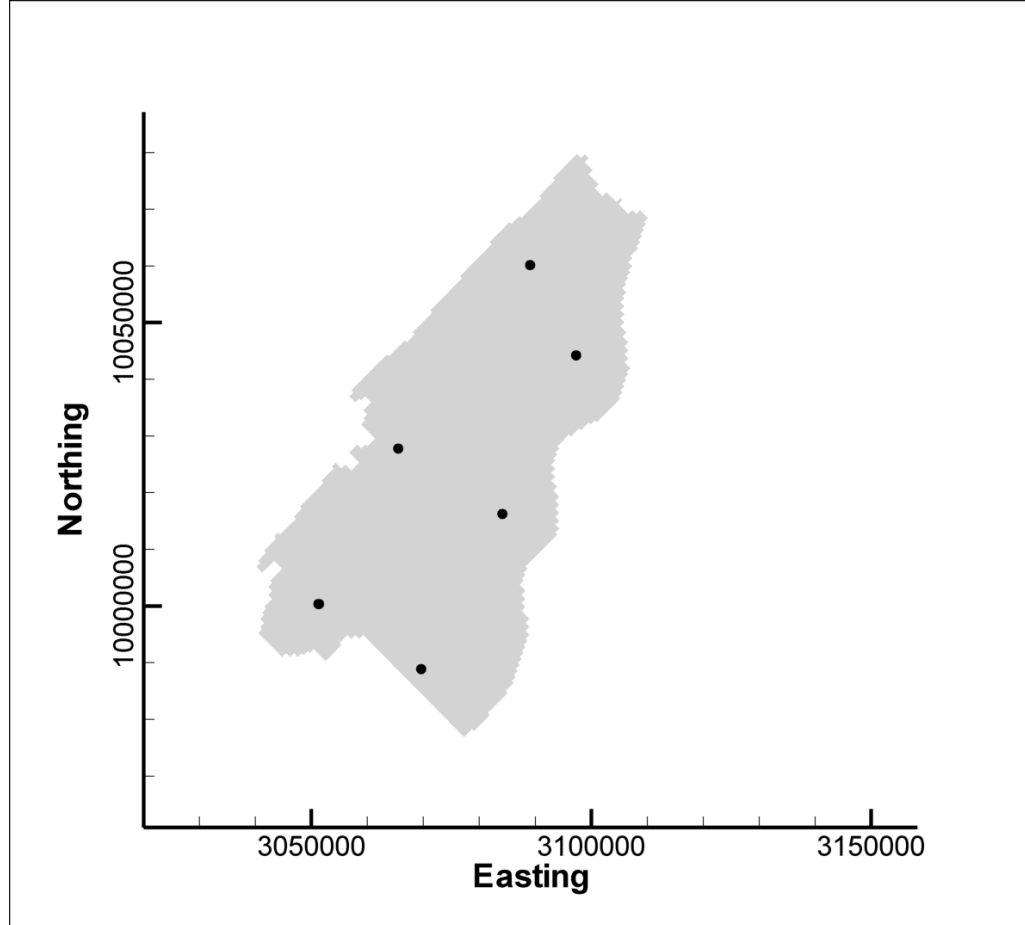


Figure 6.14 – Locations of pilot points used for sensitivity analysis of recharge in BSEA GAM. Values ranged in value from 0.0 to 3.0.

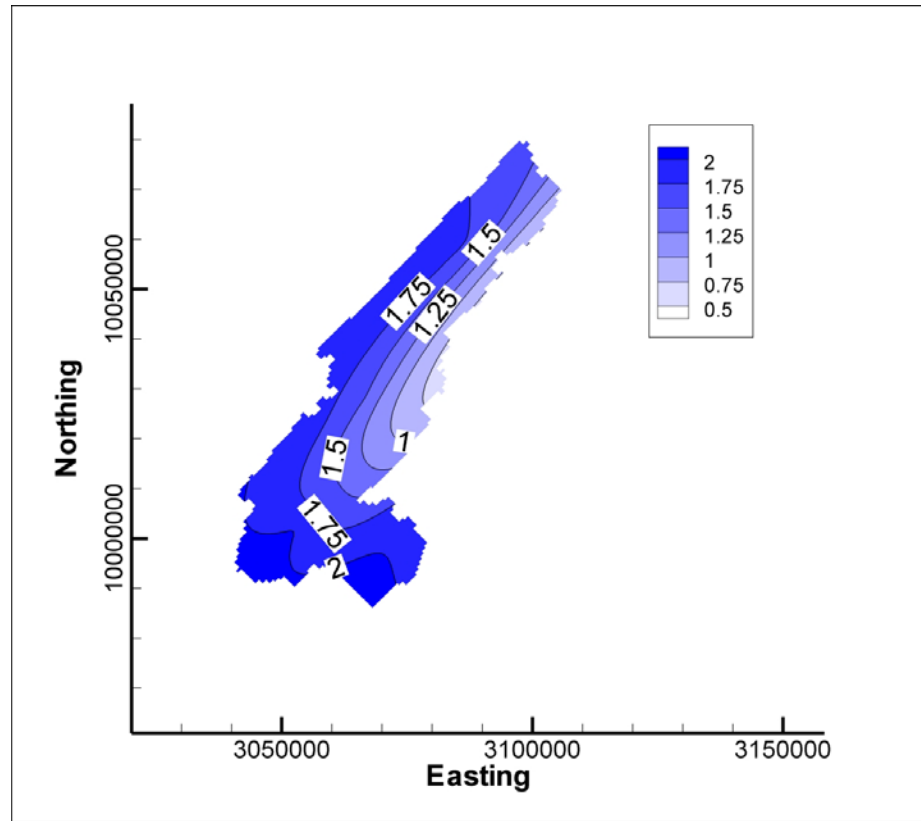


Figure 6.15 – Warping values used to multiply the model recharge when the spring discharge indicated drought conditions.

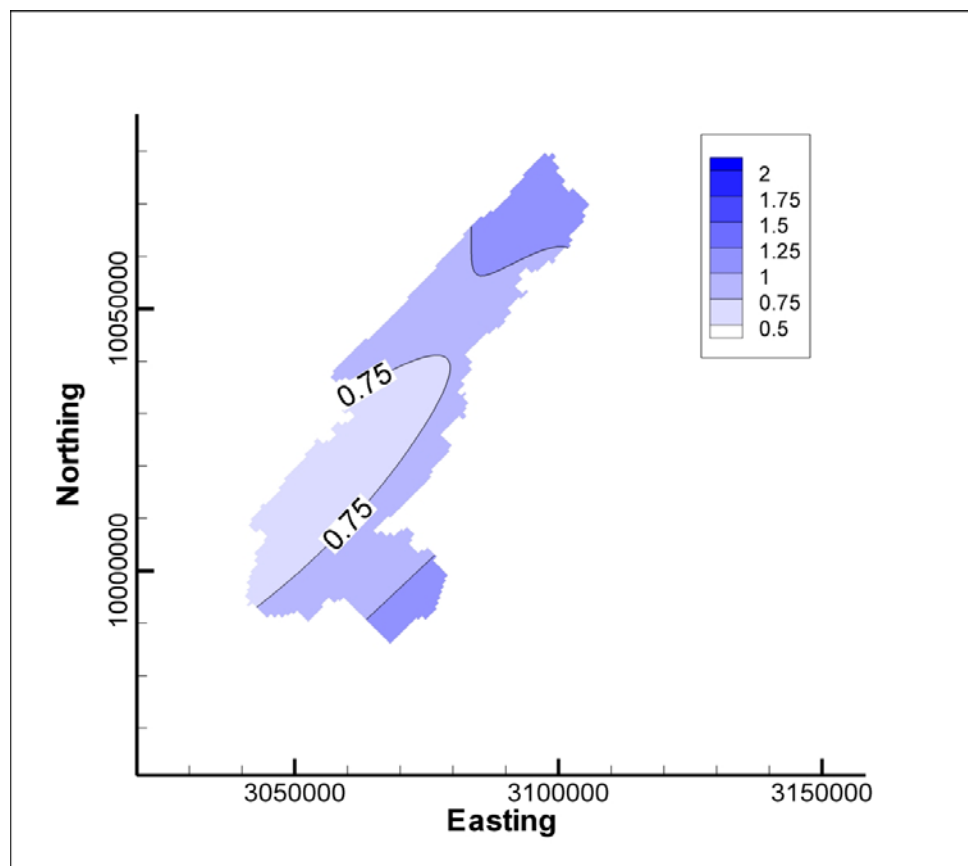


Figure 6.16 – Warping values used to multiply the model recharge when spring discharge indicated normal conditions.

Chapter 7. Summary and Conclusions

The use of NEXRAD for delineating and evaluating the recharge zones in karst aquifers has been discussed in this dissertation. By calculating the cross-correlation of each NEXRAD measurement to spring flow data for the same period of time a map showing the locations hydraulically connected to the spring can be developed. Both numerical experiments and field applications were conducted as part of the study. The numerical experiments conducted by Padilla and Pulido-Bosch are revisited using the numerical groundwater model MODFLOW. This allowed the introduction of spatially varying parameters into the model. The results show that spatially varying parameters can be inferred based on the results cross-correlation of spatially varying precipitation with respect to a single spring discharge location. Also, contributing area maps are prepared for both Barton Springs and Jacob's Well. Barton Springs has a precise estimate of the recharge area. The current map of the recharge area and the NEXRAD derived map show good agreement with the cross-correlation results. Conversely, Jacob's Well has not been sufficiently studied to delineate a contributing area map. This study provides an preliminary estimate of the area contributing to flow at Jacob's Well. Finally, the development of these maps can also be applied to the construction of regional groundwater models. An application of this methodology with the groundwater availability model for the Barton Springs portion of the Edward's aquifer is introduced. The application of spatial cross-correlation analysis to constrain recharge in the model showed a reduction in the objective function with respect to discharge at Barton Springs

of 15%. Below, a summary and conclusions of the work presented along with several possible enhancements to further this.

SUMMARY AND CONCLUSIONS

Calculating the cross-correlation at NEXRAD measurement locations with respect to spring discharge data is a useful method for developing a map of likely locations contributing to recharge at the spring. An algorithm was developed that processes the NEXRAD data and puts it in a format along with the spring discharge data to allow the calculation of the cross-correlations. These methods were used to develop these maps at two karst springs in Central Texas. Results from these analyses indicated that the cross-correlation analysis can be used with spatial precipitation estimates to develop maps of likely recharge locations for karst springs when more robust methods are not available. The methods were tested at Barton Springs near Austin, Texas, where a precise boundary of the recharge zone has been delineated. The cross-correlation analysis showed agreement with the delineated boundary with some variations along the up-dip boundary of the aquifer. The same algorithms were applied at Jacob's Well near Wimberly, Texas, where no precise map of a recharge zone has been delineated. The analysis provided a zone of recharge that appeared to follow the prevailing theory of the direction of groundwater flow in the region. Finally, the usefulness of cross-correlation analysis was demonstrated for use with regional groundwater models for constraining recharge patterns. The various applications of this algorithm each indicate that cross-correlation analysis of spring discharge data and NEXRAD precipitation data is a useful tool for developing maps of recharge likelihood for karst springs.

FUTURE WORK

There are several enhancements that may both refine the methodology and provide more insight into the karst flow system using cross-correlation and NEXRAD data. Some of these enhancements include: 1) Obtaining higher resolution NEXRAD data; 2) evaluate changes in recharge patterns with changes in land use, specifically increased urbanization; and 3) applying cross-correlation analysis to surface water modeling for developing routing equations. Each of these is briefly discussed below.

Higher Resolution NEXRAD

The NWS provides 4 km by 4 km resolution NEXRAD data on a 1-hour time step for the continental United States. However, the WSR-88D radar network has the ability to produce up to 1 km by 1 km resolution precipitation data on a 15-minute time step. It is possible that the higher resolution data would provide more detailed picture of where recharge is likely originating for spring discharge. Furthermore, in other applications, specifically small scale studies such as Birk et al. (2004), the increased resolution could be the difference in finding a solution or not. Also, the increased temporal resolution could be useful when the spring discharge has an extremely quick response to precipitation.

Land Use Changes

With over ten years of NEXRAD data it is possible that the land use within the boundary of NEXRAD cells has changed. One application of the cross-correlation analysis with NEXRAD data would be to investigate how the correlations compare before and after major land-use changes. Sharp et al. (2008) presented a similar investigation completed with gage precipitation data at the Camp Mabry gage and spring

discharge at Barton Springs. The cross-correlation results indicated that land use changes on the recharge zone had increased recharge to the spring. NEXRAD data could be used to evaluate impacts of drastic changes in land-use to spring discharge.

Surface Water Routing

Using NEXRAD data has increased in popularity in surface water projects as pre-processors for hydrologic models are increasingly adding functionality to process these data. Stream routing methods approximate the time it takes for water to flow through a channel. It is useful for merging simulated outflow from more than one basin at a single point. Because it deals with timing, cross-correlation analysis would be a good tool to define the lags between more than one time series to create calibration constraints for the surface water modeling. Using NEXRAD data for this purpose would be useful in models that are either distributed in nature or that have a large number of sub-watersheds without specific precipitation gages inside the sub-watershed.

These three enhancements provide a short list of applications of cross-correlation and NEXRAD data in hydrogeology. By analyzing these data with cross-correlations our understanding of the spatial and temporal response of hydrologic systems is enhanced.

APPENDIX A

In order to process the NEXRAD data set available from the NWS, the NWS provides a computer program called “xmrg_read.c” written in the C programming language (NWS, 2007b). The program is a command line based program that reads and converts the binary XMRG file format into an ASCII file. However, in order to process the entire period of record the program was altered to add functionality to handle multiple files and multiple naming conventions. The C program was converted to an Microsoft Visual C++ 6.0 windows console application with Microsoft Foundation Classes. Furthermore, a graphical user interface (GUI) for the program was added to aid in selecting the processing of the data. Figure A.1 shows the dialog box used as the GUI for the altered xmrg_read.c program. The GUI allows the user to select the starting and ending dates and times for the processing, whether the files were created for use with UNIX or IBM based systems, the location of the NEXRAD data on the hard drive, and the subset of the HRAP grid that will be processed. Once these inputs have been selected, the program processes the binary data and produces an ASCII output file with the NEXRAD precipitation time-series for each cell. The source code for this program is included in this Appendix. Only the computer code altered as part of this dissertation is included. The source code automatically produced by Microsoft Visual Studio 6.0 is not included.

HEADER FILE

```
// NEXRADDlg.h : header file  
//
```

```

        #if
!defined(AFX_NEXRADDLG_H__87785718_711D_498E_9388_325B6DAF4562__IN
CLUDED_)
        #define
AFX_NEXRADDLG_H__87785718_711D_498E_9388_325B6DAF4562__INCLUDE
D_

        #if _MSC_VER > 1000
        #pragma once
        #endif // _MSC_VER > 1000

        ///////////////////////////////////////////////////////////////////
        // CNEXRADDlg dialog

        class CNEXRADDlg : public CDialog
        {
        // Construction
        public:
                CString GetMonthTarFileName(COleDateTime *tmpTime1);
                CString GetDayTarFileName(COleDateTime *tmpTime1, BOOL
*blnZipped);
                CNEXRADDlg(CWnd* pParent = NULL); // standard constructor
                BOOL LaunchTarExtraction(CString *strXMRGGridName, BOOL
blnRemove);
                void GetXMRGHourlyValues(CString *strXMRGGridName, long
*ColList,
                                                long
*RowList, double *Values, long numCells);
        // Dialog Data
               //{{AFX_DATA(CNEXRADDlg)
                enum { IDD = IDD_NEXRAD_DIALOG };
                CString m_CellFileDirectory;
                CString m_XMRGDirectory;
                CString m_StartMonth;
                CString m_StartHour;
                CString m_StartDay;
                CString m_EndYear;
                CString m_StartYear;
                CString m_EndMonth;
                CString m_EndHour;
                CString m_EndDay;
                int m_Reverse;
                //}}AFX_DATA

        // ClassWizard generated virtual function overrides

```



```

support
    //{{{AFX_VIRTUAL(CNEXRADDlg)
    protected:
    virtual void DoDataExchange(CDataExchange* pDX);    // DDX/DDV

    //}}}AFX_VIRTUAL

// Implementation
protected:
    HICON m_hIcon;

    // Generated message map functions
    //{{{AFX_MSG(CNEXRADDlg)
    virtual BOOL OnInitDialog();
    afx_msg void OnSysCommand(UINT nID, LPARAM lParam);
    afx_msg void OnPaint();
    afx_msg HCURSOR OnQueryDragIcon();
    afx_msg void OnEditchangeStartMonth();
    afx_msg void OnCellFile();
    afx_msg void OnDirectory();
    afx_msg void OnKillfocusStartMonth();
    afx_msg void OnKillfocusStartDay();
    afx_msg void OnCloseupStartDay();
    afx_msg void OnKillfocusEndYear();
    afx_msg void OnKillfocusEndMonth();
    afx_msg void OnKillfocusEndHour();
    afx_msg void OnKillfocusEndDay();
    afx_msg void OnKillfocusStartHour();
    afx_msg void OnKillfocusStartYear();
    virtual void OnOK();
    afx_msg void OnRadio2();
    afx_msg void OnRadio1();
    //}}}AFX_MSG
    DECLARE_MESSAGE_MAP()
private:
    CString  GetXMRGFileName(COLEDateTime  *tmpTime1,  BOOL
*bInZipped);
    BOOL  LaunchZipExtraction(CString *strXMRGGridName);
    void  reverse_byte_order(int *in_array,int arraysize);

    void  ReadCells(CString *strCellFileName,
long *RowList, long *ColList,
double *Values,
long *numValues);
};

```

```
//{{AFX_INSERT_LOCATION}}
// Microsoft Visual C++ will insert additional declarations immediately before the
previous line.
```

```
#endif
!defined(AFX_NEXRADDLG_H__87785718_711D_498E_9388_325B6DAF4562__IN
CLUDED_)
```

SOURCE FILE

```
// NEXRADDlg.cpp : implementation file
//

#include "stdafx.h"
#include "NEXRAD.h"
#include "NEXRADDlg.h"
#include <malloc.h>

#define NUMCELLS 217
#ifdef _DEBUG
#define new DEBUG_NEW
#undef THIS_FILE
static char THIS_FILE[] = __FILE__;
#endif

//////////////////////////////////////
// CAboutDlg dialog used for App About

class CAboutDlg : public CDialog
{
public:
    CAboutDlg();

// Dialog Data
//{{AFX_DATA(CAboutDlg)
enum { IDD = IDD_ABOUTBOX };
//}}AFX_DATA

// ClassWizard generated virtual function overrides
//{{AFX_VIRTUAL(CAboutDlg)
protected:
virtual void DoDataExchange(CDataExchange* pDX);    // DDX/DDV
support
//}}AFX_VIRTUAL
```

```

// Implementation
protected:
   //{{AFX_MSG(CAboutDlg)
   //}}AFX_MSG
    DECLARE_MESSAGE_MAP()
};

CAboutDlg::CAboutDlg() : CDialog(CAboutDlg::IDD)
{
   //{{AFX_DATA_INIT(CAboutDlg)
   //}}AFX_DATA_INIT
}

void CAboutDlg::DoDataExchange(CDataExchange* pDX)
{
    CDialog::DoDataExchange(pDX);
   //{{AFX_DATA_MAP(CAboutDlg)
   //}}AFX_DATA_MAP
}

BEGIN_MESSAGE_MAP(CAboutDlg, CDialog)
   //{{AFX_MSG_MAP(CAboutDlg)
    // No message handlers
   //}}AFX_MSG_MAP
END_MESSAGE_MAP()

////////////////////////////////////
// CNEXRADDlg dialog

CNEXRADDlg::CNEXRADDlg(CWnd* pParent /*=NULL*/)
: CDialog(CNEXRADDlg::IDD, pParent)
{
   //{{AFX_DATA_INIT(CNEXRADDlg)
    m_CellFileDirectory = _T("");
    m_XMRGDirectory = _T("");
    m_StartMonth = _T("");
    m_StartHour = _T("");
    m_StartDay = _T("");
    m_EndYear = _T("");
    m_StartYear = _T("");
    m_EndMonth = _T("");
    m_EndHour = _T("");
    m_EndDay = _T("");
   //}}AFX_DATA_INIT
    // Note that LoadIcon does not require a subsequent DestroyIcon in Win32

```

```

        m_hIcon = AfxGetApp()->LoadIcon(IDR_MAINFRAME);
    }

void CNEXRADDlg::DoDataExchange(CDataExchange* pDX)
{
    CDialog::DoDataExchange(pDX);
   //{{AFX_DATA_MAP(CNEXRADDlg)
    DDX_Text(pDX, txt_CellFile, m_CellFileDirectory);
    DDX_Text(pDX, txt_XMRGLocation, m_XMRGDirectory);
    DDX_CBString(pDX, CMB_StartMonth, m_StartMonth);
    DDX_CBString(pDX, CMB_StartHour, m_StartHour);
    DDX_CBString(pDX, CMB_StartDay, m_StartDay);
    DDX_CBString(pDX, CMB_EndYear, m_EndYear);
    DDX_CBString(pDX, CMB_StartYear, m_StartYear);
    DDX_CBString(pDX, CMB_EndMonth, m_EndMonth);
    DDX_CBString(pDX, CMB_EndHour, m_EndHour);
    DDX_CBString(pDX, CMB_EndDay, m_EndDay);
   //}}AFX_DATA_MAP
}

BEGIN_MESSAGE_MAP(CNEXRADDlg, CDialog)
    {{{AFX_MSG_MAP(CNEXRADDlg)
    ON_WM_SYSCOMMAND()
    ON_WM_PAINT()
    ON_WM_QUERYDRAGICON()
    ON_CBN_EDITCHANGE(CMB_StartMonth, OnEditchangeStartMonth)
    ON_BN_CLICKED(cmd_CellFile, OnCellFile)
    ON_BN_CLICKED(cmd_Directory, OnDirectory)
    ON_CBN_KILLFOCUS(CMB_StartMonth, OnKillfocusStartMonth)
    ON_CBN_KILLFOCUS(CMB_StartDay, OnKillfocusStartDay)
    ON_CBN_CLOSEUP(CMB_StartDay, OnCloseupStartDay)
    ON_CBN_KILLFOCUS(CMB_EndYear, OnKillfocusEndYear)
    ON_CBN_KILLFOCUS(CMB_EndMonth, OnKillfocusEndMonth)
    ON_CBN_KILLFOCUS(CMB_EndHour, OnKillfocusEndHour)
    ON_CBN_KILLFOCUS(CMB_EndDay, OnKillfocusEndDay)
    ON_CBN_KILLFOCUS(CMB_StartHour, OnKillfocusStartHour)
    ON_CBN_KILLFOCUS(CMB_StartYear, OnKillfocusStartYear)
    ON_BN_CLICKED(IDC_RADIO2, OnRadio2)
    ON_BN_CLICKED(IDC_RADIO1, OnRadio1)
    }}}AFX_MSG_MAP
END_MESSAGE_MAP()

////////////////////////////////////
// CNEXRADDlg message handlers

```

```

BOOL CNEXRADDlg::OnInitDialog()
{
    CDialog::OnInitDialog();

    // Add "About..." menu item to system menu.

    // IDM_ABOUTBOX must be in the system command range.
    ASSERT((IDM_ABOUTBOX & 0xFFF0) == IDM_ABOUTBOX);
    ASSERT(IDM_ABOUTBOX < 0xF000);

    m_Reverse = 0;

    CMenu* pSysMenu = GetSystemMenu(FALSE);
    if (pSysMenu != NULL)
    {
        CString strAboutMenu;
        strAboutMenu.LoadString(IDS_ABOUTBOX);
        if (!strAboutMenu.IsEmpty())
        {
            pSysMenu->AppendMenu(MF_SEPARATOR);
            pSysMenu->AppendMenu(MF_STRING,
IDM_ABOUTBOX, strAboutMenu);
        }
    }

    // Set the icon for this dialog. The framework does this automatically
    // when the application's main window is not a dialog
    SetIcon(m_hIcon, TRUE);           // Set big icon
    SetIcon(m_hIcon, FALSE);        // Set small icon

    // TODO: Add extra initialization here
    CComboBox *pComboBox = (CComboBox*) GetDlgItem(CMB_StartMonth);

    if (!pComboBox)
        return FALSE;

    // TODO: Add extra initialization here
    char tmpString[256];

    for (int i = 1; i <= 12; i++) {
        sprintf(tmpString, "%2i", i);
        pComboBox->AddString(tmpString);
    }
}

```

```

pComboBox = (CComboBox*) GetDlgItem(CMB_EndMonth);

if (!pComboBox)
    return FALSE;

    // TODO: Add extra initialization here
for (i = 1;i<=12;i++) {
    sprintf(tmpString, "%2i",i);
    pComboBox->AddString(tmpString);
}

pComboBox = (CComboBox*) GetDlgItem(CMB_StartDay);

if (!pComboBox)
    return FALSE;

    // TODO: Add extra initialization here

for (i = 1;i<=31;i++) {
    sprintf(tmpString, "%2i",i);
    pComboBox->AddString(tmpString);
}

pComboBox = (CComboBox*) GetDlgItem(CMB_EndDay);

if (!pComboBox)
    return FALSE;

    // TODO: Add extra initialization here

for (i = 1;i<=31;i++) {
    sprintf(tmpString, "%2i",i);
    pComboBox->AddString(tmpString);
}

pComboBox = (CComboBox*) GetDlgItem(CMB_StartYear);

if (!pComboBox)
    return FALSE;

    // TODO: Add extra initialization here

for (i = 1994;i<=2007;i++) {
    sprintf(tmpString, "%2i",i);
    pComboBox->AddString(tmpString);
}

```

```

    }
    pComboBox = (CComboBox*) GetDlgItem(CMB_EndYear);

    if (!pComboBox)
        return FALSE;

        // TODO: Add extra initialization here

    for (i = 1994; i <= 2007; i++) {
        sprintf(tmpString, "%2i", i);
        pComboBox->AddString(tmpString);
    }
    pComboBox = (CComboBox*) GetDlgItem(CMB_StartHour);

    if (!pComboBox)
        return FALSE;

        // TODO: Add extra initialization here

    for (i = 1; i <= 24; i++) {
        sprintf(tmpString, "%2i", i);
        pComboBox->AddString(tmpString);
    }
    pComboBox = (CComboBox*) GetDlgItem(CMB_EndHour);

    if (!pComboBox)
        return FALSE;

        // TODO: Add extra initialization here

    for (i = 1; i <= 24; i++) {
        sprintf(tmpString, "%2i", i);
        pComboBox->AddString(tmpString);
    }

    return TRUE; // return TRUE unless you set the focus to a control
}

void CNEXRADDlg::OnSysCommand(UINT nID, LPARAM lParam)
{
    if ((nID & 0xFFF0) == IDM_ABOUTBOX)
    {
        CAboutDlg dlgAbout;
        dlgAbout.DoModal();
    }
}

```

```

        else
        {
            CDialog::OnSysCommand(nID, lParam);
        }
    }

// If you add a minimize button to your dialog, you will need the code below
// to draw the icon. For MFC applications using the document/view model,
// this is automatically done for you by the framework.

void CNEXRADDlg::OnPaint()
{
    if (IsIconic())
    {
        CPaintDC dc(this); // device context for painting

        dc.GetSafeHdc(), 0);

        SendMessage(WM_ICONERASEBKGND,          (WPARAM)

        // Center icon in client rectangle
        int cxIcon = GetSystemMetrics(SM_CXICON);
        int cyIcon = GetSystemMetrics(SM_CYICON);
        CRect rect;
        GetClientRect(&rect);
        int x = (rect.Width() - cxIcon + 1) / 2;
        int y = (rect.Height() - cyIcon + 1) / 2;

        // Draw the icon
        dc.DrawIcon(x, y, m_hIcon);
    }
    else
    {
        CDialog::OnPaint();
    }
}

// The system calls this to obtain the cursor to display while the user drags
// the minimized window.
HCURSOR CNEXRADDlg::OnQueryDragIcon()
{
    return (HCURSOR) m_hIcon;
}

void CNEXRADDlg::OnEditchangeStartMonth()
{

```



```

        // TODO: Add your control notification handler code here
    }

void CNEXRADDlg::OnCellFile()
{
    // TODO: Add your control notification handler code here
    CFileDialog *FDlog = new CFileDialog(TRUE, "Cell File, *.txt");
    if (FDlog->DoModal() == IDOK) {
        //FDlog.G
        m_CellFileDirectory = FDlog->GetPathName();

        }
    delete FDlog;

    UpdateData(FALSE);
}

void CNEXRADDlg::OnDirectory()
{
    // TODO: Add your control notification handler code here
    CString strFileName;
    CFileDialog *FDlog = new CFileDialog(TRUE, "Cell File, *.txt");
    if (FDlog->DoModal() == IDOK) {
        //FDlog.G
        m_XMRGDirectory = FDlog->GetPathName();
        strFileName = FDlog->GetFileName();
        m_XMRGDirectory
        m_XMRGDirectory.Left(m_XMRGDirectory.GetLength() - strFileName.GetLength());
    }
    delete FDlog;

    UpdateData(FALSE);
}

void CNEXRADDlg::OnKillfocusStartMonth()
{
    // TODO: Add your control notification handler code here
    UpdateData(TRUE);
}

void CNEXRADDlg::OnKillfocusStartDay()
{

```

```

        // TODO: Add your control notification handler code here
        UpdateData(TRUE);
    }

void CNEXRADDlg::OnCloseupStartDay()
{
    // TODO: Add your control notification handler code here
    UpdateData(TRUE);
}

void CNEXRADDlg::OnKillfocusEndYear()
{
    // TODO: Add your control notification handler code here
    UpdateData(TRUE);
}

void CNEXRADDlg::OnKillfocusEndMonth()
{
    // TODO: Add your control notification handler code here
    UpdateData(TRUE);
}

void CNEXRADDlg::OnKillfocusEndHour()
{
    // TODO: Add your control notification handler code here
    UpdateData(TRUE);
}

void CNEXRADDlg::OnKillfocusEndDay()
{
    // TODO: Add your control notification handler code here
    UpdateData(TRUE);
}

void CNEXRADDlg::OnKillfocusStartHour()
{
    // TODO: Add your control notification handler code here
    UpdateData(TRUE);
}

void CNEXRADDlg::OnKillfocusStartYear()
{
    // TODO: Add your control notification handler code here
    UpdateData(TRUE);
}

```

```

void CNEXRADDlg::OnOK()
{
    // TODO: Add extra validation here
    CString tmpXMRGTitle;
    CString tmpTarTitle;
    CString tmpString;
    CString tmpMonth;
    int tmpOldMonth;
    int tmpOldDay;
    CString tmpDay;
    CString tmpYear;
    CString tmpHour;
    CString tmpTitle;
    CString strXMRGGridName;
    CString strCurrentXMRG;
    CString strShellCommand;
    CString strCommandFolder;
    CString strBackSlach ( "\\\" );
    CFile theCFile;
    CFileStatus theCFileStatus;
    long RowList[NUMCELLS];
    long ColList[NUMCELLS];
    double XMRGValues[NUMCELLS];
    long numCells = 0;
    BOOL blnFirstTime;
    BOOL blnZipped;
    FILE *out_Fileptr = NULL;
    int i;

    COleDateTime tmpTime1( atol((LPCTSTR) m_StartYear),
                           atol((LPCTSTR) m_StartMonth),
                           atol((LPCTSTR) m_StartDay),
                           atol((LPCTSTR) m_StartHour), 0,
0 ); // 10:15PM March 19, 1999
    COleDateTime tmpTime2( atol((LPCTSTR) m_EndYear),
                           atol((LPCTSTR) m_EndMonth),
                           atol((LPCTSTR) m_EndDay),
                           atol((LPCTSTR) m_EndHour), 0, 0
); // 10:15PM March 21, 1999

    blnZipped = FALSE;

```

```

    blnFirstTime = TRUE;

    double crap = 0;

    ReadCells(&m_CellFileDirectory,          RowList,          ColList,
    XMRGValues,&numCells);

    out_Fileptr=fopen(strcat(m_XMRGDirectory.GetBuffer(m_XMRGDirectory.GetLength(
    )), "XMRGData.csv"), "w");
    if (out_Fileptr == NULL) {
        return;
    }

    fprintf(out_Fileptr, "Date");
    for (i=0; i<numCells; i++) {
        fprintf(out_Fileptr, "%i", i);
    }
    fprintf(out_Fileptr, "\n");
    crap = ( 1.0 / 24.0 );
    while (tmpTime1 < tmpTime2) {

        if (blnFirstTime) {
            strXMRGGridName = GetMonthTarFileName(&tmpTime1);
            if (!strXMRGGridName.IsEmpty()) {
                LaunchTarExtraction(&strXMRGGridName, FALSE);
            }

            strXMRGGridName = GetDayTarFileName(&tmpTime1, &blnZipped);
            if (blnZipped) {
                LaunchZipExtraction(&strXMRGGridName);
                blnZipped = FALSE;
                strXMRGGridName.SetAt
                ((strXMRGGridName.GetLength()-3), '\0');
            }
            if (!strXMRGGridName.IsEmpty()) {
                LaunchTarExtraction(&strXMRGGridName, TRUE);
            }

            tmpOldMonth = tmpTime1.GetMonth();
            tmpOldDay = tmpTime1.GetDay();
            blnFirstTime = FALSE;
        }
    }

```

```

    if (tmpOldMonth != tmpTime1.GetMonth()) {
        strXMRGGridName = GetMonthTarFileName(&tmpTime1);
        if (!strXMRGGridName.IsEmpty()) {
            LaunchTarExtraction(&strXMRGGridName,FALSE);
        }
    }

    if (tmpOldDay != tmpTime1.GetDay()) {
        strXMRGGridName = GetDayTarFileName(&tmpTime1, &blnZipped);
        if (blnZipped) {
            LaunchZipExtraction(&strXMRGGridName);
            blnZipped = FALSE;
            strXMRGGridName.SetAt
((strXMRGGridName.GetLength()-3),'\0');
        }
        if (!strXMRGGridName.IsEmpty()) {
            LaunchTarExtraction(&strXMRGGridName,TRUE);
        }
    }

    strXMRGGridName = GetXMRGFileName(&tmpTime1,
&blnZipped);

    if (blnZipped) {
        LaunchZipExtraction(&strXMRGGridName);
        blnZipped = FALSE;
        strXMRGGridName.SetAt
((strXMRGGridName.GetLength()-2),'\0');
    }

    if (!strXMRGGridName.IsEmpty()) {
        theCFileStatus.m_size = 0;
        theCFile.GetStatus(strXMRGGridName,theCFileStatus);
        if (theCFileStatus.m_size > 0) {
            GetXMRGHourlyValues(&strXMRGGridName,
Collist, RowList, XMRGValues,
numCells);

            fprintf(out_Fileptr, "%s",
tmpTime1.Format(_T("%m/%d/%y %H")));
            for (i=0;i<NUMCELLS;i++) {
                fprintf(out_Fileptr,
XMRGValues[i]);
            }
        }
    }

```

```

        }
        fprintf(out_Fileptr, "\n");
    }
    else {
        fprintf(out_Fileptr, "%s",
tmpTime1.Format(_T("%m/%d/%y %H")));
        for (i=0;i<NUMCELLS;i++) {
            fprintf(out_Fileptr, ",-999");
        }
        fprintf(out_Fileptr, "\n");
    }
}
else {
    fprintf(out_Fileptr, "%s", tmpTime1.Format(_T("%m/%d/%y
%H")));
    for (i=0;i<NUMCELLS;i++) {
        fprintf(out_Fileptr, ",-999");
    }
    fprintf(out_Fileptr, "\n");
}

    tmpOldMonth = tmpTime1.GetMonth();
    tmpOldDay = tmpTime1.GetDay();
    tmpTime1 += crap;
}
fclose(out_Fileptr);
//free (ColList);
//free (RowList);
//free (XMRGValues);

    CDialog::OnOK();
}

CString CNEXRADDlg::GetXMRGFileName(COLEDateTime *tmpTime1,
BOOL *blnZipped)
{
    CString tmpName;
    CFileFind tmpFindFile;
    CString tmpString;
    CString tmpMonth;
    CString tmpDay;
    CString tmpYear;

```

```

CString tmpHour;
CString tmpTitle;

tmpMonth = tmpTime1->Format(_T("%m"));
tmpDay = tmpTime1->Format(_T("%d"));
tmpYear = tmpTime1->Format(_T("%Y"));
tmpHour = tmpTime1->Format(_T("%H"));
tmpTitle = "stage3_";
tmpName = m_XMRGDirectory + tmpYear + "\\\" + tmpTitle + tmpMonth +
tmpDay + tmpYear + "_" + tmpHour + "z_WG";

CFileFind finder;
BOOL bWorking = finder.FindFile(tmpName);
if (bWorking) {
    blnZipped = FALSE;
    return tmpName;
}

tmpName = m_XMRGDirectory + tmpYear + "\\\" + tmpTitle + tmpMonth +
tmpDay + tmpYear + "_" + tmpHour + "z_WG.Z";

bWorking = finder.FindFile(tmpName);
if (bWorking) {
    *blnZipped = TRUE;
    return tmpName;
}

tmpMonth = tmpTime1->Format(_T("%m"));
tmpDay = tmpTime1->Format(_T("%d"));
tmpYear = tmpTime1->Format(_T("%Y"));
tmpHour = tmpTime1->Format(_T("%H"));
tmpTitle = "Siii_";
tmpName = m_XMRGDirectory + tmpYear + "\\\" + tmpTitle + tmpMonth +
tmpDay + tmpYear + "_" + tmpHour + "z_WG";

bWorking = finder.FindFile(tmpName);
if (bWorking) {
    blnZipped = FALSE;
    return tmpName;
}

tmpName = m_XMRGDirectory + tmpYear + "\\\" + tmpTitle + tmpMonth +
tmpDay + tmpYear + "_" + tmpHour + "z_WG.Z";

```

```
bWorking = finder.FindFile(tmpName);
if (bWorking) {
    *bInZipped = TRUE;
    return tmpName;
}
```

```
tmpName = m_XMRGDirectory + tmpYear + "\\\" + tmpTitle + tmpMonth +
tmpDay + tmpYear + \"_\" + tmpHour + \"z_WG.gz\";
```

```
bWorking = finder.FindFile(tmpName);
if (bWorking) {
    *bInZipped = TRUE;
    return tmpName;
}
```

```
tmpMonth = tmpTime1->Format(_T(\"%m\"));
tmpDay = tmpTime1->Format(_T(\"%d\"));
tmpYear = tmpTime1->Format(_T(\"%Y\"));
tmpHour = tmpTime1->Format(_T(\"%H\"));
tmpTitle = \"xmr_g_\";
tmpName = m_XMRGDirectory + tmpYear + "\\\" + tmpTitle + tmpMonth +
tmpDay + tmpYear + \"_\" + tmpHour + \"z_WG\";
```

```
bWorking = finder.FindFile(tmpName);
if (bWorking) {
    bInZipped = FALSE;
    return tmpName;
}
```

```
tmpName = m_XMRGDirectory + tmpYear + "\\\" + tmpTitle + tmpMonth +
tmpDay + tmpYear + \"_\" + tmpHour + \"z_WG.Z\";
```

```
bWorking = finder.FindFile(tmpName);
if (bWorking) {
    *bInZipped = TRUE;
    return tmpName;
}
```

```
tmpMonth = tmpTime1->Format(_T(\"%m\"));
tmpDay = tmpTime1->Format(_T(\"%d\"));
```



```
tmpYear = tmpTime1->Format(_T("%Y"));
tmpHour = tmpTime1->Format(_T("%H"));
tmpTitle = "xmrg";
tmpName = m_XMRGDirectory + tmpYear + "\\\" + tmpTitle + tmpMonth +
tmpDay + tmpYear + tmpHour + "z";
```

```
bWorking = finder.FindFile(tmpName);
if (bWorking) {
    blnZipped = FALSE;
    return tmpName;
}
```

```
tmpName = m_XMRGDirectory + tmpYear + "\\\" + tmpTitle + tmpMonth +
tmpDay + tmpYear + tmpHour + "z.Z";
```

```
bWorking = finder.FindFile(tmpName);
if (bWorking) {
    *blnZipped = TRUE;
    return tmpName;
}
tmpMonth = tmpTime1->Format(_T("%m"));
tmpDay = tmpTime1->Format(_T("%d"));
tmpYear = tmpTime1->Format(_T("%Y"));
tmpHour = tmpTime1->Format(_T("%H"));
tmpTitle = "xmrg";
tmpName = m_XMRGDirectory + tmpYear + "\\\" + tmpTitle + tmpMonth +
tmpDay + tmpYear.Right(2) + tmpHour + "z";
```

```
bWorking = finder.FindFile(tmpName);
if (bWorking) {
    blnZipped = FALSE;
    return tmpName;
}
```

```
tmpName = m_XMRGDirectory + tmpYear + "\\\" + tmpTitle + tmpMonth +
tmpDay + tmpYear.Right(2) + tmpHour + "z.Z";
```

```
bWorking = finder.FindFile(tmpName);
if (bWorking) {
    *blnZipped = TRUE;
    return tmpName;
}
```

```

    }

    tmpMonth = tmpTime1->Format(_T("%m"));
    tmpDay = tmpTime1->Format(_T("%d"));
    tmpYear = tmpTime1->Format(_T("%y"));
    tmpHour = tmpTime1->Format(_T("%H"));
    tmpTitle = "xmrg";
    tmpName = m_XMRGDirectory + tmpYear + "\\\" + tmpTitle + tmpMonth +
tmpDay + tmpYear + tmpHour + "z";

    bWorking = finder.FindFile(tmpName);
    if (bWorking) {
        blnZipped = FALSE;
        return tmpName;
    }

    tmpName = m_XMRGDirectory + tmpYear + "\\\" + tmpTitle + tmpMonth +
tmpDay + tmpYear + tmpHour + "z.Z";

    bWorking = finder.FindFile(tmpName);
    if (bWorking) {
        *blnZipped = TRUE;
        return tmpName;
    }

    tmpName.Empty();
    blnZipped = FALSE;
    return tmpName;
}

CString CNEXRADDlg::GetMonthTarFileName(COLEDateTime *tmpTime1)
{
    CString tmpString;
    CString tmpMonth;
    CString tmpDay;
    CString tmpYear;
    CString tmpHour;
    CString tmpTitle;
    CString tmpName;
    BOOL bWorking;
    CFileFind finder;

```

```

tmpMonth = tmpTime1->Format(_T("%m"));
tmpDay = tmpTime1->Format(_T("%d"));
tmpYear = tmpTime1->Format(_T("%Y"));
tmpHour = tmpTime1->Format(_T("%H"));
tmpTitle = "XMRG";
tmpName = m_XMRGDirectory + tmpYear + "\\ " + tmpTitle + tmpMonth +
tmpYear + "WG.tar";

```

```

bWorking = finder.FindFile(tmpName);
if (bWorking) {
    return tmpName;
}

```

```

tmpMonth = tmpTime1->Format(_T("%m"));
tmpDay = tmpTime1->Format(_T("%d"));
tmpYear = tmpTime1->Format(_T("%Y"));
tmpHour = tmpTime1->Format(_T("%H"));
tmpTitle = "stage3_";
tmpName = m_XMRGDirectory + tmpYear + "\\ " + tmpTitle + tmpMonth +
tmpYear + "_WG.tar";

```

```

bWorking = finder.FindFile(tmpName);
if (bWorking) {
    return tmpName;
}

```

```

tmpMonth = tmpTime1->Format(_T("%m"));
tmpDay = tmpTime1->Format(_T("%d"));
tmpYear = tmpTime1->Format(_T("%Y"));
tmpHour = tmpTime1->Format(_T("%H"));
tmpTitle = "xmrg_";
tmpName = m_XMRGDirectory + tmpYear + "\\ " + tmpTitle + tmpMonth +
tmpYear + "_WG.tar";

```

```

bWorking = finder.FindFile(tmpName);
if (bWorking) {
    return tmpName;
}
tmpName = m_XMRGDirectory + tmpYear + "\\ " + tmpTitle + tmpMonth +
tmpYear + "_WG.tar.gz";

```

```

    bWorking = finder.FindFile(tmpName);
    if (bWorking) {
        return tmpName;
    }
    tmpMonth = tmpTime1->Format(_T("%m"));
    tmpDay = tmpTime1->Format(_T("%d"));
    tmpYear = tmpTime1->Format(_T("%Y"));
    tmpHour = tmpTime1->Format(_T("%H"));
    tmpTitle = "Siii";
    tmpName = m_XMRGDirectory + tmpTime1->Format(_T("%Y")) + "\\\" +
tmpTitle + tmpMonth + tmpYear + "WG.tar";

```

```

    bWorking = finder.FindFile(tmpName);
    if (bWorking) {

        return tmpName;
    }
    tmpName.Empty();
    return tmpName;

```

```

}
CString  CNEXRADDlg::GetDayTarFileName(COLEDateTime    *tmpTime1,
BOOL *bInZipped)
{
    CString tmpString;
    CString tmpMonth;
    CString tmpDay;
    CString tmpYear;
    CString tmpHour;
    CString tmpTitle;
    CString tmpName;
    BOOL bWorking;
    CFileFind finder;

        tmpMonth = tmpTime1->Format(_T("%m"));
    tmpDay = tmpTime1->Format(_T("%d"));
    tmpYear = tmpTime1->Format(_T("%Y"));
    tmpHour = tmpTime1->Format(_T("%H"));
    tmpTitle = "XMRG";
    tmpName = m_XMRGDirectory + tmpYear + "\\\" + tmpTitle + tmpMonth +
tmpDay + tmpYear + "WG.tar";

```

```

bWorking = finder.FindFile(tmpName);
if (bWorking) {
    return tmpName;
}

tmpMonth = tmpTime1->Format(_T("%m"));
tmpDay = tmpTime1->Format(_T("%d"));
tmpYear = tmpTime1->Format(_T("%Y"));
tmpHour = tmpTime1->Format(_T("%H"));
tmpTitle = "stage3_";
tmpName = m_XMRGDirectory + tmpYear + "\\ " + tmpTitle + tmpMonth +
tmpDay + tmpYear + "_WG.tar";

```

```

bWorking = finder.FindFile(tmpName);
if (bWorking) {
    return tmpName;
}

```

```

tmpMonth = tmpTime1->Format(_T("%m"));
tmpDay = tmpTime1->Format(_T("%d"));
tmpYear = tmpTime1->Format(_T("%y"));
tmpHour = tmpTime1->Format(_T("%H"));
tmpTitle = "stage3_";
tmpName = m_XMRGDirectory + tmpYear + "\\ " + tmpTitle + tmpMonth +
tmpDay + tmpYear + "_WG.tar";

```

```

bWorking = finder.FindFile(tmpName);
if (bWorking) {
    return tmpName;
}

```

```

tmpMonth = tmpTime1->Format(_T("%m"));
tmpDay = tmpTime1->Format(_T("%d"));
tmpYear = tmpTime1->Format(_T("%Y"));
tmpHour = tmpTime1->Format(_T("%H"));
tmpTitle = "xmrg_";
tmpName = m_XMRGDirectory + tmpYear + "\\ " + tmpTitle + tmpMonth +
tmpDay + tmpYear + "_WG.tar";

```

```

bWorking = finder.FindFile(tmpName);

```

```

    if (bWorking) {
        return tmpName;
    }

    tmpName = m_XMRGDirectory + tmpYear + "\\ " + tmpTitle + tmpMonth +
tmpDay + tmpYear + "_WG.tar.gz";

    bWorking = finder.FindFile(tmpName);
    if (bWorking) {
        *bInZipped = TRUE;
        return tmpName;
    }

    tmpMonth = tmpTime1->Format(_T("%m"));
    tmpDay = tmpTime1->Format(_T("%d"));
    tmpYear = tmpTime1->Format(_T("%Y"));
    tmpHour = tmpTime1->Format(_T("%H"));
    tmpTitle = "stage3_";
    tmpName = m_XMRGDirectory + tmpYear + "\\ " + tmpTitle + tmpMonth +
tmpDay + tmpYear + "_WG.tar.gz";

    bWorking = finder.FindFile(tmpName);
    if (bWorking) {
        *bInZipped = TRUE;
        return tmpName;
    }

    tmpMonth = tmpTime1->Format(_T("%m"));
    tmpDay = tmpTime1->Format(_T("%d"));
    tmpYear = tmpTime1->Format(_T("%Y"));
    tmpHour = tmpTime1->Format(_T("%H"));
    tmpTitle = "Siii";
    tmpName = m_XMRGDirectory + tmpYear + "\\ " + tmpTitle + tmpMonth +
tmpDay + tmpYear + "WG.tar";

    bWorking = finder.FindFile(tmpName);
    if (bWorking) {
        return tmpName;
    }

    tmpMonth = tmpTime1->Format(_T("%m"));
    tmpDay = tmpTime1->Format(_T("%d"));

```

```

tmpYear = tmpTime1->Format(_T("%Y"));
tmpHour = tmpTime1->Format(_T("%H"));
tmpTitle = "Siii";
tmpName = m_XMRGDirectory + tmpYear + "\\\" + tmpTitle + tmpMonth +
tmpDay + tmpYear.Right(2) + "WG.tar";

```

```

bWorking = finder.FindFile(tmpName);
if (bWorking) {
    return tmpName;
}
tmpName.Empty();
return tmpName;
}

```

```

BOOL CNEXRADDlg::LaunchTarExtraction(CString *strXMRGGridName,
BOOL blnRemove)
{

```

```

    CString strShellCommand;
    CString strCommandFolder;
    CString strBackSlach ( "\\\" );

```

```

        STARTUPINFO si;
        PROCESS_INFORMATION pi;

```

```

        ZeroMemory( &si, sizeof(si) );
        si.cb = sizeof(si);
        ZeroMemory( &pi, sizeof(pi) );

```

```

        strCommandFolder = strXMRGGridName->Left(strXMRGGridName-
>ReverseFind(strBackSlach.GetAt(0))+1);
        strShellCommand = "\"C:\\UnxUtils\\usr\\local\\wbin\\tar.exe\" -xf "
+ strXMRGGridName-
>Right(strXMRGGridName->GetLength()
- strXMRGGridName-
>ReverseFind(strBackSlach.GetAt(0))-1);

```

```

        // Start the child process.
        if( !CreateProcess( NULL, // No module name (use
command line).

```

```

        strShellCommand.GetBuffer(strShellCommand.GetLength()),
        NULL, // Process handle not inheritable.

```

```

        NULL,          // Thread handle not inheritable.
        FALSE,        // Set handle inheritance to FALSE.
        0,            // No creation flags.
        NULL,         // Use parent's environment block.

    strCommandFolder.GetBuffer(strCommandFolder.GetLength()), // Use
parent's starting directory.
        &si,          // Pointer to STARTUPINFO structure.
        &pi )        // Pointer to
PROCESS_INFORMATION structure.
    )
    {
//
        strXMRGGridName = GetLastError() ;
        return FALSE;
    }

// Wait until child process exits.
WaitForSingleObject( pi.hProcess, INFINITE );

if (blnRemove) {
    remove(strXMRGGridName-
>GetBuffer(strXMRGGridName->GetLength()));
    strXMRGGridName->ReleaseBuffer(-1);
}

strCommandFolder.ReleaseBuffer(-1);
strShellCommand.ReleaseBuffer(-1);

// Close process and thread handles.
CloseHandle( pi.hProcess );
CloseHandle( pi.hThread );
return TRUE;
}
BOOL CNEXRADDlg::LaunchZipExtraction(CString *strXMRGGridName)
{
    CString strShellCommand;
    CString strCommandFolder;
    CString strBackSlach ( "\\");

    STARTUPINFO si;
    PROCESS_INFORMATION pi;

    ZeroMemory( &si, sizeof(si) );

```



```

        si.cb = sizeof(si);
        ZeroMemory( &pi, sizeof(pi) );

        strCommandFolder = strXMRGGridName->Left(strXMRGGridName-
>ReverseFind(strBackSlach.GetAt(0))+1);
        strShellCommand = "\"C:\\UnxUtils\\usr\\local\\wbin\\gunzip.exe\" "
+ strXMRGGridName-
>Right(strXMRGGridName->GetLength()
- strXMRGGridName-
>ReverseFind(strBackSlach.GetAt(0))-1);

        // Start the child process.
        if( !CreateProcess( NULL, // No module name (use
command line).

        strShellCommand.GetBuffer(strShellCommand.GetLength()),
        NULL, // Process handle not inheritable.
        NULL, // Thread handle not inheritable.
        FALSE, // Set handle inheritance to FALSE.
        0, // No creation flags.
        NULL, // Use parent's environment block.

        strCommandFolder.GetBuffer(strCommandFolder.GetLength()), // Use
parent's starting directory.
        &si, // Pointer to STARTUPINFO structure.
        &pi ) // Pointer to
PROCESS_INFORMATION structure.
        )
        {
            // strXMRGGridName = GetLastError() ;
            return FALSE;
        }

        // Wait until child process exits.
        WaitForSingleObject( pi.hProcess, INFINITE );

        strCommandFolder.ReleaseBuffer(-1);
        strShellCommand.ReleaseBuffer(-1);

        // Close process and thread handles.
        CloseHandle( pi.hProcess );
        CloseHandle( pi.hThread );

    return TRUE;
}

```

```

void CNEXRADDlg::GetXMRGHourlyValues(CString *strXMRGGridName,
long *ColList,
long
*RowList, double *Values, long numCells)
{
FILE *in_file_ptr;

char user_id[10], date[10], time[10], process_flag[8];
char date2[10],time2[10];

int intWrote=0;

int rfchd[4];
int numsuccess,numbytes;
int numbytes_a[2];

long MAXX, MAXY, XOR, YOR;
long nrows, ncols;
long i, j;
/*short precip[1000];*/
short *onerow;
/*int rainfall[1000][1000];*/
float **matrix;
// float outval;
float xstereo,ystereo;
void reverse_byte_order(int *,int);
void reverse_byte_order_short(short *,int);
/* end variable declaration */

in_file_ptr=fopen(strXMRGGridName->GetBuffer(strXMRGGridName-
>GetLength()),"rb");
if (in_file_ptr == NULL)
{
(void)printf("Can not open file %s for input.\n", (LPCTSTR)
strXMRGGridName);
return;
}
strXMRGGridName->ReleaseBuffer(-1);
/* start reading the XMRG file*/
/*SEEK_SET specifies the position offset from the beginning of the file*/
fseek(in_file_ptr, 4, SEEK_SET);
for(i=0;i<4;i++)

```

```

        {
            fread(&rfchd[i], sizeof(int), 1, in_file_ptr);
        }
    if (rfchd[0] == 290) {
        m_Reverse = 0;
    }
    else {
        m_Reverse = 1;
    }

    if (m_Reverse == 1) {
        (void) reverse_byte_order(rfchd,4);
    }
    XOR=rfchd[0];
    YOR=rfchd[1];
    xstereo=XOR*4762.5-401.0*4762.5;
    ystereo=YOR*4762.5-1601.0*4762.5;
    MAXX=rfchd[2];
    MAXY=rfchd[3];
    nrows = MAXY;
    ncols = MAXX;

    /*print to header file*/
    /*echo to screen*/
    (void)printf("ncols %d\n",MAXX);
    (void)printf("nrows %d\n",MAXY);

    /*each record is preceded and followed by 4 bytes*/
    /*first record is 4+16+4 bytes*/
    fseek(in_file_ptr, 24, SEEK_SET);
    /*read second FORTRAN record*/
    fread(numbytes_a,sizeof(int),2,in_file_ptr);
    if (m_Reverse == 1) {
    (void)reverse_byte_order(numbytes_a,2);
    }
    fseek(in_file_ptr, 4, SEEK_CUR);
    numbytes = numbytes_a[0];

    numsuccess=fscanf(in_file_ptr, "%10s %10s %10s %8s %10s %10s",
user_id, date, time, process_flag,date2,time2);
    /*numsuccess=fscanf*/

    /*first record (24) plus second record(46) is 70*/
    /*if (strlen(date2)>0)*/

```

```

    if ((int) numbytes == 66)
    {
        fseek(in_file_ptr, 98, SEEK_SET);
(void)printf("user_id %10s\n",user_id);
        (void)printf("date %10s\n",date);
        (void)printf("time %10s\n",time);
        (void)printf("process_flag %8s\n",process_flag);
        (void)printf("datelen %d\n",strlen(date));
        (void)printf("timelen %d\n",strlen(time));
        (void)printf("user_id %d\n",strlen(user_id));
        (void)printf("date2 %s\n",date2);
        (void)printf("time2 %s\n",time2);
        (void)printf("numbytes %d\n",numbytes);
    }
    else if ((int) numbytes==38)
    {
        fseek(in_file_ptr, 70, SEEK_SET);
        /*(void)printf("gothere\n");*/
(void)printf("user_id %10s\n",user_id);
        (void)printf("date %10s\n",date);
        (void)printf("time %10s\n",time);
        (void)printf("process_flag %8s\n",process_flag);
        (void)printf("numbytes %d\n",numbytes);
    }
    else if ((int) numbytes==37)
    {
        /* read first header line */
        fseek(in_file_ptr, 4, SEEK_SET);
        for(i=0;i<4;i++)
        {
            fread(&rfchd[i], sizeof(int), 1, in_file_ptr);
        }
    if (m_Reverse == 1) {
        (void) reverse_byte_order(rfchd,4);
    }

        /* read second header line */
        (void)printf("Reading June 1997 - Summer 1999 AWIPS format.\n");
        /*first record (24) plus second record(45) is 70*/
        fseek(in_file_ptr, 69, SEEK_SET);

        /*(void)printf("gothere\n");*/
        (void)printf("WARNING: SECOND RECORD ONLY HAS 37
BYTES\n");
        (void)printf("SHOULD HAVE 38 BYTES\n");
        (void)printf("Assuming data is still valid. . . \n");

```

```

        (void)printf("user_id %10s\n",user_id);
        (void)printf("date %10s\n",date);
        (void)printf("time %10s\n",time);
        (void)printf("process_flag %8s\n",process_flag);
        (void)printf("numbytes %d\n",numbytes);
    }
    else if ((int) numbytes == (ncols*2))
        /* the second record of the files was nonexistent in pre-June 1997 files.*/
        {
            /* read first header line */
            fseek(in_file_ptr, 4, SEEK_SET);
            for(i=0;i<4;i++)
            {
                fread(&rfchd[i], sizeof(int), 1, in_file_ptr);
            }
            if (m_Reverse == 1) {
                (void) reverse_byte_order(rfchd,4);
            }
            (void)printf("Reading pre-1997 format.\n");
            fseek(in_file_ptr,24, SEEK_SET);
        }
        else
        {
            (void)printf("numbytes %d\n",numbytes);
            (void)printf("Header file is in a nonstandard format. Data NOT
READ!\n");
            exit(1);
        }

        /* allocate memory for arrays */
        onerow = (short int*) malloc(sizeof(short int)*ncols);
        matrix = (float**) malloc(sizeof(float)*nrows);
        for (i=0;i<nrows;i++)
            matrix[i]=(float*) malloc(sizeof(float)*ncols);
        printf("out5");
        for(i=nrows-1;i>-1;i--)
        {
            fseek(in_file_ptr, 4, SEEK_CUR);
            /* read one row */
            fread(onerow,sizeof(short),ncols,in_file_ptr);
            if (m_Reverse == 1) {
                (void) reverse_byte_order_short(onerow,ncols);
            }
            fseek(in_file_ptr, 4, SEEK_CUR);
            for(j=0;j<ncols;j++)

```

```

        {
            matrix[i][j] = (float) onerow[j];
        } /* close j */
    } /* close i */

    for(i=0; i<NUMCELLS; i++)
    {
        if ((nrows*ncols) <= 200000) {
            Values[i] = matrix[nrows-(RowList[i]+1)][ColList[i]]/100.0;
        }
        else {
            Values[i] = matrix[nrows-(RowList[i]+10)][ColList[i]+30]/100.0;
        }
        /* convert from hundredths of mm to mm*/
        //printf("%lf", matrix[RowList[i]-1][ColList[i]-1]);
    }
}

```

```
fclose(in_file_ptr);
```

```

for (i=0;i<nrows;i++)
    { free(matrix[i]);}
    free(matrix);// }
free(onerow);
return;

}

```

```
void reverse_byte_order(int *in_array,int arraysize)
{
```

```

    unsigned int i,k;
    signed char *p_data; /*data pointer*/
    signed char *p_temp; /*temporaty data pointer */
    int temp;

```

```

    /*printf("before %d %d\n",input_data[0],input_data[1]);*/
    p_data = (signed char *) in_array - 1;

```

```

for ( k = 0 ; k < arraysize ; k++ )
{
    temp = *( in_array + k );
    p_temp = ( signed char * ) ( &temp ) + 4;

    for ( i = 0 ; i < 4 ; i++ )
    {
        *(++p_data) = *(--p_temp);
    }
}
/*printf("after %d %d\n",input_data[0],input_data[1]);*/

/*free(start_ptr);*/
}

void reverse_byte_order_short(short *in_array,int arraysize)
{
    unsigned int  i,k;
    signed char *p_data; /*data pointer*/
    signed char *p_temp; /*temporaty data pointer */
    short temp;

    /*printf("before %d %d\n",input_data[0],input_data[1]);*/
    p_data = (signed char *) in_array - 1;
    for ( k = 0 ; k < arraysize ; k++ )
    {
        temp = *( in_array + k );
        p_temp = ( signed char * ) ( &temp ) + 2;

        for ( i = 0 ; i < 2 ; i++ )
        {
            *(++p_data) = *(--p_temp);
        }
    }
    /*printf("after %d %d\n",input_data[0],input_data[1]);*/

    /*free(start_ptr);*/
}

void CNEXRADDlg::ReadCells(CString *strCellFileName,
                           long *RowList, long *ColList,
double *Values,
                           long *numValues)

```

```

{
    FILE    *in_file_ptr;
    int i=0;
    long numValuesII;
    long tmpValue;

    in_file_ptr=fopen(strCellFileName->GetBuffer(strCellFileName-
>GetLength()),"r");
    //    in_file_ptr=fopen((LPCTSTR) strCellFileName,"r");
    if (in_file_ptr == NULL)
    {
        (void)printf("Can not open file %s for input.\n",(LPCTSTR)
strCellFileName);
        return;
    }

    fscanf(in_file_ptr,"%i", numValues);//(&numValues, 3, 1 , in_file_ptr);

    numValuesII = *numValues;

    //    *RowList = (long*) malloc(90*numValuesII);
    //    *Values = (double*) malloc(90*numValuesII);
    //    *ColList = (long*) malloc(90*numValuesII);

    /* start reading the XMRG file*/
    /*SEEK_SET specifies the position offset from the beginning of the file*/
    for(i=0;i<NUMCELLS;i++)
    {
        fscanf(in_file_ptr,"%i",&tmpValue);
        //    fscanf(in_file_ptr,"%i",&(RowList[i]));
        ColList[i] = tmpValue;
        fscanf(in_file_ptr,"%i",&tmpValue);
        //    fscanf(in_file_ptr,"%i",&(ColList[i]));
        RowList[i] = tmpValue;
    }
    fclose(in_file_ptr);
}

void CNEXRADDlg::OnRadio2()
{
    // TODO: Add your control notification handler code here
    if (m_Reverse == 1) {
        m_Reverse = 0;

```



```
        }  
    }  
void CNEXRADDlg::OnRadio1()  
{  
    // TODO: Add your control notification handler code here  
    if (m_Reverse == 0) {  
        m_Reverse = 1;  
    }  
}
```

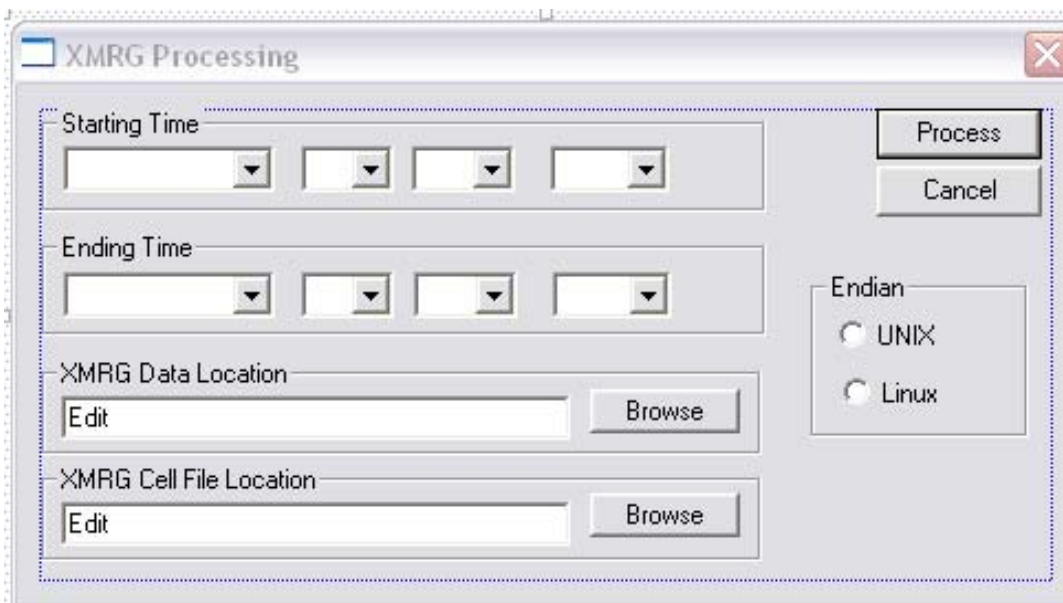


Figure A.1 – Graphical user interface for the NEXRAD data processing software to facilitate the conversion of xmrp file format into an ASCII format.

Bibliography

- Aquilina, L., Ladouche, B., Dorfliger, N., 2005, Recharge processes in karstic systems investigated through correlation of chemical and isotopic composition of rain and spring-waters: *Applied Geochemistry*, v. 20, p. 2189-2206.
- Ashworth, J. B., 1983, Ground-water availability of the lower Cretaceous formations in the Hill Country of south-central Texas: Texas Department of Water Resources Report 273, 65 p.
- Barrett, M. E., and Charbeneau, R. J., 1996, A parsimonious model for simulation of flow and transport in a karst aquifer: Technical Report Center for Research in Water Resources, Report No. 269, 149 p.
- Bebout, D. G., and Loucks, R. G., 1974, Stuart City trend, lower Cretaceous, south Texas, a carbonate shelf-margin model for hydrocarbon exploration: Univ. Texas, Bureau of Economic Geology Report of Inv. no. 78, 80 p.
- Bluntzer, R. L., 1992, Evaluation of the ground-water resources of the Paleozoic and Cretaceous aquifers in the Hill Country of central Texas: Texas Water Development Board Report 339, 130 p.
- Birk, S., Liedl, R., Sauter, M., 2004, Identification of localized recharge and conduit flow by combined analysis of hydraulic and physico-chemical spring responses (Urenbrunnen, SW-Germany): *Journal of Hydrology*. v. 286, p. 179-193.
- BSEACD, 2008, Proposed Management Plan: Barton Springs Edwards Aquifer Conservation District, 74 p.
- BSEACD, 2003, Summary of Groundwater Dye Tracing Studies (1996-2002), Barton Springs Segment of the Edwards Aquifer, Texas, Barton Springs/Edwards Aquifer Conservation District Newsletter, April 2003.
- Budge, T.J., and Sharp, J.M. Jr., 2008, Delineating contributing areas in two Texas karst aquifers using NEXRAD rainfall estimates, in *Proceedings of Water Down Under 2008*, p. 203-214.
- Carpenter, T.M., Georgakakos, K.P., Sperflagea, J.A., 2001, On the parametric and NEXRAD-radar sensitivities of a distributed hydrologic model suitable for operational use: *Journal of Hydrology*, v. 253, p. 169-193.
- Connair, D.P., Murray, B.S., 2002, Karst groundwater basin delineation, Fort Knox, Kentucky: *Engineering Geology*, v. 65, p. 125-131.

- Cunningham, K. J., Renken, R. A., Wacker, M. A. and Zygnerski, M., 2003, Application of Carbonate Cycle Stratigraphy to Delineate Porosity and Preferential Flow and to Assess Advective Transport in the Karst Limestone of the Biscayne Aquifer: Geological Society of America Abstracts with Programs, v. 35, no. 6, p. 453
- Deeds, N., Budge, T.J., Kelley, V., Young, S.C., Saunders, G.P., and Waugh, J, 2007, Estimation of Spatially Varying Recharge for a Regional Scale Ground Water Model in the Texas Gulf Coast, Abstract Book of the 2007 Ground Water Summit Program.
- Diersch, H.-J. G.: 2002, "FEFLOW--Reference Manual," Berlin: WASY Ltd., 292 p.
- Doherty, J., 2003, Groundwater model calibration using Pilot Points and Regularisation: Groundwater v.41, no. 2, p. 170-177.
- Dufresne, D.P., Drake, C.W., 1999, Regional groundwater flow model construction and wellfield site selection in a karst area, Lake City, Florida: Engineering Geology, v. 52, p. 129-139.
- ESI, 2007, Environmental Science Institute at the University of Texas at Austion Jackson School of Geosciences, www.esi.utexas.edu/outreach/caves/karst.php
- Fulton, R.A., Breidenbach, J.P., Seo, D., Miller, D.A., O'Bannon, T., 1998, The WSR-88D rainfall algorithm: Weather and Forecasting, v. 13, p. 377-395.
- Geological Society of America, 2007, Session No. 40: Inverse Methods in Practice: Perspectives and Future Directions: Geological Society of America Abstracts with Programs, v. 39, no. 6, p. 111.
- George, W. O., and others, 1952, Geology and ground-water resources of Comal County, Texas: U.S. Geol. Survey Water-Supply Paper 1138, 126 p.
- Glenn, S., 2003, Ground Water Modeling using NEXRAD-Generated Data and MODFLOW: Evaluating the Parameters of Rainfall and Discharge in a GIS Framework, [PhD Thesis]: Rice University, 234 p.
- Grimshaw, T.W., 1970, Geology of the Wimberley area, Hays and Comal Counties, Texas. [Masters Thesis]: University of Texas and Austin. 104 p.
- Halihan, T, 2000, Permeability structure in Fractured Aquifers, [PhD Thesis]: University of Texas at Austin, 133 p.
- Harbaugh, A.W., and McDonald, M.G., 1996, User's documentation for MODFLOW-96, an update to the U.S. Geological Survey modular finite-difference ground-water flow model: U.S. Geological Survey Open-File Report 96-485, 56 p.

- Hanson, J. A., and Small, T. A., 1995, Geologic framework and hydrogeologic characteristics of the Edwards aquifer outcrop, Hays County, Texas: U.S. Geological Survey, Water-Resources Investigations Report 95-4265, 10 p. (1 sheet).
- Hauwert, N.M., 2006, Summary of some recent studies on recharge and groundwater flow within the Barton Springs Segment of the Edwards Aquifer: Austin Geological Society Bulletin, v. 2, p 15-16.
- Hauwert, N., and Vickers, S., 1994, Barton Springs/Edwards aquifer hydrogeology and groundwater quality: Austin, TX, Barton Springs/Edwards Aquifer Conservation District, report prepared for Texas Water Development Board under contract no. 93483-346, 92 p.
- Hunt, B.B., Smith, B.A., and Beery, J., 2007, Potentiometric maps for low to high flow conditions, Barton Springs Segment of the Edwards Aquifer, Central, Texas: BSEACD Report of Investigations 2007-1201, 64 p.
- HGL, 2005, MODFLOW-SURFACT Software (version 2.2) Overview: Installation, Registration, and Running Procedures. HydroGeoLogic, Inc., Herndon, VA., 543 p.
- Jenks, G.F., Caspall, F.C., 1971, Error on Choroplethic Maps: Definition, Measurement, Reduction: *Annals of the Association of American Geographers*, v. 61, no. 2, p. 217-244.
- Johnson, D., Smith, M., Koren, V., Finnerty, B., 1999, Comparing mean areal precipitation estimates from NEXRAD and rain gauge networks: *Journal of Hydrologic Engineering*, v. 4, no. 2, p. 117-124.
- Johnson, C.A., Yung, A.C., Nixon, K.R., Legates, D.R., 2001, The Use of HEC-GeoHMS and HEC-HMS To Perform Grid-based Hydrologic Analysis of a Watershed: Dodson and Associates, 2001
- Jones, I.C., 2003, Groundwater Availability Modeling: Northern Segment of the Edwards Aquifer, Texas: Texas Water Development Board Report 358, 75 p.
- Karst Waters Institute, 2007, Karst Waters Institute - Home, <http://www.karstwaters.org/index.htm>, Leesburg, Va.
- Kwan, H.C., Cheng, A.C., Liu, R., Borrett, D.S., 2004, Human cortical perfusion and the arterial pulse: a near-infrared spectroscopy study: *BMC Physiology*, v. 4, no. 7.
- Larocque, M., Mangin, A., Razack, M., Banton, O., 1998, Contribution of correlation and spectral analyses to the regional study of a large karst aquifer (Charente, France): *Journal of Hydrology*, v. 205. p. 217-231

- Lee, E.S., Krothe, N., 2003, Delineating the karstic flow system in the upper Lost River drainage basin, south central Indiana: using sulphate and delta-SSO₄ as tracers: *Applied Geochemistry*, v. 18, p. 145-153.
- Lin, H.C.J., Richards, D.R., Talbot, C.A., Yeh, G.T., Cheng, J.R., Cheng, P., and Jones, N.L., 1997, FEMWATER: A Three-Dimensional Finite Element Computer Model for Simulating Density-Dependent Flow and Transport in Variably Saturated Media. Version 3.0, 143p.
- Long, A.J., Putnam, L.D., 2004, Linear model describing three components of flow in karst aquifers using Oxygen-18 data: *Journal of Hydrology*, v. 296, p. 254-270.
- Mace, R. E., Chowdhury, A. H., Anaya, R., and Way, S. C., 2000, Groundwater availability of the Trinity Aquifer, Hill Country Area, Texas: numerical simulations through 2050: Texas Water Development Board Report 353, 117 p.
- Maddox, R.A., Zhang, J., Gourley, J.J., Howard, K.W., 2002, Weather radar coverage over the contiguous United States: *Weather and Forecasting*, v.17, p. 927–934.
- Mahler, B., 2006, personal conversation with Barb Mahler, Head of Barton Springs Characterization Project, United States Geological Survey, Austin, Texas.
- Massei, N., Mahler, B.J., Bakalowicz, M., Fournier, M., and Dupont, J.P., 2007, Quantitative Interpretation of Specific Conductance Frequency Distributions in Karst: *Ground Water*, v. 45, no. 3, p. 288-293.
- Moore, G.K., 1992, Hydrographs analysis in fractured rock terrane: *Ground Water*, v. 30, no. 3, p. 390-395.
- Nativ, R., Gunay, G., Hozl, H., Reichert, B., Solomon, D.K., Tezcan, L., 1999, Separation of groundwater-flow components in a karstified aquifer using Environmental tracers: *Applied Geochemistry*, v. 14, p. 1001–1014.
- NWS, 2007, NWS River Forecast Centers. <http://www.weather.gov/ahps/rfc/rfc.php>
- NWS, 2007b, National Weather Service Hydrology Laboratory. <http://www.weather.gov/ohd/hrl/dmip/nexrad.html>
- NWS, 2002, About the Stage III data. http://www.weather.gov/ohd/hrl/dmip/stageiii_info.htm
- NWS/OH, 1997, Stage III precipitation processing system, system guide. Hydrologic Research Laboratory. <http://www.nws.noaa.gov/oh/hrl/pps/pps.htm>
- NWS/OH, 1999, Displaying and using NWS XMRG/HRAP files within ArcView or ArcInfo GIS. <http://www.nws.noaa.gov/oh/hrl/distmodel/hrap.htm>.

- Padilla, A., Pulido-Bosch, A., 1995, Study of hydrographs of karst aquifers by means of correlation and cross-spectral analysis: *Journal of Hydrology*, v. 168, p. 73-89.
- Painter, S.L., 2004, A MODFLOW-based approach for modeling flow in karst aquifers, *Abstracts with Programs – Geological Society of America*, v. 36, no. 5, p. 30.
- Panagopoulos, G., Lambrakis, N., 2006, The contribution of time series analysis to the study of the hydrodynamic characteristics of the karst systems: Application on two typical karst aquifers of Greece (Trifilia, Alymyros Crete): *Journal of Hydrology*, v. 329, p. 368-376.
- PEST, 2007, *Model-Independent Parameter Estimation, User Manual: 5th Edition*, Watermark Computing. 333 p.
- Pollock, D.W., 1994, *User's Guide for MODPATH/MODPATH-PLOT, Version 3: A particle tracking post-processing package for MODFLOW, the U.S. Geological Survey finite-difference ground-water flow model: U.S. Geological Survey Open-File Report 94-464*, 249 p.
- R Development Core Team, 2006, *R: A language and environment for statistical computing: R Foundation for Statistical Computing, Vienna, Austria. ISBN 3-900051-07-0*, URL <http://www.R-project.org>.
- Rose, P. R., 1972, Edwards Group, surface and subsurface, central Texas: *Univ. Texas, Bureau of Economic Geology Report. of Inv.*, no. 74, 198 p.
- Scanlon, B.R., Mace, R.E., Smith, B., Hovorka, S., Dutton, A.R., Reedy, R., 2001, *Groundwater Availability of the Barton Springs Segment of the Edwards Aquifer, Texas: Numerical Simulations Through 2050: Bureau of Economic Geology*, 99 p.
- Scanlon, B.R., Mace, R.E., Barrett, M.E., Smith, B., 2003, Can we simulate regional groundwater flow in a karst system using equivalent porous media models? Case study, Barton Springs Edwards aquifer, USA: *Journal of Hydrology*, v. 276, p. 137-158.
- Seo, D.J., Breidenbach, J., Fulton, R., Miller, D, Vignal, B., Krajewski, W, 2000, *Final Report for June 1, 1999 to May 31, 2000 Interagency Memorandum of Understanding Among The NEXRAD Program, The WSR-88D Operational Support Facility, and The National Weather Service Office of Hydrology, Hydrologic Research Laboratory Office of Hydrology National Weather Service, July 28, 2000*
- Senger, R. K., and Kreitler, C. W., 1984, *Hydrogeology of the Edwards aquifer, Austin area, Central Texas: The University of Texas at Austin, Bureau of Economic Geology Report of Investigations No. 141*, 35 p.

- Sharp, J. M., Jr., 1990, Stratigraphic, geomorphic and structural controls of the Edwards aquifer, Texas, U. S. A.: in Selected Papers on Hydrogeology (E. S. Simpson and J. M. Sharp, Jr., eds.), International Association of Hydrogeologists, Heise, Hannover, v. 1, p. 67-82.
- Sharp, J. M. Jr., Llado, L.E., Wiles, T.J., Budge, T.J., and Garcia-Fresca, B., 2008, Alterations to recharge to the Edwards Aquifer, Barton Springs Segment, caused by urbanization: Geological Society of America Abstracts with Programs, v. 40, no. 3, p. 30
- Shelton, G., 2008, personal communication with with Greg Shelton, Hydrologist at the West Gulf River Forecast Center, National Weather Service, Dallas, Texas.
- Slade, R. M., Jr., Dorsey, M. E., and others, 1986, Hydrology and water quality of the Edwards aquifer associated with Barton Springs in the Austin area, Texas: U.S. Geological Survey, Water-Resources Investigations Report 86-4036, 96 p.
- Slade, R. M., Ruiz, L., and others, 1985, Simulation of the flow system of Barton Springs and associated Edwards aquifer in the Austin area, Texas: U.S. Geological Survey, Water Resources Investigations Report 85-4299, 49 p.
- Small, T. A., Hanson, J. A., and Hauwert, N. M., 1996, Geologic framework and hydrogeologic characteristics of the Edwards aquifer outcrop (Barton Springs segment), northeastern Hays and southwestern Travis Counties, Texas: U.S. Geological Survey, Water-Resources Investigations WRI 96-4306, 15 p. (1 sheet).
- Smart, C.C., 1988, Artificial tracer techniques for the determination of the structure of conduit aquifers: Ground Water, v. 26, no. 4, p. 445-453.
- Smith, B., 2006, personal communication with Brian Smith, Senior Hydrogeologist for the Barton Springs Edwards Aquifer Conservation District, Austin, Texas
- Smith, J.A., Seo, D.J., Baeck, M.L., Hudlow, M.D., 1996, An intercomparison study of NEXRAD precipitation estimates: Water Resources Research 31, 2035–2045.
- Smith, M.B., Dong-Jun, S., Koren, V.I., Reed, S.M., Zhang, Z., Duan, Q., Moreda, F., Cong, S., 2004, The distributed model intercomparison project (DMIP): motivation and experiment design, Journal of Hydrology, Vol. 298, pp. 4-26
- Texas Water Development Board, 2001, Estimating Groundwater Availability in Texas, In proceedings of the 1st annual Texas Rural Water Association and Texas Water Conservation Association Water Law Seminar: Water Allocation in Texas: The Legal Issues: Texas Water Development Board, 15 p.
- Texas Water Development Board. 2007, Water for Texas 2007. Document No. GP-8-1, v. 1, 43 p.

- Therrien R., McLaren R.G., Sudicky E.A., and Panday S.M. 2004, HydroSphere; A three-dimensional numerical model describing fully-integrated subsurface and surface flow and solute transport: User manual, 275 p.
- USGS, 2007, Barton Springs Characterization Project. http://tx.usgs.gov/projects/aquifer_springs/bartonsprings/index.html,
- USGS, 2006, Estimated Recharge to the Edwards Aquifer in the San Antonio Area, Texas, 1934–2006, http://tx.usgs.gov/projects/aquifer_springs/estimatedrecharge.htm
- UT, 2005, Characterization of Jacob’s Well near Wimberley, Texas. University of Texas at Austin 2005 Hydrogeology Field Methods Class Report.
- URS, 2005, Numerical Simulations of Groundwater Withdrawal from the LSWP Using the Northern and Southern Gulf Coast GAMs, prepared for the Lower Colorado River Authority, 39 p.
- Vandenschrick, G., van Wesemael, B., Frot, E., Pulido-Bosch, A., Molina, L., Stievenard, M., Souchez, R., 2002, Using stable isotope analysis (delta-D-deltaO-18) to characterize the regional hydrology of the Sierra de Gador, south east Spain: *Journal of Hydrology*, v. 265, p. 43-55.
- Wang, X., Xie, H., Sharif, H., Zeitler, J., 2008, Validating NEXRAD and Stage III precipitation products for uniform rainfall on the Upper Guadalupe River Basin of the Texas Hill Country: *Journal of Hydrology*, v. 348, p. 73-86.
- Worthington, S. R. H., Smart, S. C. and Ruland, W. W.: 2002, Assessment of Groundwater Velocities to the Municipal Wells at Walkerton, *in* Proceedings of the 56 th Canadian Geotechnical and 3 rd Joint IAH-CNC and CGS Groundwater Specialty Conferences, Niagara Falls, Ontario, Canada, October 20–23, 2002, p. 1,081–1,086.
- Wiegner, A.W. Wierzbicka, M.M., 1987, A method for assessing significance of peaks in cross-correlation histograms: *Journal of Neuroscience Methods*. v. 22, p. 125-131.
- WVMA, 2007, Wimberly Valley Watershed Association – Jacob’s Well in Wimberley, Texas. <http://www.visitwimberley.com/water/>.
- Xie, H., Zhou, X., Vivoni, E.R., Hendrickx, J.M.H., Small, E.E., 2005, GIS-based NEXRAD Stage III precipitation database: automated approaches for data processing and visualization: *Computers and Geosciences*, v. 31, p. 65-76.
- Xie, H., X. Zhou, J. Hendrickx, E. Vivoni, H. Guan, Y. Tian, and E. Small, 2006, comparison of NEXRAD Stage III and gauge precipitation estimates in central New Mexico: *Journal of the American Water Resources Association*, v. 42, no. 1, p. 237-256

- Young, C.B., 2000, Evaluation of NEXRAD precipitation estimates and their potential use for nonpoint source pollution modeling [PhD thesis]: University of Iowa, 229 p.
- Young, C.B., Bradley, A.A., Krajewski, W.F., Kruger, A., Morrissey, M.L., 2000, Evaluating NEXRAD multisensor precipitation estimates for operational hydrologic forecasting: *Journal of Hydrometeorology*, v. 1, p. 241–254.
- Zygierewicz, J. Mazurkiewicz, J. Durka, P.J. Franaszczuk, P.J. and Crone, N.E., 2006, Estimation of short-time cross-correlation between frequency bands of event related EEG: *Journal of Neuroscience Methods*, v. 157, no. 2, p. 294-302.

Vita

Trevor Jones Budge was born in Portland, Oregon in 1974. He is the son of Ronald and Rosalind Budge. He graduated from Reynolds High School in Troutdale, Oregon where he served as Student Body President and was a captain on the varsity football team. He attended Brigham Young University from 1993 to 2000 where he earned a Bachelor and Master of Science in Civil and Environmental Engineering. During his undergraduate education he spent two years on a mission for his church in Santiago, Chile. Also, he married the former Camea Amber Dullum in 1997. They have three daughters Courtney, MacKenzie, and Alexis. After graduation from BYU he was employed by both HydroGeoLogic, Inc. and URS Corporation as a graduate engineer and hydrogeologist. He returned to school at the University of Texas at Austin in Spring 2004 to pursue his doctoral studies.

Permanent address: 1116 Pine Portage Loop, Leander, Texas, 78641

This dissertation was typed by the author.